Role of aPKCλ in epidermal morphogenesis and homeostasis

Inaugural-Dissertation

zur

Erlangung des Doktorgrades

der Mathematisch-Naturwissenschaftlichen Fakultät

Der Universität zu Köln

vorgelegt von

Michaela Tosca Niessen

aus Remagen

Köln, 2013

Berichterstatter: **Prof. Dr. rer. nat. Thomas Langer**

Prof. Dr. rer. nat. Carien M. Niessen

Tag der mündlichen Prüfung: 13.04.2012

Abstract

Cell polarity, defined as the asymmetric distribution of proteins, lipids and structural elements within a cell, is crucial for tissue homeostasis by regulating a variety of functions such as barrier formation, cell fate, migration and cell shape. The overall aim of this study was to examine how polarity pathways regulate epidermal morphogenesis and homeostasis and more specifically, the balance between differentiation and proliferation in a self-renewing stratified epithelium. Atypical protein kinase C (aPKC) is a key player in the regulation of polarity, although most of its functions have been studied in lower organisms or in mammalian simple epithelial cells. In mammals, two aPKC isoforms have been identified, aPKCλ and aPKCζ. To elucidate the role of aPKCλ in the stratifying epithelium of mice, aPKCλ was deleted specifically in all epidermal lineages (aPKCλ$^{epi-/-}$ mice). Loss of aPKCλ resulted in a progressive phenotype characterized by a hyperthickened interfollicular epidermis (IFE), enlarged sebaceous glands and deformed hair follicles (HFs). We observed increased differentiation of sebaceous glands and IFE whereas HF differentiation was perturbed after aPKCλ deletion, suggesting cell fate changes within the epidermal lineage. aPKCλ$^{epi-/-}$ HFs increasingly failed to enter resting phases of the hair cycle, which was associated with increased proliferation and a loss of quiescence in HF bulge stem cells. Concomitantly with inappropriate HF stem cell activation, immunohistochemical and FACS analyses revealed a gradual loss of bulge stem cell marker expression, indicating a depletion of bulge stem cells over time in aPKCλ$^{epi-/-}$ mice. This was accompanied by a gradually increased number of cells expressing markers of more committed progenitors suggesting altered cellular fate of aPKCλ$^{-/-}$ HF stem cells. The gradual loss of stem cell function was confirmed *in vitro* by a loss of proliferative potential of adult keratinocytes. Moreover, aged mice showed complete alopecia and a premature aging phenotype indicating exhaustion of stem cells. Together, these data demonstrate that loss of aPKCλ exhausts the bulge stem cell compartment over time. Cellular analyses revealed that epidermal deletion of aPKCλ increased the ratio of asymmetric versus symmetric divisions in the IFE as well as HFs providing a mechanistic explanation for how aPKC regulates epidermal cell fate decisions. On the molecular level this was linked to altered Rac1 activation and changes in the expression and *in vitro* localization of the cell fate protein Numb. Moreover, loss of aPKCλ increased Wnt/β-catenin signaling in keratinocytes, which provides a potential link to altered HF cycling. In summary, this work revealed that aPKCλ is crucial for epidermal homeostasis and HF stem cell maintenance and demonstrates a key role for aPKCλ in the regulation of epidermal cell fate decisions, likely by controlling the balance of asymmetric versus symmetric cell divisions.

Zusammenfassung

Zellpolarität ist definiert als die asymmetrische Verteilung von Proteinen, Lipiden und strukturellen Elementen in der Zelle und ist eine unerlässliche Bedingung für die Funktionalität von Geweben, zum Beispiel durch die Regulation von Barrierefunktion und Zellschicksal. Ziel dieser Arbeit war es herauszufinden, wie Zellpolarität die Homeostase eines stratifizierten Epitheliums regultiert. Atypical protein kinase C (aPKC) ist ein essentieller Regulator von Zellpolarität, wobei die Funktion von aPKC vor allem in *C.elegans*, *D. melanogaster* und in Zellkultur untersucht wurde. In Säugetieren existieren zwei aPKC Isoformen, aPKCλ und aPKCζ. Um die Rolle des Polaritätsproteins aPKCλ in der Epidermis zu charakterisieren, wurde aPKC spezifisch in allen epidermalen Kompartimenten inaktiviert (aPKCλ$^{epi-/-}$ Mäuse). Die epidermale Depletion von aPKC resultierte in einem auffälligen Phänotyp. Die interfollikuläre Epidermis von aPKCλ$^{epi-/-}$ Mäusen war stark verdickt, die Talkdrüsen vergrößert und die Haarfollikel zeigten eine abnormale Form. Während Talgdrüsen und interfollikuläre Epidermis eine verstärkte Differenzierung zeigten, war die Differenzierung von Haarfollikeln gestört, was auf ein verändertes Zellschicksal in aPKCλ$^{-/-}$ Keratinozyten hindeutet. Weiterhin traten aPKCλ$^{-/-}$ Haarfollikel nicht mehr in Ruhephasen des follikulären Zyklus (Telogen) ein und zeigten eine verstärkte Proliferation. Die Stammzellen der Wulstregion im Haarfollikel befinden sich normalerweise in einem Ruhezustand, in dem sie sich selten teilen. Ruhende Haarfollikelstammzellen konnten in aPKCλ$^{epi-/-}$ Mäusen kaum detektiert werden. Weitere Studien mittels FACS und Immunohistochemie zeigten, dass die Zahl der Haarfollikelstammzellen der Wulstregion während des postnatalen Lebens von aPKCλ$^{epi-/-}$ Mäusen graduell abnimmt. Gleichzeitig wurde eine Vergrößerung der Population von Progenitorzellen, welche im oberen Teil des Haarfollikels oberhalb der Wulstregion lokalisiert sind, festgestellt, was eine Veränderung des Zellschicksals von Haarfollikelstammzellen der Wulstregion vermuten lässt. Der Verlust der Funktion der Stammzellen wurde durch eine starke Verminderung des proliferativen Potentials von adulten aPKCλ$^{-/-}$ Keratinozyten bestätigt. Ein Jahr alte aPKCλ$^{epi-/-}$ Mäuse hatten all ihr Haar verloren. Mittels einer Analyse auf zellulärer Ebene fanden wir heraus, dass der Anteil von asymmetrischer Zellteilung, verglichen mit symmetrischer Zellteilung, in allen epidermalen Kompartimenten erhöht war. Wir detektierten eine verminderte Aktivierung der kleinen GTPase Rac1 und eine reduzierte Expression des Proteins Numb in aPKCλ- negativer Epidermis. Darüber hinaus ist der aPKCλ$^{epi-/-}$ Phänotyp mit einer erhöhten Aktivität des Wnt/β-catenin Signalweges assoziiert. Unsere Ergebnisse zeigen, das aPKCλ unerlässlich für epidermale Homeostase und die Erhaltung des Stammzellkompartiments der Wulstregion des Haarfollikels ist. Unsere Analyse demonstriert, dass aPKCλ Zellschicksal in der Epidermis reguliert und eine wichtige Rolle in der Kontrolle der Balance von asymmetrischer gegen symmetrischer Zellteilung spielt.

Content

List of Figures

Introduction

Results

List of Tables

Abbrevations

ACD	Aymmetric cell division
BCA	bicinchoninic acid
bp	base pairs
BrdU	bromdesoxyuridine
BSA	bovine serum albumin
°C	degree Celsius
Ctr	Control
Cre	site specific recombinase from phage P1(causes recombination)
DAPI	4`6-Diamidino-2-phenylindol
DNA	deoxyribonucleic aciid
E	embryonic day
ECL	enzymatic chemiluminescence
EDTA	ethylenediaminetetraacetic acid
EGF	epidermal growth factor
EtOH	ethanol
FACS	fluorescence activated cell sorting
FCS	fetal calf serum
Fig.	figure
floxed/ floxed	lox P flanked
FSC	Foward scatter
g	acceleration of gravity
GFP	green fluorescent protein
GTP	Guanosintriphosphat
HF	hair follicle
HFSC	hair follicle stem cells
hrs	hours
H&E	hematoxylin and eosin
HRP	horse radish peroxidase
IFE	interfollicular epidermis
Inscuteable	Insc

IRS	Inner root sheath
K	keratin
kDa	kilo Dalton
LRC	label retaining cells
mg	milligram
min	minutes
µl	microliter
ml	milliliter
NGS	normal goat serum
ORS	Outer root sheeth
P	postnatal day
PAGE	polyacrylamide gel electrophoresis
PBS	phosphate buffered saline
PCR	polymerase chain reaction
PFA	paraformaldehyde
PMSF	phenylmethylsulphonylfluorid
qRT-PCR	quantitative Real Time PCR
Rac1	Ras-related C3 botulinum toxin substrate 1
rpm	rounds per minute
SDS	sodium dodecyl sulphate
sec	seconds
SOP	sensory organ precursor
str.	*stratum*
Tamoxifen	Tam
TBS	tris buffered saline
U	unit
vs.	versus
v/v	volume by volume
w/v	weight by volume
α6Int	α-6- Intergrin

1 Introduction

1.1. The skin

The mammalian skin protects the organism from dehydration and forms a barrier against harmful influences, such as UV, temperature changes, mechanical stress and microbes. It is composed of two distinct compartments, the dermis and the epidermis, separated by the dermal-epidermal basement membrane zone, which acts as a permeability barrier and forms an adhesive interface between the two main skin compartments (Ko and Marinkovich, 2010). The underlying, mesenchymically derived dermis is composed of fibro-elastic extracellular matrix tissue, contains many sensory receptors and is highly vascular. The outermost layer of the skin, the epidermis, is a complex self-renewing tissue, encompassing the interfollicular epidermis and epidermal appendages, such as hair follicles, sebaceous glands and sweat glands. To provide a functional barrier, cells are sealed to each other by adherens junctions, desmosomes and in the upper epidermal layers, tight junctions (Fig. 1.1) (Niessen and Niessen, 2010; Fuchs and Raghavan, 2002).

1.1.1.The interfollicular epidermis

The interfollicular epidermis (IFE) is organized into four distinct layers of keratinocytes. The innermost layer of the IFE, the basal layer (*stratum basale*) is composed of proliferating, undifferentiated keratinocytes characterized by expression of the intermediate filament pair Keratin14 (K14) and Keratin5 (K5). In response to not yet completely defined stimuli, keratinocytes exit the basal layer, stop dividing and commence a program of terminal differentiation by entering the spinous layer (*stratum spinosum*). Basal cells begin to differentiate into spinous cells by switching from the expression of basal cytoskeletal markers (K14/K5) to spinous cytoskeletal proteins (K10) and by increasing their cell-cell adhesions. The journey of epidermal differentiation continues as keratinocytes progress upwards from the spinous layer through the granular layer (*stratum granulosum*), which forms the apical viable boundary of the epidermis and is characterized by loricrin expression. Finally, the cells end in the *stratum corneum* where cells undergo terminal differentiation by loosing their nuclei and become corneocytes. In the *stratum corneum*, numerous proteins and lipids are tightly crosslinked and thus provide a protective barrier, called cornified envelope (Kalinin et al., 2002). The outermost cells will eventually slough off to be replaced from below (Fig. 1.1B) (Blanpain and Fuchs, 2009; Fuchs, 2007).

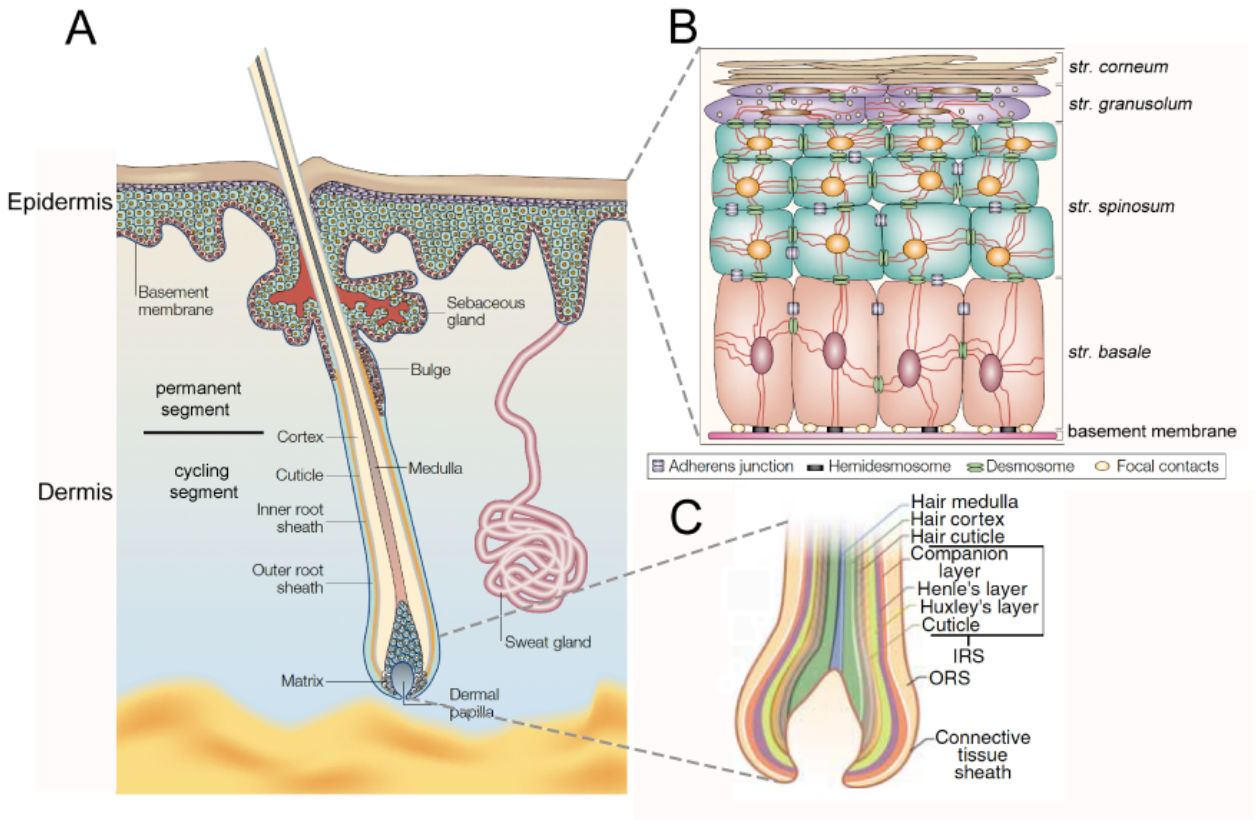

Figure 1. 1: The skin and its appendages

(A) The skin consists of the epidermis and dermis. The epidermis is separated from the dermis by the basement membrane and is composed of the interfollicular epidermis and its appendages. A cycling hair follicle is depicted, with proliferating matrix cells at the bottom of the hair bulb. (B) Proliferating basal keratinocytes *(str. basale)* of the interfollicular epidermis give rise to cells of the *stratum* (*str.*) *spinosum*, *granulosum* and *corneum*. Cells are tightly sealed to each other by adherens junctions, hemidesmosomes, desmosomes and tight junctions (not shown). (C) The transient portion of the hair follicle harbors matrix cells of the bulb, which differentiate into several cell lineages organized into concentric layers of the outer root sheath (ORS), inner root sheath (IRS) and the hair shaft. (A) and (B) modified from (Fuchs and Raghavan, 2002); (C) modified from (Cotsarelis, 2006).

1.1.2 The hair follicle

HFs cycle throughout life to provide steady replenishment of hair. The outermost layer of the HF, the outer root sheath (ORS), is continuous with the basal layer of the IFE and thus is in direct contact to the basement membrane separating the follicle from dermal cells (Fuchs, 2007). HFs cycle through phases of rest (telogen), regression (catagen) and growth (anagen) and thus are present in different states: during resting phases, only the permanent part of the HFs exists (s. 1.3.3) (Fig. 1.3). This permanent portion harbors the hair follicle stem cell (HFSC) niche called bulge, the upper isthmus, the junctional zone and the opening of the hair channel being connected to the IFE, the infundibulum (Blanpain and Fuchs, 2009). Proliferating keratinocytes are located in the outer root sheath (ORS) and the secondary hair germ of resting HFs. During HF growing phases, the cycling lower part of the HF is formed. Cycling follicles are lengthened and proliferating cells are located in the hair bulb at the HF

base. At the center of the hair bulb, the HF contains the dermal papilla, a region of condensed mesenchyme surrounded by matrix cells. Signaling from the dermal papilla regulates proliferation required to form the hair shaft (Fig.1.1, Fig. 1.3) (Rendl et al., 2005).

The follicle consists of multiple tissue layers that are characterized by their distinct morphology and program of differentiation. Terminal differentiation happens in the inner HF layers, such as the inner root sheath (IRS) towards the centrally localized, highly keratinized hair shaft (HS). The IRS comprises the Henle and Huxley layers and the cuticle. The companion layer is a single layered band of vertically orientated cells layers located between the ORS cells and the IRS and harbors unique adhesions required for HS attachment during growth (Panteleyev et al., 2001; Hanakawa et al., 2004). The morphogenetic differentiation of the single layers of the HF is reflected by the expression of a range of HF-specific keratins (Moll et al., 1982). For example, Keratin (K) 28 is a type I acidic keratin specifically expressed in all layers of the IRS as well as the medulla. In the adjacent companion layer, the type II Keratin (K) 75 is exclusively expressed (Langbein et al., 2006; Langbein et al., 2003).

1.1.3 The sebaceous gland

The sebaceous gland (SG) develops during late embryogenesis and arises from ORS keratinoctyes in the developing HF bulge region that differentiate into sebocytes (Niemann, 2009). The SG will remain attached to the follicle and secretes lipid-rich sebum into the hair canal that empties out to the skin surface. Comparatively little insight has been gained about SG function so far. However, SGs are important for barrier formation and protection against pathogens and environmental assaults (Schneider et al., 2009). Moreover, SG function has been recently shown to be required for skin homeostasis and function, e.g. hair development and immunity (Binczek et al., 2007; Blount et al., 2008; Zouboulis et al., 2008).

1.1.4 Embryonic epidermal development

In mice, the formation of a stratifying epidermis from a single-layered epithelium is executed in approximately 10 days, from embryonic day (E) E8.5 to E18.5 (Moll et al., 1982). Stratification starts by turning on the expression of K5 and K14. At E15.5, the epidermis forms the spinous and granular layer and starts to express the differentiation markers K10, K1 and loricrin (Koster and Roop, 2007). The switch between proliferating basal cells into differentiated suprabasal cells is not yet well understood, however one important mechanism proposed to drive epidermal stratification is the rotation of the plane of division in basal cells towards the suprabasal layers (asymmetric cell division), which peaks at around E16.5 (s. 1.4.1) (Lechler and Fuchs, 2005; Smart, 1970). Reciprocal signaling between dermis and epidermis coordinates the development of epidermal appendages (Watt, 2001). Primary HFs first appear from epidermal condensates by down-growth of basal cells at embryonic day (E)

13.5. Successive waves of secondary HF induction from E16 until postnatal day 1 precede primary HF morphogenesis. Placode formation is followed by HF organogenesis (hair germ and hair peg stage) and HF maturation (Schneider et al., 2009).

1.2 Stem cell compartments of the murine skin

In the murine epidermis, several stem/progenitor cell populations have been described that maintain turnover of epidermal compartments (Bickenbach et al., 1986; Cotsarelis et al., 1990; Morris et al., 2004; Blanpain et al., 2004). A stem cell (SC) may be defined as a multipotent cell that retains a high capacity to self renew throughout life and has been associated with infrequent cycling. Upon stimuli from the surrounding microenvironment (SC niche), SCs are able to produce daughter cells committed to differentiate into different lineages (Lajtha, 1979; Li and Clevers, 2010).

1.2.1 Stem cells in the interfollicular epidermis

The lifelong process of self-renewal in the IFE is driven by a high proliferative capacity of progenitor cells in the basal layer of the IFE maintaining the balance between proliferation and differentiation (Kaur, 2006; Levy et al., 2005). Indeed, slow-cycling cells have been found in the IFE (Potten, 1974; Braun et al., 2003). Whereas human IFE progenitors are relatively well characterized on the molecular level, e.g. by differential expression of β1 integrin or Desmoglein3 (Jones et al., 2007), the spatial localization and molecular identity of murine IFE progenitor cells is not yet clearly defined (Jaks et al., 2010). Additionally, niche identity of IFE progenitor cells has still not been determined (Jones and Wagers, 2008). In the IFE, several mediators of IFE progenitor cell determination, maintenance and proliferative potential, such as Rac1, p63 and c-Myc, have been defined (Arnold and Watt, 2001; Castilho et al., 2007; Senoo et al., 2007).

1.2.2. Stem cells in the hair follicle

Recently, several studies in the adult HF uncovered a collection of diverse and dynamic progenitor cell populations located in distinct regions of the HF (Jaks et al., 2010).

1.2.2.1 Stem cell markers of hair follicle bulge

HFs contain the most pluripotent and best-characterized SC population of the epidermis. These SCs reside in a discrete microenvironment called bulge region, a contiguous part of the ORS forming a niche, which is histologically visible after HF morphogenesis (3 weeks of life) (Nowak et al., 2008; Cotsarelis et al., 1990). Progeny isolated from a single bulge HFSC can generate all epidermal lineages (IFE, HF, SG) when engrafted onto the back of immunocompromised (*Nude)* mice. In addition, bulge HFSCs show enhanced colony-forming capacity in cell culture (Blanpain et al., 2004). Keratinocytes residing in the bulge are quiescent, as identified by their ability to retain labeled nucleotides (^{3}H-thymidine and 5-

bromo-2-deoxyuridine) over long periods of time (Cotsarelis et al., 1990; Bickenbach et al., 1986). The contribution of bulge cells to epidermal regeneration has been *in vivo* examined by a series of lineage-tracing experiments revealing that bulge HFSCs do regenerate the whole HF under homeostatic conditions (Morris et al., 2004b; Greco et al., 2009; Jaks et al., 2008; Petersson et al., 2011; Zhang et al., 2010). Bulge SCs are activated at the start of each hair cycle to generate the lower non-permanent part of HFs under homeostatic conditions (s. 1.3.2) (Zhang et al., 2009; Morris et al., 2004b). Moreover, these cells continuously contribute to the turnover of the SG (Petersson et al., 2011) and can be induced to proliferate upon wounding or challenge (TPA treatment) to provide cells for HF regeneration and repair of the epidermis (Ito et al., 2005; Cotsarelis et al., 1990; Morris and Potten, 1999). Bulge SCs have been well characterized at the molecular marker level. Transcriptional profiling revealed that bulge HFSCs express the surface markers CD34 and Keratin 15 (K15) as well as the transcription factors Sox9 (SRY box9), Tcf3 (T-cell factor 3) and NFATc1 (Nuclear factor of activated T-cells, cytoplasmic1) (Cotsarelis et al., 1990; Tumbar et al., 2004; Morris et al., 2004a; Horsley et al., 2008) (Fig.1.2). So far, CD34 is the most specific bulge SC marker and an important tool for bulge HFSC isolation. CD34 positive cells are multipotent and highly clonogenic (Blanpain et al., 2004). CD34 itself is important for HFSC activation and tumorigenesis (Trempus et al., 2007). Genetic targeting of the bulge by a truncated version of the K15 promotor demonstrated that K15 positive cell populations were competent to regenerate the entire HF (Morris et al., 2004a).

Recently, a population of Lgr5 (Leucin-rich G protein-coupled receptor 5) expressing cells has been demonstrated to have SC properties *in vivo*. Lgr5 positive cells are located in the lower bulge, in the secondary germ of telogen HFs and in the lower ORS of anagen HFs. Interestingly, these cells are actively cycling, supporting the idea of coexisting quiescent and proliferative SC populations in the bulge SC niche (Jaks et al., 2008). Notably, the bulge region is also the niche for melanocyte SCs, the melanoblasts. Differentiating melanocytes migrate from the bulge region to the hair bulb where they supply melanin to the hair-building keratinocytes (Trempus et al., 2007).

1.2.2.2 Progenitor cells of the isthmus/infundibulum

Additionally, progenitor cell populations residing above the HF bulge have been identified, which do not express bulge SC markers as e.g. CD34 and K15. For example, highly clonogenic cells reside in the upper isthmus region, express the thymic SC marker Plet1 (glycoylphosphatidylinositol-anchored protein1) and are recognized by the MTS24 antibody (Depreter et al., 2008). Plet1 is expressed in differentiated keratinocytes of the ORS, the companion layer and the SG duct (Raymond et al., 2010). Additionally, keratinocytes of the HF junctional zone above the MTS24 positive region express the transmembrane protein

Lrig1 (leucin-rich repeats and immunoglobulin-like domain protein 1). MTS24/Plet1 and Lrig1 positive cells are also able to generate adult epidermal lineages in skin reconstitution assays (Nijhof et al., 2006; Jensen et al., 2009). During skin homeostasis, Lrig1 positive SCs are rather bipotent, replenishing IFE and SG, but not HF lineages (K. B. Jensen u. a. 2009). Finally, a primitive SC pool has been localized to the central isthmus of adult HFs. This population is characterized by Lgr6 expression, a protein closely related to Lgr5. Embryonic Lgr6 positive cells have been shown to be able to establish all parts of the epidermis. In adult tissue, Lgr6 positive cells mainly contribute to the generation of the IFE and the SG, while their role in follicle lineages reduces with age (Snippert et al., 2010). Also the SG contains a small number of progenitors, producing proliferative progeny that differentiates into lipid-filled sebocytes. The small number of progenitors expresses the transcriptional repressor Blimp1 and resides near the base of the SG (Fuchs and Horsley, 2008).

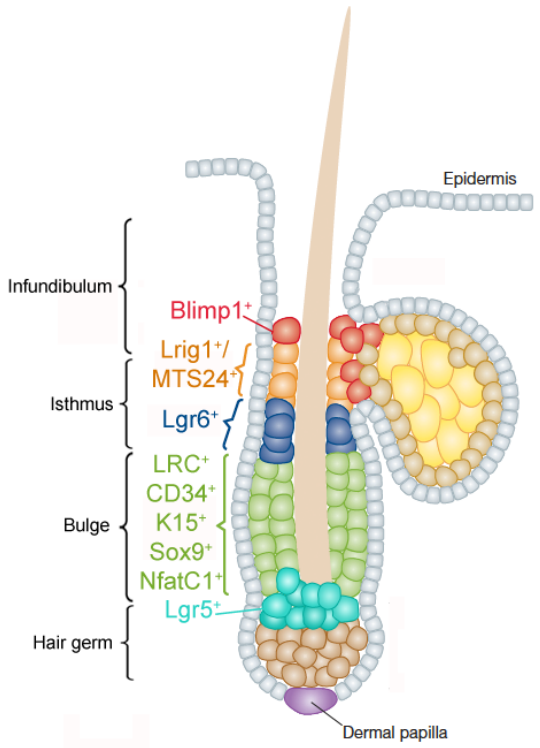

Figure 1. 2: Schematical representation of progenitor cell populations in the telogen HF

Several progenitor populations are depicted by their different gene/protein expression or promotor activity. Lgr5: turquois (hair germ and bulge); NfatC1, Sox9, K15, CD34, Label retaining cells (LRC): green (bulge); Lgr6: blue (isthmus); Lrig1, Plet1/MTS24: orange (upper isthmus/infundibulum); Blimp1: red (infundibulum). Modified from (Horsley, 2011).

The successive discovery of the above-mentioned progenitor populations of the bulge and isthmus/infundibulum region provokes the question for the significance of the single populations and their cell-autonomous role under homeostatic conditions. Moreover, how do these different subpopulations of progenitor cells relate to each other? A recent study

demonstrated that HF bulge SCs are able to give rise to keratinocytes of other progenitor cell compartments of the pilosebaceous unit, suggesting a hierarchy of competent multipotent keratinocytes. For example, progeny of slow-cycling bulge cells are able to migrate through the Lgr6 and Lrig1 positive compartments up to the SG (Zhang et al., 2009; Petersson et al., 2011). However, the underlying signaling networks regulating and maintaining these different progenitor cell identities and their exact hierarchy are still subject of investigation.

1.3 Epidermal homeostasis

The major function of the epidermis is to provide a functional barrier against outside influences. Therefore, an essential characteristic is its ability of life long self-renewal to maintain its homeostasis throughout postnatal life (Halprin, 1972).

1.3.1 Regeneration of the IFE

At present two conflicting models have been postulated on how the IFE is maintained during adult life. The epidermal proliferative unit (EPU) model proposes that the IFE is organized into columns maintained by a single SC surrounded by transit amplifying (TA) cells (Potten, 1974). In line with this model, slow cycling, label-retaining cells are dispersed among the basal layer, positioned within units of cells corresponding to these slow cycling cells (Mackenzie and Bickenbach, 1985; Morris et al., 1985). In contrast, recent clonal analysis of genetically labeled basal proliferating cells revealed insight into behavior of interfollicular progenitors of tail or ear IFE. These data suggest, that single populations of resident and more committed progenitors with random fate, which share neither SC nor TA characteristics, maintain the IFE (Clayton et al., 2007; Doupé et al., 2010).

1.3.2 Cyclic regeneration of the HF

The hair coat requires a constant supply of new hairs throughout an animals life requiring that murine HFs undergo cyclic HF renewal. To produce new hairs, existing follicles undergo cycles of growth (anagen), regression (catagen), and rest (telogen) (Alonso and Fuchs, 2006). After morphogenesis, HFs enter catagen, a phase characterized by regression of the lower part of the HF. During catagen, the lower non-permanent “cycling” portion of the HF regresses in a process that includes apoptosis of the epithelial cells of the hair bulb and the ORS. Next, the HFs will enter a phase of rest (telogen), in which HFs are inactive and bulge SCs are in a quiescent state. During late telogen, some bulge and hair germ cells are activated by signals from the dermal papilla (e.g. FGF and BMP inhibitors) in a two-step mechanism to initiate the HF growth phase. First, hair germ cells are mobilized to migrate and proliferate towards the newly forming matrix to support hair growth. Next, these activated bulge cells will replenish hair germ cells (Greco et al., 2009; Zhang et al., 2009). The following growth (anagen) phase is characterized by lengthening of the HF, pushing of the dermal papilla downwards from the bulge and proliferation of the cells in the HF bulb.

Moreover, bulge progenitors proliferate to refill the hair germ and the bulge compartment. During each anagen, the HF produces an entire new hair shaft and the new HF forms adjacent to the old (club) hair that eventually will be shed (Milner et al., 2002). Since the first two hair cycles are well defined in murine skin and synchronized, they provide an excellent model to study SC activation and quiescence.

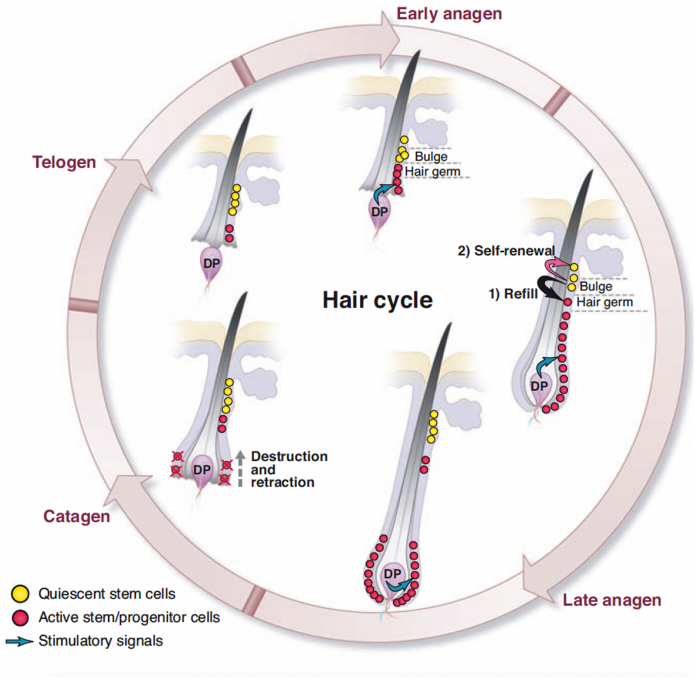

Figure 1. 3: The murine hair cycle

During catagen, the cycling part of the HF undergoes apoptosis. In telogen, HF progenitors of the hair germ and bulge are quiescent. At the end of telogen, bulge SCs and hair germ cells are activated by signals from the dermal papilla. During anagen, bulge SC proliferate to refill the hair germ and the bulge compartment and keratinocytes of the hair bulb proliferate to fuel cells into the differentiating HF layers. Modified from (Li and Clevers, 2010).

1.3.4 Signaling pathways in hair follicle regeneration

Self-renewal of epidermal SCs must be tightly controlled to ensure life-long epidermal homeostasis. At present, the Wnt/β-catenin and the BMP signaling pathways are among the main signaling pathways that regulate SC activation, quiescence and cell type specification (Yang and Peng, 2010) and will therefore be discussed in more detail. FGF signaling, Hedgehog and Notch signaling are additional pathways reported to be essential for epidermal regeneration and SC homeostasis (Watt and Jensen, 2009).

1.3.4.1 Wnt/β-catenin signaling

The Wnt/β-catenin signaling pathway is crucial for HFs to enter anagen phases of the hair cycle. In the absence of a Wnt signal, β-catenin is phosphorylated and targeted for proteasomal degradation by a destruction complex. Binding of Wnt to its receptor inactivates the destruction complex resulting in β-catenin stabilization and translocation to the nucleus to bind to TCF/Lef transcription factors and induce the expression of target genes. Wnt/β-catenin signaling is crucial to induce epithelial cells to adopt HF fate and necessary for placode formation during embryogenesis (Huelsken et al., 2001; DasGupta and Fuchs, 1999). Quiescence of HFSCs is achieved by Wnt-inhibitory signals from the dermal papilla (Lo Celso et al., 2004; Gat et al., 1998). When β-catenin is artificially elevated in adult HFs, this can stimulate SC proliferation and bulge expansion and instructs resting HFs to enter anagen. Expression of constitutively active β-catenin induces *de novo* ectopic HF morphogenesis (Lo Celso et al., 2004; Lowry et al., 2005; Baker et al., 2010). Fate decisions of matrix cells are dependent on Wnt/β-catenin-mediated Lef1 (lymphoid-enhancer factor1) signaling determining lineage commitment towards HF differentiation (Merrill et al., 2001). Hence, Wnt/β-catenin signaling controls HFSC specification, activation and HF differentiation.

1.3.4.2 TGF-β/BMP signaling

The refractory stage of telogen is controlled by BMP signaling. BMPs are secreted signaling molecules, which bind to specific BMP receptors. The activity of BMPs is modulated by several antagonists and transmitted to the nucleus by the BMP-Smad or BMP-MAPK signaling pathways (Botchkarev and Sharov, 2004). Several loss of function studies demonstrated that BMP signaling in the SC niche is required for SC quiescence. Perturbed BMP signaling triggers activation of Wnt/β-catenin signaling in quiescent SCs and entry into anagen phase of the hair cycle (Kobielak et al., 2007; Yang et al., 2009b). The BMP pathway activates the SC-marker NfatC1, which in turn represses CDK4 (cyclin dependent kinase 4) and stimulates the expression of cell cycle inhibitors. During SC activation, BMP inhibitory signals from the DP lead to the inactivation of NfatC1 followed by cell cycle progression (Horsley et al., 2008).

1.3 Cell polarity

Cell polarity is defined as the unequal distribution of constituents (RNAs, lipids, proteins) within a cell thus producing asymmetry in structure and function. Cell polarity is critical for a variety of biological processes such as tissue morphogenesis, organelle positioning, signaling, cytoskeletal organization, directional cell migration and asymmetric cell division (Macara, 2004; Knoblich, 2008).

1.3.1 Molecular mediators of cell polarity

Polarity is established and maintained by the activity of a core set of polarity proteins that are highly conserved throughout *metazoa*. The first polarity proteins, the Par (partitioning-defective) proteins, were initially identified through their role in asymmetric cell division of the *C. elegans* zygote (Kemphues et al., 1988). The *PAR* genes encode various proteins ranging from adaptor proteins such as the PDZ domain containing proteins Par3 and Par6 to serine/threonine kinases like Par1 and Par4. Par3 and Par6 bind the serine/threonine kinase aPKC forming a dynamic complex (Suzuki and Ohno, 2006). Next to the Par3/Par6/aPKC complex, two additional protein complexes have been identified in *Drosophila* and demonstrated to be crucial for cell polarization: the Crumbs/Patj/Pals1/Lin7 and Scribble/Lgl/Dlg polarity complexes. To establish and maintain polarity, these complexes and proteins interact and mutually regulate each other's activity (Fig. 1.6A). An overview of the most important cell polarity proteins as well as the so far identified mammalian isoforms is presented in table 1 (Macara, 2004; Niessen and Niessen, 2010).

Table 1: Mediators of cell polarity

The original name in the organism they were first identified in and their most common mammalian name as well as the so far known function of the respective protein is shown. *: identified in *C. elegans*. ±: identified in *D. melanogaster*. ND: not determined. TM: transmembrane protein. h: human, m: mouse.

Original name	Mammalian name	Function
Partitioning-defective (Par)1*	MARK2 MARK1, 3, 4, 5?	Ser/Thr kinase
Par3*	Par3a (ASIP) Par3b	PDZ containg scaffold
Par4*	Lkb1	Ser/Thr kinase
Par5*	14-3-3 family (7 members, β, γ, ε, δ, σ, ζ,η)	phosphoserine/ threonine binding scaffold
Par6*	Par6a Par6b Par6c	PDZ containing scaffold
aPKC+	aPKCλ (m)/aPKCι (h) aPKCζ	Ser/Thr kinase
Lethal Giant Larvae (Lgl) #	Lgl1 (Hugl1) Lgl2	WD40 repeats containg scaffold
Scribble#	Scribble (Vartul, Crib1, LAP4)	LAP protein/scaffold

Original name	Mammalian name	Function
Disc Large (Dlg)#	Dlg1 (Sap97) Dlg2 (PSD-93) Dlg3 (SAP-102) Dlg4 (PSD95, SAP90) Dlg5	MAGUK protein/ scaffold
Crumbs (Crb)#	Crb1 (RP12, LCA8) Crb2 Crb3	TM protein/scaffold
Stardust (Std) #	Protein associated with Lin7 (Pals)1 (MMP5) Pals2 (MMP6, VAM-1, p55T) MMP 1-3, 7	MAGUK protein/ scaffold
dros.Pals1-associated tight junction protein (Patj)#	Patj Mup1	PDZ containing scaffold
Lin7*	Lin7A (Velis1, MALS-1) Lin7B (Velis2, MALS-2) Lin7C (Velis3, MALS-3)	PDZ containing scaffold

1.3.2 Asymmetric cell division

Cells can divide either symmetrically resulting in two daughter cells with similar fate or asymmetrically leading to differential daughter cell identities (Nelson, 2003). Organisms use this asymmetric cell division (ACD) to generate different cell types during development and under homeostatic conditions to replace cells that are turned-over. For example, a variety of SCs, also in mammals, use ACD to simultaneously self-renew and differentiate. ACD requires the polarization of two opposite domains within the cell, each of which associated with a different set of cell fate determinants and orientation of the mitotic spindle (Knoblich, 2008). One of the best-studied examples of asymmetric division occurs in *Drosophila* neuroblasts, progenitors of the central nervous system, which undergo multiple rounds of SC like divisions. Here, the initial polarization cue comes from the apical enrichment of the Par3/Par6/aPKC complex. However, the mechanism that positions Par3/Par6/aPKC asymmetrically is not yet well understood. Par3 recruits Cdc42 to the cortical neuroblast membrane resulting in polarized localization and at least partial activation of Par6/aPKC at the cortex. Active aPKC then phosphorylates Lgl, thereby dissociating it from the Par6/aPKC complex. This has two consequences, it allows for association of Par3 with Par6/aPKC

thereby coupling the complex to different downstream substrates, such as the fate determinant Numb. Secondly, it dissociates Lgl from the apical neuroblast cortex resulting in enrichment of Lgl at the basal side, which then recruits fate determinants (Miranda, Numb, Brat, Prospero, Pon) crucial for turning on the more differentiated ganglion mother cell fate in this daughter cell (Wirtz-Peitz et al., 2008; Atwood and Prehoda, 2009). Hence, apical aPKC localization is essential for asymmetric localization of cell fate determinants. Par3 couples cell polarity to spindle orientation by binding the adaptor protein Inscuteable (Insc). Insc then recruits a protein complex consisting of the heterotrimeric Gα1 (G protein α1-subunit), PINS (partner of Inscuteable) and MUD (Microtubule-associated dynein binding protein), which provides attachment sites for astral microtubules (Fig. 1.4) (Knoblich, 2010).

Asymmetric division is also observed in diverse mammalian systems, such as T-cells, neuronal progenitor cells in the developing brain and the epidermis (Fig. 1.5). Although the underlying mechanisms are less clear than in *Drosophila*, the same players, such as aPKC or Par3, have been implicated in the regulation of mammalian ACDs (Plusa et al., 2005; Hao et al., 2010; Zheng et al., 2010).

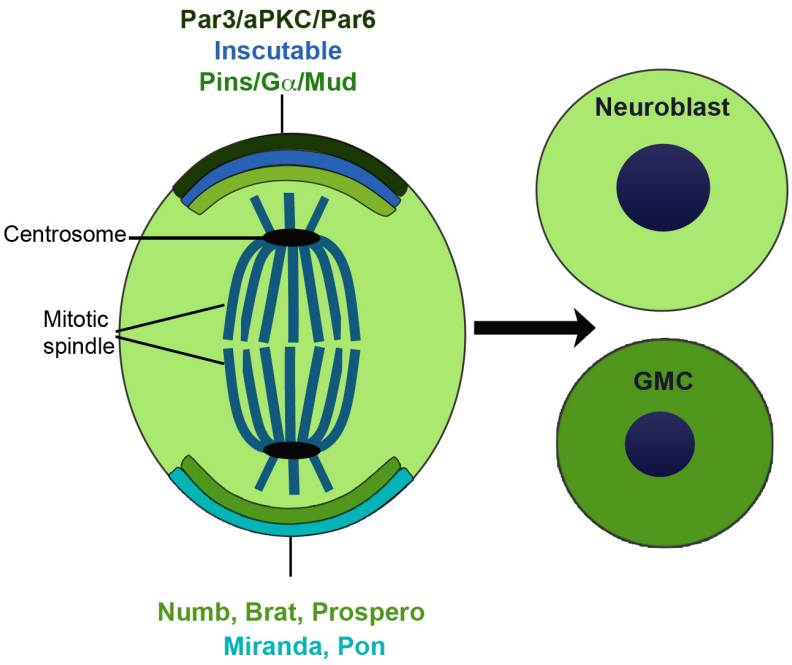

Figure 1. 4: Asymmetric cell division in *Drosophila* neuroblasts

Neuroblasts divide asymmetrically to generate two daughter cells of different cell fate, a ganglion mother cell (GMC) and a neuroblast progenitor cell. Distribution of components important for polarity establishment, spindle positioning and cell fate determination are illustrated. Apically localized polarity proteins (Par3/Par6/aPKC) bind the spindle-positioning complex (Pins, Gai, Mud) via Inscuteable. Next to Miranda and Pon (Partner of Numb), the cell fate determinants Numb, Brain tumour (Brat) and Prospero are localized to the basal cell cortex.

1.3.3 Apico-basal polarity

Simple epithelial cells polarize to establish an apical and a basolateral membrane domain, with distinct structural and functional characteristics. An apical junctional complex, consisting of tight junctions, adherens junctions and desmosomes, separates these membrane domains. This form of cell polarity is essential for the formation of a protective barrier and for vectorial functions, such as directed secretion of components. The establishment of apico-basolateral polarity in simple mammalian epithelial cells is achieved by complex agonistic and antagonistic interactions of cell polarity protein complexes that allow spatial targeting of polarity complexes to different domains within the cell (Fig. 1.6A) (St Johnston and Sanson, 2011).

1.4 Cell polarity in the mammalian skin

The skin is a highly polarized tissue and thus an excellent model system to study a range of processes that require cell polarization. These are for example the formation and maintenance of the self-renewing epidermis or the behaviour of different populations of progenitor cells that drive self-renewal. Thus, using skin several open questions on cell polarity can be addressed, such as e.g. how a life long self-renewing tissue regulates the balance between asymmetric and symmetric divisions under homeostatic and regenerating conditions (s. 1.4.1) or how apico-basolateral polarity is established over multiple layers (s. 1.4.2) (Niessen and Niessen, 2010).

1.4.1. Asymmetric cell division in epidermal morphogenesis and homeostasis

In the epidermis, a rotation of the plane of cell cleavage in basal dividing cells is observed concurrent with the onset of stratification from E16.5 on. This results in apical/basal divisions (asymmetric) as opposed to basal/basal (symmetric) cell divisions (Fig. 1.4A) (Smart, 1970; Lechler and Fuchs, 2005). Lechler and Fuchs reported an apical localization of the polarity proteins LGN and Par3 in asymmetrically dividing cells, which is lost when ACDs are perturbed. Follow-up studies demonstrated that after ACD, the daughter remains K14 positive whereas the suprabasal daughter turns on the suprabasal marker K10, strongly suggesting that asymmetric divisions indeed promote differentiation and cell fate changes during the stratification process (Poulson and Lechler, 2010). Furthermore, an *in vivo* lentiviral knockdown system provided additional direct evidence that ACDs drive differentiation. Interfering with the molecular machinery that determines spindle positioning in asymmetrically dividing *Drosophila* neuroblasts, e.g. the mammalian PINS homologue LGN or the MUD homologue NuMA, resulted in a strong reduction of asymmetric division concomitant with an increase in symmetric divisions (Fig.1.4B). These changes were accompanied by a thinner, less differentiated epidermis with less suprabasal layers thus coupling key regulators of spindle positioning to differentiation in mammalian epithelial cells

(Williams et al., 2011). These recent findings suggest that the core machinery that control spindle orientation during asymmetric divisions in *Drosophila* is conserved in the mammalian epidermis.

Unlike in *Drosophila* neuroblasts, the decision to divide either symmetrically or asymmetrically is not predetermined cell-autonomously in epidermal progenitors (Poulson and Lechler, 2010), indicating that the microenvironment might play an important role in the overall outcome of divisions. In line with this, epidermal loss of cell adhesive cues such as β1-integrins or the adherens junction molecule α-catenin, resulted in random spindle orientation and altered differentiation (Lechler and Fuchs, 2005).

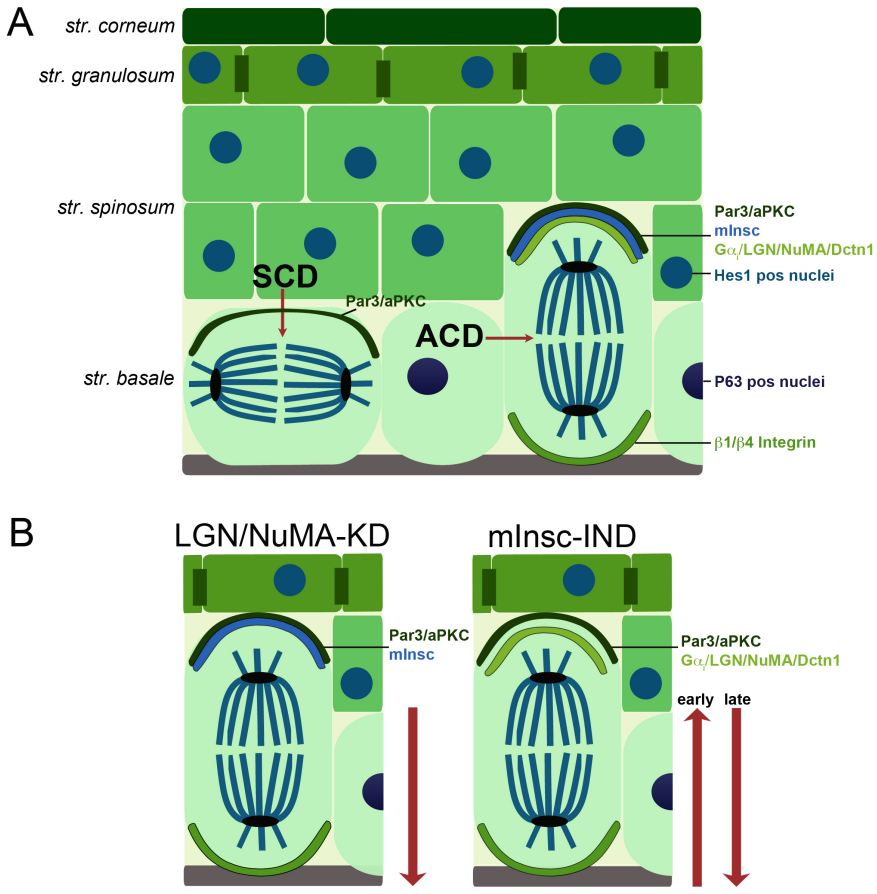

Figure 1. 5: Asymmetric cell division in embryonic murine epidermis

(A) Asymmetric cell division (ACD) in the E16.5 IFE. ACDs produce one basal and one suprabasal cell, whereas symmetric cell divisions (SCD) result in two basal daughter cells. The mammalian homologues of mediators of ACD in *Drosophila* (aPKC/Par3, mInsc, Ga1/LGN/NuMA/Dcnt1), basal P63 expression and suprabasal activity of the Notch signaling pathway (indicated by Hes1 pos nuclei) are crucial for the regulation of this process. (B) Effects of deletion/induction of molecular mediators on the ratio of ACD vs. SCD. Basal cells were biased towards symmetric spindle orientation after transfection with shRNAs targeting either LGN or NuMA (Williams et al., 2011). Forced expression of mInscuteable induces increased ACD in the epidermis shortly after induction (early), whereas 3 days after induction, this effect is reversed (later) (Poulson and Lechler, 2010). KO: Knock-out, IND: inducible, KD: Knock-down.

It has not yet been elucidated whether asymmetric divisions regulate cell fate decisions of SCs in adult IFE and HFs. Bulge cells represent a heterogenous population with regard to their proliferative features (Sotiropoulou et al., 2008; Tumbar et al., 2004), however divisions perpendicular to the basement membrane have been reported in HFs (Blanpain and Fuchs, 2009; Zhang et al., 2009). Lineage tracing experiments in the HF bulge suggest that symmetric divisions during anagen replenish bulge SCs cells, whereas more committed progenitors located in the hair germ of late telogen HFs divide perpendicular to the basement membrane (Fig. 1.5) (Zhang et al., 2010). So far, tracing-studies of the divisions have not yet directly revealed whether ACDs in regard to the basement membrane in hair germ SCs indeed result in differential cell fate (Zhang et al., 2010). Nevertheless, indirect evidence from RNA expression microarrays suggests that dividing SCs in the bulge retain their SC signature, whereas more committed progenitors of the hair germ change their expression profile towards more differentiated cells already after one division (Zhang et al., 2009). It will be interesting to further decipher which molecular and cellular mechanisms govern the regulation of ACD/SCD and cell fate decisions in HFs. Perpendicular spindles have also been observed in the hair bulb (Blanpain and Fuchs, 2009), suggesting that these divisions may regulate the differentiation of the various HF layers (Fig. 1.5) (Blanpain and Fuchs, 2009).

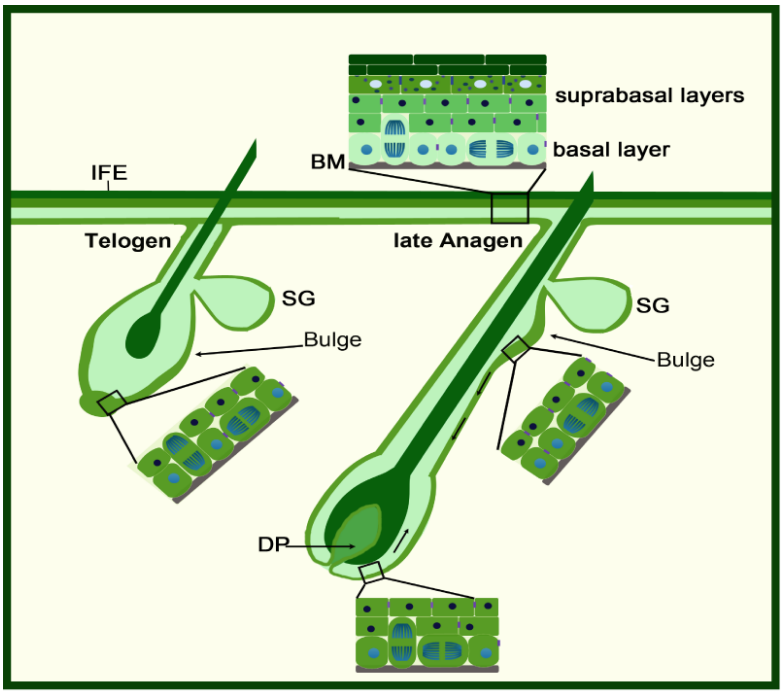

Figure 1. 6: Asymmetric cell division in different epidermal compartments

Next to ACD in the IFE (Fig. 1.4A), ACD is believed to take place when HFSCs move outwards the bulge region to differentiate, whereas inside the bulge, SCDs serve to replenish the SC pool during anagen phases of the hair cycle (Zhang et al., 2010). ACD are also observed in the bulb region of the HF. SCDs are oriented in parallel to the basal layer, ACD perpendicular to the basal layer. IFE: interfolliclular epidermis. BM: basement membrane. SG: sebaceous gland. DP: dermal papilla.

1.4.2 Apico-basal polarity in the skin

The stratifying epidermis is not a classically polarized epithelium, in which tight junctions separate basolateral and apical membrane domains. Instead, the epidermis establishes polarity along the basal to apical axis of the tissue, with the *str. granulosum* forming the viable apical boundary. Interestingly, functional tight junctions are found in the *str. granulosum* and these may, as in simple epithelia, serve as a fence necessary for "apical" protein and lipid targeting. The mechanisms that regulate the formation of apico-basolateral tissue polarity in a stratifying epithelium are largely unknown. If similar mechanisms are in place as in simple epithelia, the mutual antagonistic actions of polarity complexes have to be established over several cell layers. A relatively simple system could consist of counter-gradients of mutually inhibiting complexes over the basal-apical axis of the epidermis (Niessen and Niessen, 2010; Goldstein and Macara, 2007).

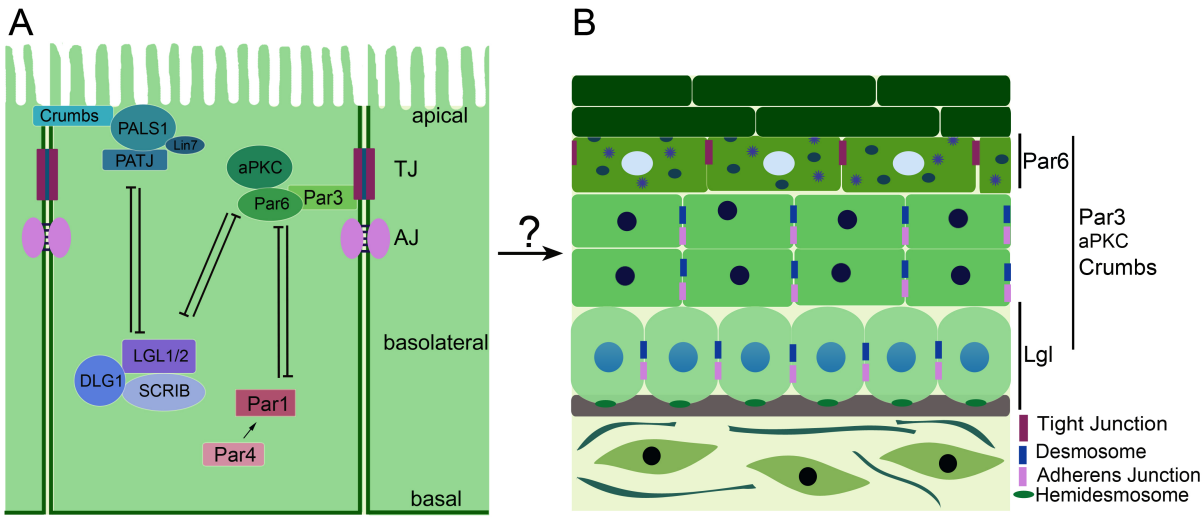

Figure 1. 7: Similarities and differences of polarity in simple vs. stratifying epithelia

(A) Apico-basal polarity in simple epithelia. The apical junctional complex consisting of tight junctions (TJ) and adherens junctions (AJ) forms a border to establish apico-basal polarity. Mutual interactions of Par3/Par6/aPKC with other polarity complexes/ proteins regulate apico-basal polarity and barrier formation in simple epithelia. (B) Polarity in the epidermis. In contrast to simple epithelia, the epidermis has no apical vs. basolateral membrane domain but displays apico-basal polarity over the tissue. This is reflected in differential expression/localization of polarity and differentiation markers and adhesive junctions. Moreover, lamellar bodies (dark green) and keratohyalin granules (purple asterisks) are targeted towards the *str. corneum*. Indicated is the localization pattern of different cell polarity proteins and adhesion complexes.

1.5 The PKC family of serine/threonine kinases

This thesis focuses on the role of aPKCλ, a polarity protein, in epidermal homeostasis and cell fate decisions. This protein is a member of the PKC family of serine/threonine kinases. PKCs belong to the AGC (cAMP-dependent protein kinase/PKG/PKC) protein kinases family, which is important for controlling key cellular events by phosphorylation of a range of substrates on serine and threonine amino acids. This phosphorylation modifies the activity of

its substrates, including receptors, enzymes, cytoskeletal proteins and transcription factors, thereby regulating cell proliferation, differentiation, survival and death. The PKC family comprises at present at least 11 members. These enzymes have been categorized into three subfamilies, conventional (α,βI, βII, γ), novel (δ,ε,θ, η) and atypical (ζI, ζII, ζ`,ι/λ,) PKCs. Specific cofactor requirement, tissue distribution and cellular compartmentalization suggest differential functions for each isoform (Nishizuka, 1995; Rosse et al., 2010). All PKCs consists of a C-terminal catalytical and a N-terminal regulatory domain, with the catalytic domain being highly conserved throughout the PKC family. Each member also contains a pseudosubstrate domain located in the regulatory region, which is able to bind to the catalytic domain thus creating a closed confirmation that prevents activation and association of the catalytic region with its substrates (House and Kemp, 1987). Specific activator proteins that differ between subfamilies relieve the pseudosubstrate-domain mediated inhibition. Many actions of PKCs require translocation form the cytosol to the membrane. In accordance, all family members require phosphatidylserine, a component of the phospholipid bilayer, for their activation. Classical cPKCs need DAG or phorbol esters for activation and are sensitive for Ca^{2+}. Novel nPKCs are Ca^{2+} independent but still require DAG or phorpbol esters. aPKCs are independent of phorbol esters and lack Ca^{2+} and DAG binding sites (Fig. 1.7) (s. 1.5.2.3) (Chauhan et al., 1990).

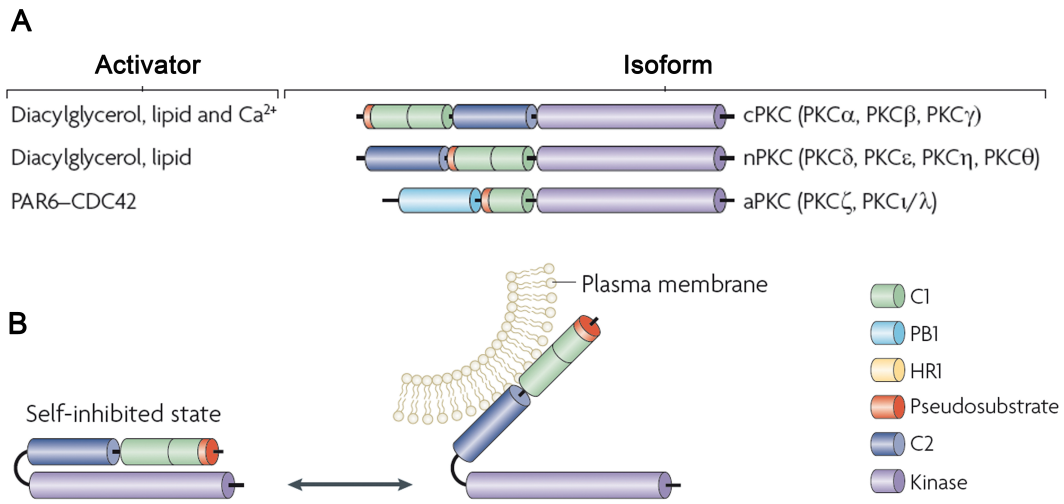

Figure 1. 8: The protein kinase C family

(A) Schematical drawing of the domain structure of the PKC family members. Mammalian PKC family members can be divided into three subgroups (cPKCs, nPKCs and aPKCs) based on the organization of their regulatory domain. (B) The pseudosubstrate domain of a cPKC binds to the substrate-binding pocket in the kinase domain, thus leading to self-inhibition. Autoinhibition is relieved by binding of the regulatoy domain to the plasma membrane. Modified from (Rosse et al., 2010)

1.5.2 atypical PKCs

The atypical PKCs differ structurally from their family members, as they lack DAG/phorbol binding sites and the tandem like cystein-rich repeats (C2) of classical and novel PKCs. Instead, their relatively short N-terminal regulatory region is characterized by the presence of a single cystein-rich region (C1, zinc-finger) responsible for lipid binding and the pseudosubstrate domain. Additionally, aPKCs harbor a N-terminal Phox/Bemp1 dimerization/ oligomerization (PB1) domain, through which they can bind adapter and activator proteins (Fig. 1.7) (Hirano et al., 2004; Suzuki et al., 2003). The two highly related mammalian aPKC isoforms, aPKCι/λ and aPKCζ are encoded by different genes, *PKCI* and *PKCZ,* and were cloned in the early nineties (Ono et al., 1989; Selbie et al., 1993). Mouse aPKCλ and human aPKCι are orthologues with 98% overall aminoacid sequence identity and are therefore referred to as aPKCι/λ. aPKCι/λ and aPKCζ share 72 % sequence identity, with the most homologous region (app. 86 %) in the kinase (catalytic) domain (Nishizuka, 1995). In addition to the two most-studied aPKC isoforms, a short isoform of aPKCζ (aPKCζ`) was detected in rat brains. Expression of this isoform under the control of a brain-specific promotor results in a short constitutive-active protein lacking the regulatory region (Marshall et al., 2000). Furthermore, a distinct *PKCZ* gene, *PKCZII* has been described. It is highly homologous to *PKCZ*, but frame shifted, thus leading to the expression of a short aPKCζII isoform, which lacks the catalytic domain but is still able to interact with binding partners, as for example Par6. This isoform has been reported to inhibit tight junction formation *in vitro* (Parkinson et al., 2004). Despite their similar structure, differences in the expression of aPKCλ vs. aPKCζ transcripts have been reported. For example, the two isoforms show non-overlapping expression patterns during embryogenesis and in the central nervous system or the skin of adult mice (Oster et al., 2004; Kovac et al., 2007; Helfrich et al., 2007), strongly suggesting isoform-specific functions in these tissues.

1.5.2.1 Substrates/binding partners of aPKC

aPKCs have been implicated in a range of functions as for example cell polarity, metabolic pathways and immunity (s. 1.6). To exert these diverse roles, aPKCs interact with a plethora of proteins, which act both upstream or downstream of aPKCs (Rosse et al., 2010). Most aPKC substrates have been identified through candidate approaches by identification of aPKC phosphorylation consensus sites (S/T-X-K/R) (Djiane et al., 2005). The physiological relevance of specific interactions is still largely unknown. Moreover, how far the aPKCs have isoform-specific substrates and how conserved the binding to specific substrates is throughout species is still under investigation. An overview of the most relevant binding partners and substrates is presented in table 2.

Table 2: Substrates and binding partners of aPKC

Table shows name of the binding partner (molecule), the mammalian aPKC isoform it was reported to be phosphorylated by (isoform), the process the interaction was shown to play a role in (process), the organism the interaction was discovered in (organism), whether the binding partner is directly phosphorylated by aPKCs (+) (substrate), and the original work where binding was first described (Reference). dm= *Drosophila melanogaster*, mcc= mammalian cell culture, xl= *Xenopus laevis*, rn= *Rattus norvegus*, hs= *homo sapiens*.

Molecule	isoform	Process	Organism	Substrate	Reference
Lgl1/2	aPKCλ; aPKCζ	Cell polarity	dm;mcc	+	Yamanaka, T. et al., 2003, Curr. Biol., Plant, P. et al., 2003, Nature
Pins/LGN	aPKCλ; aPKCζ	Cell polarity	mcc	+	Hao, Y. et al., 2010, Cell
Par1	aPKCλ; aPKCζ	Cell polarity	mcc; xl	+	Suzuki, A., 2004, Curr. Biol., Kusakabe and Nishida, 2004, EMBO
Par3	aPKCζ	Cell polarity	rn	+	Li, D. et al., 2000, Nature Cell Biology
Par6	aPKCλ; aPKCζ	Cell polarity	mcc		Joberty, G. et al., 2000, Nat. Cell Biol.
Cdc42	aPKCλ; aPKCζ	Cell polarity	hs;mm;mmc; rn		Joberty, G. et al., 2000, Nat. Cell Biol., Qiu, R.-G. et al., 2000, Curr. Biol.
Rac1		Cell polarity	mm, rn, hs		Qiu, R.-G. et al., 2000, Curr. Biol.
ZO1	aPKCλ; aPKCζ	Cell polarity/ Junction formation	mcc	+	Nunbhakdi-Craig, V. et al., 2002, JCB
Crumbs	aPKCζ	Cell polarity/ Junction formation	mcc; dm	+	Sotillos, S. et al., 2004, JCB
Dsh		Cell polarity/ Planar polarity	rn		Zhang, X. et al., 2007, Nat. Cell Biol.
Frz1	aPKCζ	Cell polarity/ Planar polarity	dm	+	Djiane, A. et al., 2005, Cell
Dap160		Vesicle traffiking	dm		Chabu and Doe, 2008, Development
Numb	aPKCζ	Cell polarity/ACD	hs	+	Smith, C. et al., 2001, EMBO
LIN-5/NuMA		Cell polarity/ACD	ce	+	Galli, M. et al., 2011, Nat. Cell Biol.
Miranda		Cell polarity/ACD	dm	+	Atwood and Prehoda, 2009, Curr. Biol.
Zif		Cell polarity/ACD	dm	+	Chang K. et al., 2010, Dev Cell
Par4/LKB1	aPKCζ	Cell polarity/NfκB	mm		Deepa, S. et al., 2011, Mol. Cell. Endocrinol.
Ajuba	aPKCζ	Apoptosis/NfκB	mcc	+	Feng and Longmore, 2005, Mol. Cell. Biol.
IRAK	aPKCλ; aPKCζ	Apoptosis/NfκB	hs		Mamidipudi, V. et al., 2004, JBC
RelA/P65		Apoptosis/NfκB	mm	+	Duran A. et al., 2003. EMBO
P62		Apoptosis/NfκB	hs		Huang, H-C, et al., 2009, Mol. Carcinog.
BAD	aPKCλ; aPKCζ	Apoptosis	hs		Desai, S. et al., 2011, Biochim Biophys Acta
IRS-1, IRS-3, IRS-4	aPKCζ	Insulin signaling	mm	+	Lee, S. et al., 2008, Endocrinology
Akt1	aPKCζ	Insulin signaling	mm		Powell, D. et al., 2003, Mol. Cell. Biol.
Vamp2	aPKCζ	Insulin signaling	mm	+	Braiman, L. et al., 2001,Mol. Cell. Biol.
MEK5		EGF signaling	hs		Diaz-Meco and Moscat, 2001, Mol. Cell. Biol.
RKIP	aPKCζ	EGF signaling	rn	+	Corbit, K. et al., 2003,JBC

1.5.2.2 Regulation and activation of aPKCs

As aforementioned, membrane-interaction of the regulatory domain of aPKC initiates the release of the pseudosubstrate site from the kinase domain leading to activation. The sphingholipid ceramide directly binds and activates aPKCζ, recruiting it to structured microdomains (Fox et al., 2007; Wang et al., 2009). An important mechanism to regulate aPKC activity is the binding of different adaptors/scaffold proteins to achieve functional specificity during cell signaling. For example, binding of the adaptor Par6 is central for the control of cell polarity, whereas binding of P62 is critical for NfκB activation. (Moscat and Diaz-Meco, 2000). Moreover, aPKCs themselves are subject to phosphorylation. For example, PDK1 (Phosphoinositise-dependent kinase 1) was found to phosphorylate and activate aPKCζ *in vitro* in a phosphatidylinositol- 3,4,5-$(PO_4)_3$ (PIP3) dependent manner. Here, PDK1 phsophorylates Thr410 in the so-called activation loop of aPKCζ/λ (Nakanishi et al., 1993; Akimoto et al., 1996). Additionally, autophosphorylation at T560 is required for maximal activation (Standaert et al., 2001). In summary, a complex network of fine-tuned mediators maintains regulation and activation of aPKCs.

1.6 Mammalian functions of aPKC

1.6.1. Diverse roles of aPKC

Whereas overexpression studies have shed light on overlapping roles of both aPKC isoforms *in vitro* (Rosse et al., 2010), is still not clear if the two main aPKC isoforms have partially overlapping and/or separate functions *in vivo*. The effort to assign unique functions to the two major aPKC isoforms is further hampered by the lack of isoform specific antibodies. *In vivo* loss of function studies have recently started to shed light on the specific functions of aPKCι/λ vs. aPKCζ. aPKCζ knock-out (aPKCζ$^{-/-}$) mice are born in mendelian ratios and viable, but display alterations in the development of secondary lymphoid organs and a reduced percentage of B cells. Further analysis of these mice revealed that aPKCζ is crucial for T-cell (Th2-cell) activation, IL4 secretion and NfκB-dependent gene transcription (Martin et al., 2002; Leitges et al., 2001). aPKC seems to control the NfκB pathway on two levels: First, aPKCζ phosphorylates and activates IKK *in vivo* in lung tissue and transformed prostate cancer cell lines (Leitges et al., 2001; Win and Acevedo-Duncan, 2008). Secondly, aPKCζ can phosphorylate RelA (P65), a subunit of the NfκB complex, thus directly facilitating NfκB-target gene transcription (Leitges et al., 2001; Duran et al., 2003; Anrather et al., 1999).

In contrast to the relatively mild aPKCζ$^{-/-}$ phenotype, genetic inactivation of aPKCλ in mice results in embryonic lethality at early stages (E9.5) with abnormalities seen as early as E6.5. This was attributed to defects in cell polarity (Soloff et al., 2004). The aPKCλ$^{-/-}$ phenotype is

in agreement with observations in lower organisms, in which functional inactivation of aPKC orthologues also results in early lethality. For example, in the absence of the *C.elegans* aPKC orthologue PKC3, establishment of embryonic polarity and first asymmetric divisions are disrupted (Tabuse et al., 1998). *Drosophila* aPKC regulates ooctyte polarity and ACD (Cox et al., 2001; Knoblich, 2008). Furthermore, when aPKCζ is downregulated in *Xenopus*, mitogenesis and oocyte inhibition is abrogated (Dominguez et al., 1992; Berra et al., 1993). Overall, these loss of function studies demonstrate that aPKCs, especially the mammalian aPKCλ isoform, are essential for embryonic development.

To examine the mammalian function of aPKCλ *in vivo* at later stages of development as well as in adult tissues, conditional tissue-specific knock-out mouse models were analyzed: Specific ablation of aPKCλ from the embryonic central nervous system results in disturbed tissue architecture in the telencephalon, caused by a loss of adherens junctions in neuroepithelial cells (Imai et al., 2006). Similarly, deletion of aPKCλ in embryonic lens cells causes disruption of apical cell junctions and mislocalization of cell polarity proteins leading to cataract formation (Sugiyama et al., 2009). Lack of aPKCλ in differentiating photoreceptors induces retinal disorganization due to loss of adherens junctions (Koike et al., 2005). These reports have confirmed an important role for mammalian aPKCλ in the formation and maintenance of adherens junctions. This function of aPKCλ seems to be conserved, since in zebrafish *heart and soul* (has) mutants, where the aPKCλ gene is mutated, dysfunctional adherens junctions were reported as well (Horne-Badovinac et al., 2001). Thus, a crucial function of aPKCλ seems to be to control adherens junction formation, possibly by regulating cell polarity proteins in several tissues *in vivo*.

Additional conditional knock-out mouse models have revealed a plethora of aPKCλ-specific functions. For example, selectively deleting aPKCλ in activated T-cells showed that aPKCλ regulates the activation of Th2 transcription factors in allergic airway inflammation. Notably, the researchers demonstrated that aPKCλ is indispensable for Th2 cell polarization (Yang et al., 2009a). Furthermore, aPKCs are implicated into several metabolic pathways. For example, aPKCs are involved in signaling by various growth factors, including IGF-1 and Insulin that act through phosphatidyl-3 kinase (PI-3 kinase) to activate aPKC. Muscle-specific aPKCλ$^{-/-}$ mice showed reduced insulin resistance and glucose tolerance as well as dyslipidemia (Farese et al., 2007a). Depletion of aPKCλ in skeletal muscle cells revealed a role of aPKCλ in glucose transport and GLUT4 glucose transporter translocation to the plasma membrane (Farese et al., 2007b, Kotani et al., 1998). aPKCλ is crucial for glucose-induced insulin secretion and glucose tolerance in the pancreas, as demonstrated by studying mice harboring a deletion of aPKCλ in pancreatic B-cells (Hashimoto et al., 2005).

Conditional deletion of aPKCλ from the liver results in increased insulin sensitivity and revealed contributions of aPKCλ on lipogenesis by regulating the expression of sterol-receptor element binding protein 1c (SREBP1c) (Matsumoto et al., 2003). Since loss of cell polarity is a hallmark of cancer it is not surprising that aPKCs are involved in tumorigenesis. Overexpression of aPKCλ is associated with a range of human carcinomas. Both aPKC isoforms have been implicated in cancer progression in human lung and colon cancer through gene amplification and the regulation of Ras signaling pathways (Fields et al., 2007). aPKCλ enhances tumorigenesis in either a colon (Murray et al., 2009) or lung carcinoma mouse model (Regala et al., 2009). On the other hand, loss of aPKCζ leads to increased tumorigenicity due to overexpression of IL6 (Galvez et al., 2009).

In summary, aPKCs are molecular mediators of several signaling pathways, including cell polarity, immunity and metabolic pathways. Hence, aPKCs may couple cell architecture to regulation of cell growth, inflammation and survival in mammals.

1.6.2 aPKC in cell polarity

The aPKC complex has been described to be a crucial mediator in several forms of cellular polarity. The members of the aPKC complex display a mutually dependent asymmetric localization and activity within the cell, thereby creating complementary membrane domains (Etienne-Manneville and Hall, 2003). Hence, asymmetric localization of aPKC is crucial for aPKCs function in several processes. For example, polarized aPKC localization is necessary for proper spindle positioning in dividing *Drosophila* neuroblasts (Fig.1.8A) and MDCK cells (Lee et al., 2006; Hao et al., 2010). In the asymmetrically dividing *C. elegans* embryo, the aPKC complex localizes to the anterior cortex, whereas Par1 translocates to the posterior cortex (Kemphues, 2000). In mammalian simple epithelial cells, the aPKC complex localizes apically to tight junctions and is essential for their formation and maintenance (Fig. 1.8B) (Suzuki and Ohno, 2006). Axon specification is controlled by positioning of the aPKC/Par6/Par3 complex to the cell body and the end tip of axons (Fig. 1.8C) (Shi et al., 2003). Finally, the aPKC complex also acts in centrosomal reorientation and microtubule polarization of migrating cells and localizes to the leading edge (Fig. 1.8D) (Etienne-Manneville and Hall, 2003).

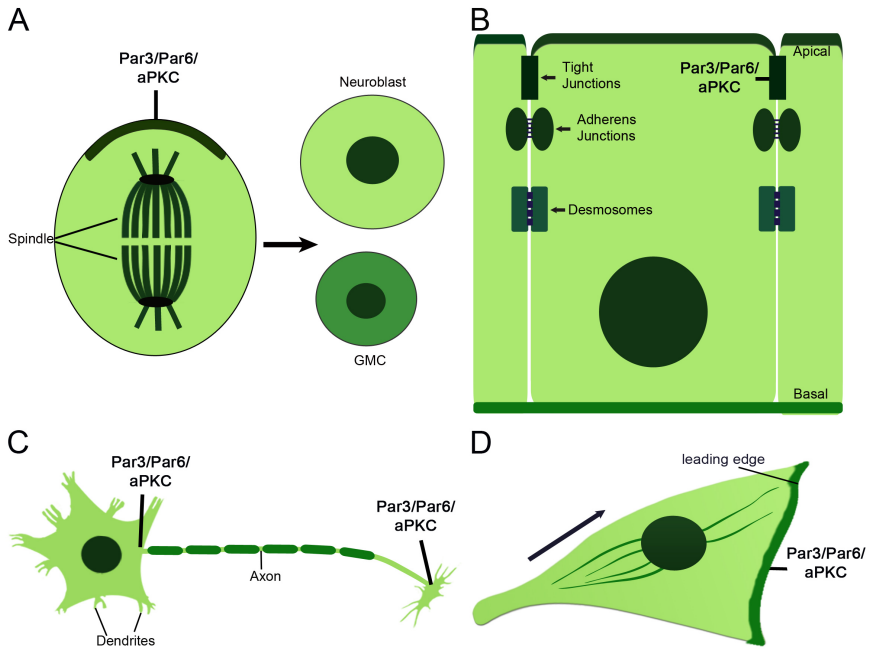

Figure 1. 9: Examples of cell polarity, in which the aPKC/Par complex is involved

(A) Asymmetric cell division of *Drosophila* neuroblasts. The Par/aPKC complex localizes apically promoting progenitor (neuroblast) cell fate. GMC=Ganglion mother cell. (B) Apico/basal polarity in mammalian epithelial cells and colocalization of the PAR/aPKC complex to tight junctions. (C) Mammalian hippocampal neuronal cells localize Par3, Par and aPKC to the cell body and the tip of the axon. (D) Localization of the PAR/aPKC complex to the leading edge during directed cell migration.

Par3, Par6 and aPKC directly interact with each other in a dynamic complex. The adaptor protein Par6 binds to aPKC through a constitutive PB1-PB1 domain interaction. Moreover, Par6 contains a CRIB domain that binds the active GTP-bound form of the small Rho GTPases Rac and Cdc42, leading to aPKC phosphorylation and activation (Joberty et al., 2000; Lin et al., 2000). Par3 binds to Par6 via its PDZ domain and interacts with the kinase domain of aPKC. Par3 association with the complex is subject to regulation, which allows switching between Par6/aPKC dependent and independent functions of Par3. For example, phosphorylation of Par3 by aPKC decreases Par3 binding affinity for aPKCs. Par3 can function both as an upstream regulator of the complex by recruiting aPKC/Par6 to the membrane as well as a downstream effector of aPKC by connecting aPKC to several signaling pathways. Moreover, Par3 has functions independent of aPKC/Par6 and, vice versa, that Par6/aPKC have Par3-independent roles (Iden and Collard, 2008; Niessen and Niessen, 2010).

The aPKC/Par complex interacts with several additional polarity proteins, some of which are also substrates, to regulate establishment and maintenance of polarity. An important aspect in the set up of polarity is the antagonizing activities of different polarity protein complexes. For example, atypical PKC and its substrate Par1 exist in a mutually inhibitory relationship. In mammalian epithelia, aPKC phosphorylates Par1 at tight junctions and thus induces its

dissociation from the basolateral membrane (Suzuki et al., 2004). In turn, *Drosophila* Par1 phosphorylates Par3, which leads to the disruption of the aPKC/Par6 complex (Benton and St Johnston, 2003). The aPKC substrate Lethal giant larvea (Lgl) has a similar role to Par1 since it also antagonizes the aPKC/Par complex to regulate apico-basal polarity of epithelial cells and *Drosophila* neuroblasts. Lgl competes with Par3 for binding to the Par6/aPKC complex and thus restricts aPKC/Par3/Par6 to the apical domain (s. 1.3.1.1) (Hutterer et al., 2004; Betschinger et al., 2005). These complex and dynamic interactions within polarized cells are crucial for the function of the aPKC complex.

1.6.3 aPKC in asymmetric cell division and cell fate determinantion

Since polarity processes regulate oriented divisions, these proteins may directly or indirectly influence cell fate choices to generate cell diversity in simple systems and mammals (Niessen and Niessen, 2010). The impact of polarity proteins, as for example aPKC, on cell fate determination has been studied in several systems ranging from *C. elegans* to mammals (Knoblich, 2008). The Par proteins and aPKC were identified as the first molecular regulators of cell fate by screening for mutants that failed to properly partition cell fate determinants during the first *C. elegans* asymmetric division (Kemphues et al., 1988). aPKCs role in cellular fate is best studied in *Drosophila* neuroblasts (Knoblich, 2008), where cortical aPKC is required and sufficient to promote self-renewal of neuroblasts. Thus, decreased aPKC levels reduce neuroblasts numbers whereas overexpression an aPKC-CAAX mutant, which is constitutively localized at the membrane, induces ectopic neuroblast renewal (Lee et al., 2006; Rolls et al., 2003). On the molecular level, the aPKC complex seems to balance asymmetric segregation of cell fate determinants by their phosphorylation, thus excluding them from the apical cortex (s. 1.3.1.1) (Knoblich, 2008). In lower vertebrates, aPKC also has been implicated in the set up of spindle orientation and cell fate determination. For example in *Xenopus,* localized aPKCλ promotes ectodermal fate by antagonizing Lgl1 and Par1, which promote neurogenesis (Sabherwal et al., 2009; Tabler et al., 2010). In zebrafish, aPKCs are crucial for spindle orientation in the neuroepithelium. Knock-down of both aPKC isoforms promotes neuroepithelial progenitor maintenance on the expense of divisions that produce differentiating cells (Baye and Link, 2007). In summary, aPKC seems to promote undifferentiated progenitor cell fate in *Drosophila* and *Xenopus*, whereas in *Danio rerio,* aPKC rather promotes differentiation of progenitor cells.

Whereas molecular details have been described in simple organisms, the *in vivo* role of aPKC in cell fate determination remains elusive in the mammalian system. The aPKC/Par complex has also been recently implicated in spindle orientation and cell fate determination *in vitro*. Here, the aPKC complex was shown to ensure proper symmetric spindle orientation in mitotic MDCK cells in *in vitro* three-dimensional matrigel cyst models (Qin et al., 2010). *Ex*

vivo work demonstrated, that aPKCλ-dependent stabilization of cortical domains is crucial for lineage specification in murine preimplantation embryos. Expression of an aPKC dominant-negative version in 4-cell stage blastomeres results in an increase of asymmetric cell divisions, triggering cell fate towards pluripotent inner cell mass (Plusa et al., 2005). aPKCλ controls junction formation and cortical tension thus regulating cell positioning inside the embryo (Dard et al., 2009b).

The effect of aPKC on cell fate determination in adult mammalian tissue is not yet clear. A recent *in vitro* study demonstrated that in murine neuronal fate determination, aPKCζ prevents differentiation by binding the cell fate determinant TRIM32 (Hillje et al., 2011). In contrast, in the mouse cortex, aPKCλ depletion affects tissue architecture but not affect cell fate (Imai et al., 2006). In the developing chicken neural tube, aPKC does not seem to have any influence on cell specification (Ghosh et al., 2008). In accord with these data, genetic knock-out studies focusing on eye function revealed that cell fate specification is not altered after deletion of aPKCλ in differentiating murine photoreceptor cells or lens cells (Koike et al., 2005; Sugiyama et al., 2009). Finally, a recent report documents that mice harboring a constitutive or hematopoietic-specific deletion of aPKCζ or λ respectively, display no alterations in activity, differentiation or fate specifiction of hematopoietic stem cells (Sengupta et al., 2011). These data suggest that despite aPKCs role in cell fate determination in lower organisms, aPKCλ might not be necessary for cell fate specification in adult mammalian tissue *in vivo*, however this has not been tested in the murine skin so far.

1.7 aPKCλ in epidermal cell polarity

Little is known about the role of aPKCζ and aPKCλ in epidermal cell polarity, however localization studies suggest non-overlapping functions for aPKCλ vs. aPKCζ. For example in the embryonic epidermis, strong expression of aPKCλ was observed in all epidermal layers and HFs, whereas aPKCζ was only found in outermost embryonic periderm cells (Kovac et al., 2007). Both aPKCλ and aPKCζ are detected in newborn murine epidermis, but aPKCλ is much stronger expressed as compared to aPKCζ (Frederik Tellkamp). The two isoforms also display a distinct localization in the epidermis of newborn mice. Whereas both isoforms showed strong cytoplasmic and weak nuclear localization in basal cells, only the aPKCλ isoform was expressed in suprabasal layers at sites of cell-cell contacts (Fig. 1.9A) (Helfrich et al., 2007), suggesting a role of aPKCλ in barrier formation. Indeed, aPKCζ is not required for nascent epidermal contacts but for the maturation and maintenance of cell-cell contacts *in vitro* (Helfrich et al., 2007). The small GTPase Rac1 was reported to control tight junction formation and maintenance by activation of the aPKCζ/Par3/Par6 complex in keratinocytes (Mertens et al., 2005). In addition, loss of cell adhesion molecules like E-cadherin (Tunggal

et al., 2005) impairs skin barrier function associated with altered Par3/aPKC activity or localization. These data demonstrate that aPKC is crucial for epithelial polarity and junction formation and suggest, that adhesive contacts and polarity signaling pathways cooperate in the epidermis, similar to simple epithelial cells, to drive epithelial barrier function.

The function of aPKC in other forms of cell polarity in the epidermis, as for example ACD, has not been studied in detail yet. Using a different antibody than Helfrich et al., (2007), aPKCλ was detected apically in the basal layer in both asymmetrically and symmetrically dividing cells of E16.5 embryonic skin (Fig. 1.9B) (Susanne Vorhagen; (Lechler and Fuchs, 2005)). This suggests, that aPKC is not promoting exclusively asymmetric or symmetric divisions and raises the question whether aPKCλ is also, as in *Drosophila*, mediating establishment of ACDs and thus cell fate decisions in the murine epidermis.

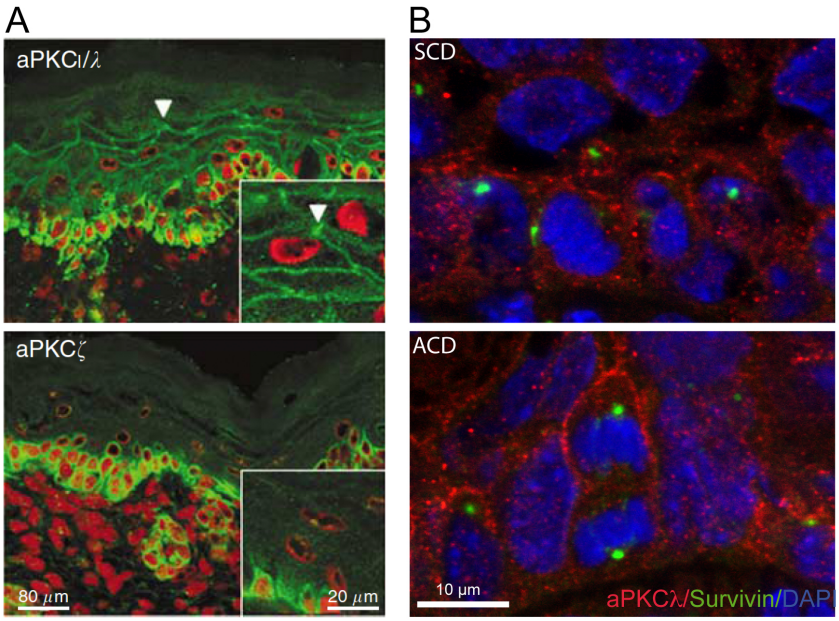

Figure 1. 10: Localization of aPKCs in the murine epidermis

(A) Localization of aPKCι/λ versus aPKCζ in the epidermis of newborn mice (Helfrich et al., 2007). (B) Localization of aPKCλ in asymmetrically (ACD) and symmetrically (SCD) dividing cells of embryonic skin (E16.5). Staining was performed using paraffin sections of dorsal skin. Survivin staining marks late anaphase spindles, nuclei were counterstained with DAPI. Staining was performed by Susanne Vorhagen.

1.8 Aims of this study

The overall goal of this study was to determine how polarity processes regulate epidermal homeostasis and how cell polarity is established and maintained in a stratified epithelium. To answer these questions, the polarity protein aPKCλ was specifically inactivated in all compartments of the mouse epidermis. aPKCs are crucial regulators of apico-basal polarity, asymmetric cell division, and cell fate in lower organisms. The aim of this work was to clarify if mammalian aPKCs regulate these processes in the epidermis.

The specific questions addressed in this study were

1. Does aPKCλ regulate epidermal morphogenesis and homeostasis?
2. Does loss of aPKCλ affect polarity and polarity signaling in the epidermis?
3. Does aPKC regulate cell fate decisions in the epidermis?
    A. Does aPKCλ control differentiation of the interfollicular epidermis and hair follicles?
    B. Does aPKCλ regulate hair follicle stem cell identity and maintenance?
    C. Is aPKCλ important for balancing asymmetric versus symmetric cell division in different compartments of the epidermis?
4. Through which molecular pathways does epidermal aPKCλ function?

2 Results

2.1 Generation of mice lacking aPKCλ in the epidermis

To examine the function of aPKCλ exclusively in the epidermal compartment of the skin, epidermis-specific knock-out mice were generated by crossing mice homozygous for the floxed aPKCλ allele (Farese et al., 2007a) to mice expressing Cre-recombinase under the control of the K14 promoter (Hafner et al., 2004). The K14 promoter targets Cre-recombinase expression to the mitotically active basal layer of mouse epidermis, including the outer root sheath of the hair follicles as well as oral and thymic epithelia. K14 promotor activity starts at embryonic day (E) 9.5 and is fully active by E 14.5 (Byrne et al., 1994; Vasioukhin et al., 1999), allowing the inactivation of genes of interest during epidermal morphogenesis. In the following report the resulting K14-Cre/+; aPKCλ$^{floxed/floxed}$ mice will be referred to as aPKCλ$^{epi-/-}$ mice. aPKCλ$^{fl/+}$, Cre/+ and aPKCλ$^{fl/fl}$,+/+ mice appeared normal and fertile. aPKCλ$^{fl/fl}$,+/+ were analyzed as control mice in all experiments and will be hereafter referred to as control (ctr) mice. PCR analysis of DNA isolated from tail cuts identified fragments of the expected size for floxed and wt alleles and showed efficient deletion only in the presence of the K14-Cre allele (Fig 2.1A.). Quantitative Real-time PCR (qRT-PCR) analysis demonstrated efficient deletion of aPKCλ also on the transcriptional level, whereas aPKCζ was slightly, but not significantly, upregulated (Fig. 2.1B). Western blot analysis revealed the absence of total and active, phosphorylated aPKCλ in primary keratinocytes isolated form newborn mice (Fig. 2.1C). Overall, this demonstrates that aPKCλ was efficiently deleted in aPKCλ$^{epi-/-}$ but not ctr mice resulting in the complete absence of protein expression in newborns.

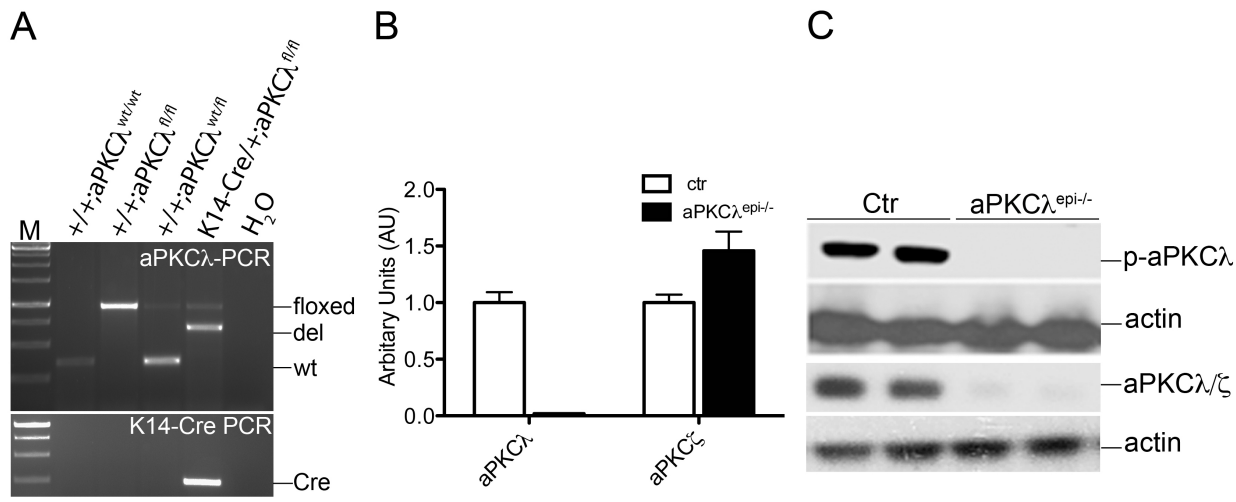

Figure 2. 1: Efficient epidermis-specific deletion of aPKCλ in aPKCλ$^{epi-/-}$ mice

(A) PCR genotyping using aPKCλ-specific and K14-Cre-specific primers on genomic DNA isolated from tail biopsies showing the different genotypes of the mice. Wt= Wildtype, fl= floxed. (B) QRT-PCR of aPKCλ and aPKCζ expression using epidermal RNA of newborn control (ctr) and aPKCλ$^{epi-/-}$ mice, N=5 independent RNA isolations of different mice. (C) Immunoblot analyses of ctr and aPKCλ$^{-/-}$ keratinocytes lysates using an antibody recognizing total aPKCλ/ζ or p-aPKCλ. Western blot for β-actin served as a loading control.

2.2 aPKCλ regulates postnatal interfollicular epidermal homeostasis

2.2.1 Increased thickening of postnatal aPKCλ$^{epi-/-}$ IFE

Histological analysis of the interfollicular epidermis (IFE) showed that loss of aPKCλ resulted in a thinner epidermis in newborn mice. Interfollicular thickness was similar in 6 days old aPKCλ$^{epi-/-}$ and ctr epidermis, whereas from postnatal day (P) 9 on, a significant thickening (hyperkeratinization) of the epidermis was observed in aPKCλ$^{epi-/-}$ compared to ctr mice. This feature was maintained at least until P100 (Fig. 2.2A/B). As a side note, quantifications from P0 skin were performed in mice of a mixed 129SV/Bl6 background, whereas quantifications from later time points were performed using material exclusively from C57/Bl6 mice.

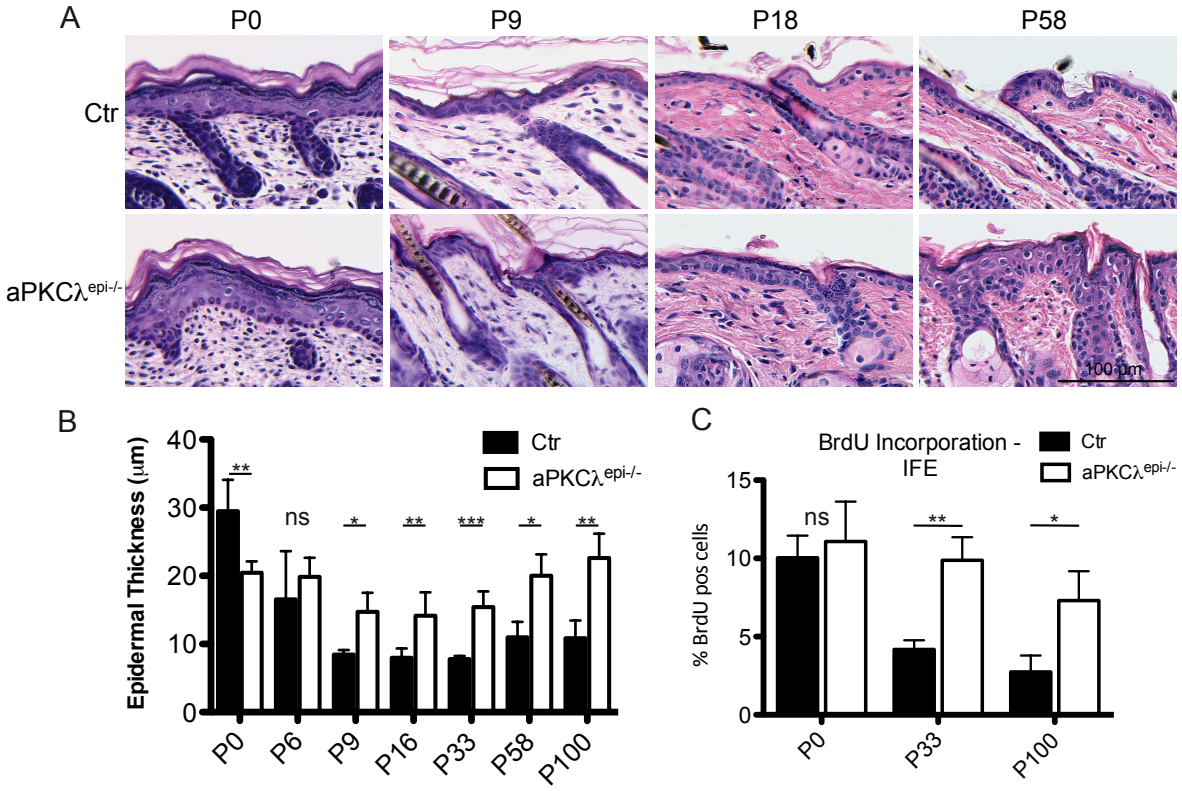

Figure 2. 2: Thickening of the IFE in adult aPKCλ$^{epi-/-}$ mice

(A) Haematoxylen and Eosin (H&E) staining of paraffin sections of back skin from ctr and aPKCλ$^{epi-/-}$ mice from the indicated postnatal (P) days. At birth, the IFE appears thinner in aPKCλ$^{epi-/-}$ mice whereas it is thickened in adult aPKCλ$^{epi-/-}$ mice. (B) Epidermal thickness measurement (without the *str. corneum*) using H&E stained sections of back skin from indicated postnatal (P) days. N>4 mice for each genotype. Data are presented in mean+/- SD. (C) Quantification of BrdU positive cells in the IFE of dorsal skin from adult mice from indicated postnatal (P) days. BrdU positive cells were quantified after a short BrdU (100 mg/ml, 0.5 hrs) pulse before sacrifice. N>4 mice for each genotype. Data are presented in mean+/- SD. ns=p>0.05; *= p<0.05; **= p<0.01; ***=p<0.001 for (B) and (C).

In line with the observations of hyperkeratinization in aPKCλ$^{-/-}$ epidermis, BrdU incorporation after short pulses of BrdU (0,5 hrs) was not increased in newborn aPKCλ$^{epi-/-}$ mice compared to ctr mice, but significantly enhanced in adult skin (P33, P100) (Fig. 2.2C). Expression and localization of several differentiation markers (K14, K10, Loricrin) was not affected by aPKCλ-deletion in newborn IFE (data not shown). In contrast, in older (P58) mice increased epidermal thickness was accompanied by a slightly, but consistently enhanced staining of the differentiation markers K14 (*str. basale*) and Loricrin (*str. granulosum*) demonstrating that deletion of aPKCλ affects postnatal interfollicular differentiation (Fig. 2.3A).

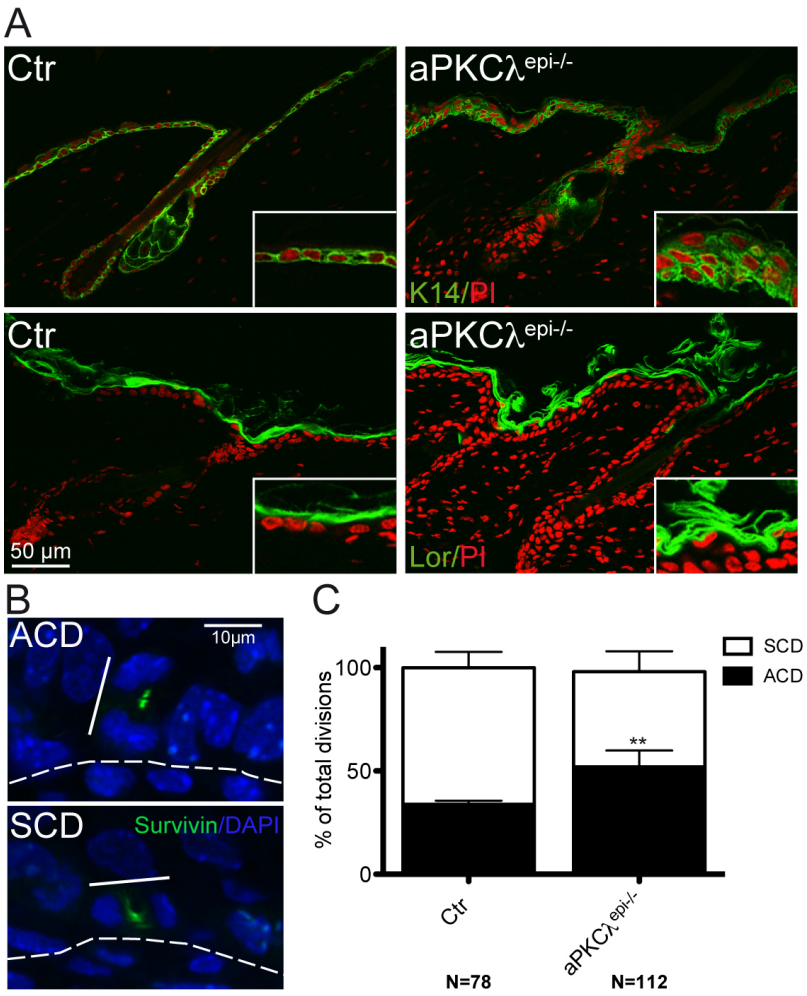

Figure 2. 3: Loss of aPKCλ results in increased differentiation and asymmetric cell division

(A) Keratin (K) 14 and Loricrin staining of paraffin sections from 58 days old mice. Nuclei were counterstained with propidium iodide (PI). (B) Co-staining of Survivin and DAPI to visualize dividing cells in the basal layer of E.16.5 embryonic skin. ACD: asymmetric cell division, perpendicular to the basal layer (broken line). SCD= symmetric cell sivision, parallel to the basal layer (broken line) (Susanne Vorhagen) (C) Quantification of the percentage of asymmetric (60-90°C), symmetric (0-30°C) or random (30-60°) cell division in regard to the basal layer of 33 days old mice. N=3 mice per genotype. Data are presented as mean values +/- SD. **= p<0.01. N=number of divisions analyzed for the respective genotype.

2.2.2 Increased asymmetric cell division in adult aPKCλ$^{-/-}$ IFE

During embryogenesis, interfollicular differentiation is regulated by symmetric (SCD) and asymmetric cell divisions (ACDs) (Smart, 1970; Lechler and Fuchs, 2005). Since aPKC regulates ACDs in *Drosophila* and *C.elegans* (Knoblich, 2008), we therefore asked whether divisions are oriented symmetrically versus asymmetrically in postnatal IFE and if so, if loss of aPKCλ alters spindle orientation. To identify mitotic cells in anaphase, nuclei were visualized by DAPI staining. Co-staining of the anaphase/telophase marker Survivin was performed to identify late-stage mitotic cells. Survivin localized to the central spindle during anaphase/telophase and to the mid-body during cytokineses (Williams et al., 2011). The angle of late-stage mitotic divisions in regard to the basement membrane of the IFE was determined, and divisions were classified as asymmetric (45°-90°) or symmetric (0°-45°). Quantification of ACD revealed a significant increase of spindles oriented perpendicularly to the basal layer in adult (P33) aPKCλ$^{epi-/-}$ (52+/-7,8%) compared to ctr (33+/-1,7%) mice (Fig. 2.3B). These data infer that aPKCλ regulates epidermal differentiation by balancing symmetric vs. asymmetric cell divisions in the adult interfollicular epidermis.

2.3 Epidermal aPKCλ deletion results in hair loss

At birth, aPKCλ$^{epi-/-}$ mice were generally undistinguishable form their littermates, except that a few aPKCλ$^{epi-/-}$ mice (around 40%) lacked vibrissae and displayed a slightly more translucent skin. The mice were born in mendelian ratios, but dependent on the mouse facility, varying percentages (between 10% and 100%) of aPKCλ$^{epi-/-}$ mice died during the first 3 days of postnatal life. A striking macroscopic phenotype of aPKCλ$^{epi-/-}$ mice became apparent from P6 on that was characterized by a decreased body size of the mice, differential eye morphology (inflamed eyes) and most remarkably, a sparse hair coat. Fur growth of aPKCλ$^{epi-/-}$ mice was delayed 1-2 days and hair was oilier. During the two first postnatal hair cycles, aPKCλ knock-out mice lost their hair coat and regained it in a cyclic fashion. However, this effect of cyclic alopecia was not synchron when comparing several aPKCλ$^{epi-/-}$ mice. The aPKCλ$^{epi-/-}$ phenotype became more pronounced with age resulting in complete alopecia at P100, except for occasional hair remaining in the facial region. P100 mice showed macroscopic cutaneous lesions, possibly originating from skin scratches. In addition, the eye phenotype became more pronounced over time, resulting in approximately 40% of aPKCλ$^{epi-/-}$ mice showing obvious clouding of the lenses (cataract) as reported for lens-cell-specific aPKCλ- knock-out mice (Fig. 2.4) (Sugiyama et al., 2009).

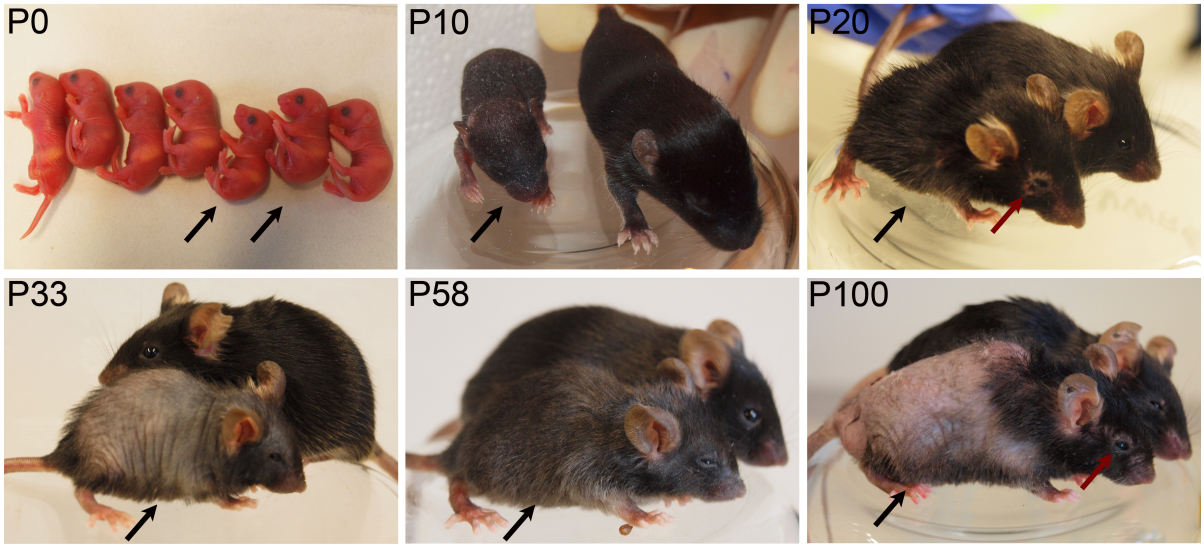

Figure 2. 4: Epidermis-specific deletion of aPKCλ results in cyclic hair loss

Macroscopic appearance of aPKCλ$^{epi-/-}$ mice and ctr littermates at several postnatal (P) days. aPKCλ$^{epi-/-}$ mice are marked by black arrows, inflamed eyes are indicated by red arrows.

2.4 aPKCλ is crucial for the homeostasis of epidermal appendages

Because aPKCλ$^{epi-/-}$ mice showed cyclic hair loss and more oily hair, histological analysis was performed on ctr and aPKCλ$^{epi-/-}$ back skin at different postnatal days to examine the phenotypic appearance of hair follicles (HF) and sebaceous glands (SG) (Fig. 2.4).

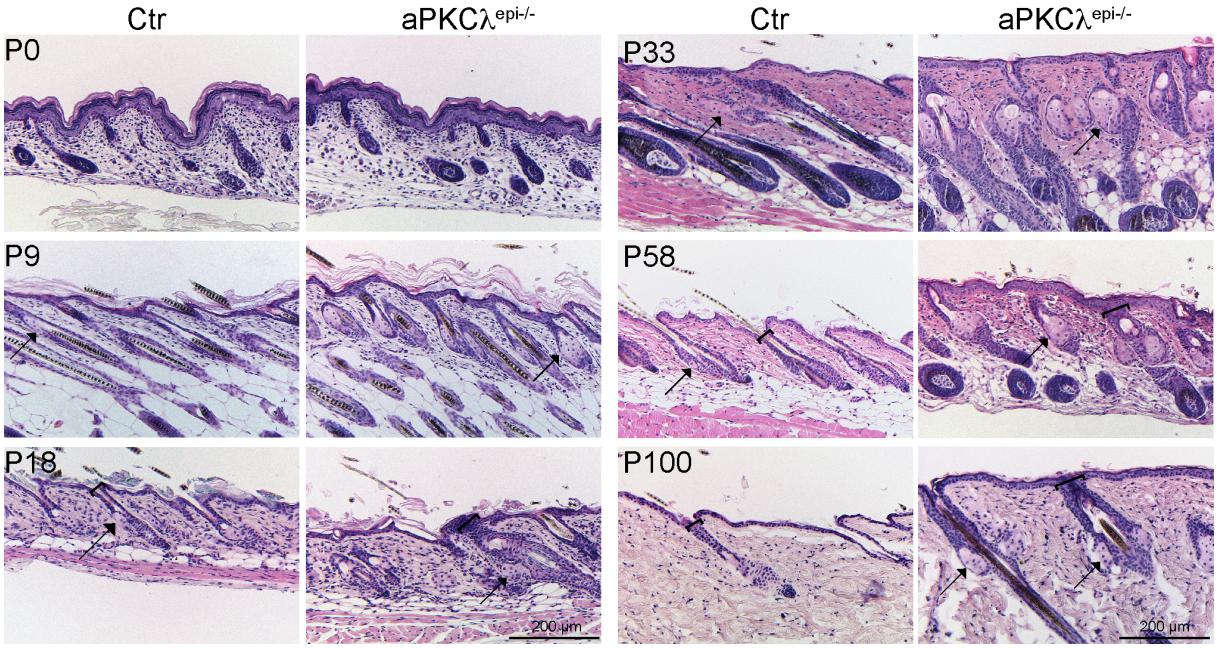

Figure 2. 5: SG and HF phenotype dof aPKCλ$^{epi-/-}$ mice during postnatal life

H&E staining of paraffin sections of back skin from ctr and aPKCλ$^{epi-/-}$ mice from the indicated postnatal (P) days. Black arrows indicate SGs and black brackets indicate width of the infundibulum.

2.4.1 Increased sebaceous gland differentiation

Whereas not identifiable at P0, SGs were first visible and already slightly enlarged in aPKCλ$^{epi-/-}$ compared to ctr mice at P9. During adult life (P58, P77, P100), SGs in aPKCλ$^{epi-/-}$ mice were strongly enlarged when compared to ctr littermates. Interestingly, SG size seemed to gradually increase with ageing of aPKCλ$^{epi-/-}$ mice (Fig. 2.5). High magnification revealed that SGs enlargement is a consequence of an increased cell number per gland (Fig. 2.6A). Increased Nile red staining indicative of lipid droplet incorporation demonstrated that these cells are indeed fully matured sebocytes at P6 (Fig. 2.6B). This was further confirmed by staining for SCD1, a marker for differentiated sebocytes at P9 (Miyazaki et al., 2001) (Fig. 2.6C). These findings demonstrate that loss of epidermal aPKCλ promotes sebaceous gland differentiation.

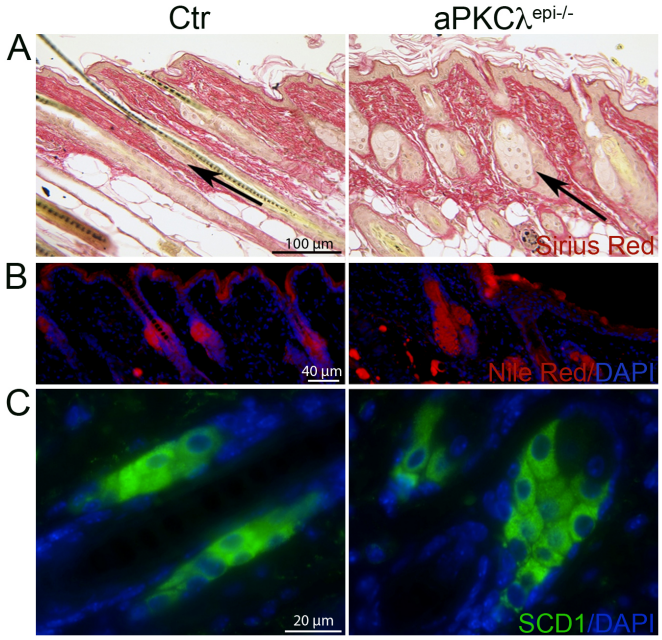

Figure 2. 6: Loss of aPKCλ increases sebaceous gland differentiation

(A) Sirius red staining using paraffin sections of 16 days old ctr and aPKCλ$^{epi-/-}$ mice. (B) Nile red staining of Cryo-preserved dorsal skin sections from 6 days old ctr and aPKCλ$^{epi-/-}$ mice. Nuclei were counterstained with DAPI. (C) Immunohistochemical staining of SCD1 on cryo-preserved sections from 9 days old mouse back skin. Nuclei were counterstained with DAPI. Staining was performed by Jeanie Scott.

2.4.2 Altered hair follicle morphology

Histological analysis revealed that at birth, aPKCλ$^{epi-/-}$ HFs were indistinguishable from ctr HFs, however during postnatal development, aPKCλ$^{epi-/-}$ mice developed a striking HF phenotype. The HFs became gradually enlarged and the infundibulum, the region between the SG and IFE, was widened from P18 on (Fig. 2.5). To visualize HF structure three-dimensionally, whole-mounts of tail skin from P25 and P100 mice were stained for K14.

Analysis confirmed histological observation that HFs displayed an irregular shape, were widened and misaligned. Mouse tail HFs are arranged in groups of three follicles and in parallel rows (Braun et al., 2003). Overall, this pattern was maintained, however with an irregular appearance. The morphological differences developed gradually during postnatal life: the phenotype of enlarged, widened, misaligned HFs was more pronounced in 100 day old mice as compared to 25 day old aPKCλ$^{epi-/-}$ mice (Fig. 2.7A). No difference in infudibulum width or HF length was detected in newborn mice. In contrast, in adult aPKCλ deficient HFs the width of the infundibulum was significantly increased compared to ctr littermates (P33; P58). Although this effect was no longer significant during later postnatal stages, the infundibulum of aPKCλ-deficient follicles retained its tendency of being wider at P100 (Fig. 2.7B). Ctr follicles declined in HF length and volume from P33 to P58, reflecting entry into resting phase of the hair cycle (telogen). This effect was not as pronounced in aPKCλ$^{epi-/-}$ follicles, which were significantly longer than ctr follicles (Fig. 2.7C).

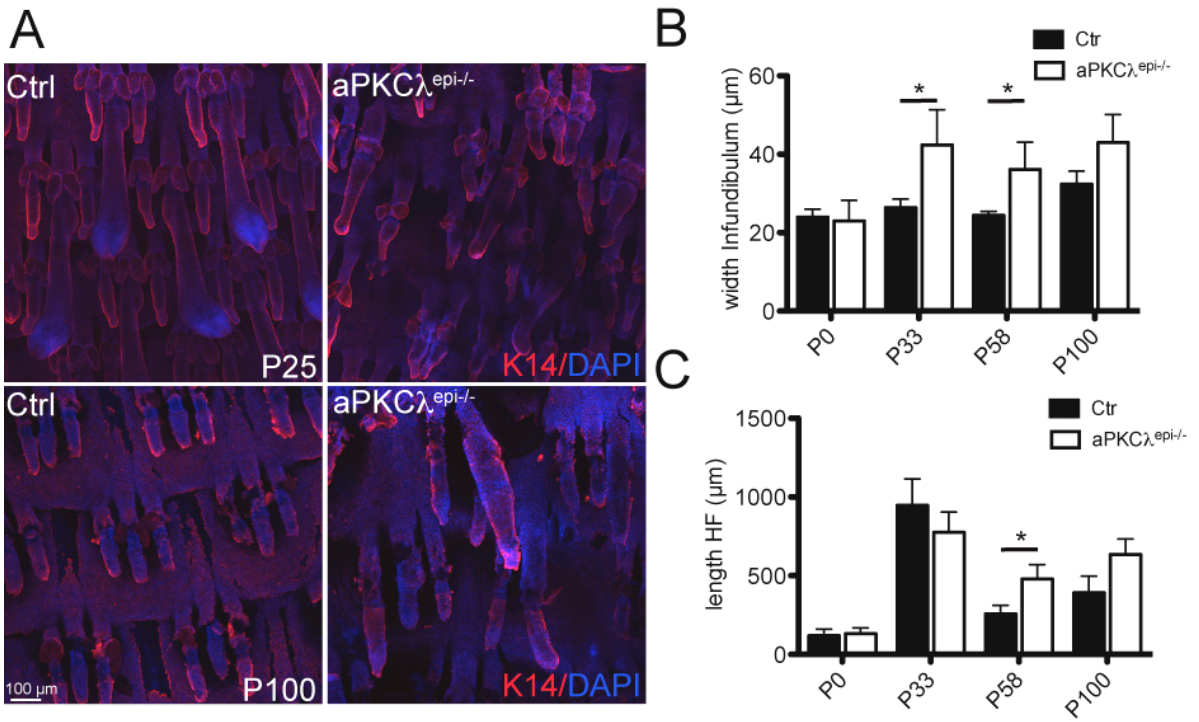

Figure 2. 7: Altered hair follicle morphology in aPKCλ$^{epi-/-}$ mice

(A) Macroscopic appearance of hair follicles visualized by K14 staining of whole-mount tail skin of 25 or 100 day old (P) mice. Nuclei were counterstained with DAPI. (B) Quantification of the width of the infundibulum zone at the indicated postnatal (P) days using H&E stainings of paraffin sections from dorsal skin. (C) Quantification of the length of HFs at the indicated postnatal (P) days using H&E stainings of paraffin sections from dorsal skin. For (B) and (C): N >4 different mice for each genotype. Data are presented in mean+/- SD. *= p<0.05.

2.4.3. Perturbed hair follicle differentiation

Altered HF morphology suggested defects in hair follicle differentiation. To examine if the specific layers of the HF of aPKCλ$^{epi-/-}$ mice differentiate properly, the localization of the hair layer-specific keratins Keratin 28 (K28), 75 (K75), 82 (K82) and 85 (K85) was investigated. K28 was localized in the inner rooth sheath (IRS) and the medulla and K85 was detected in the matrix, cortex and cuticle to a similar extend in ctr and aPKCλ$^{epi-/-}$ mice (Fig. 2.8A). In contrast, in aPKCλ$^{epi-/-}$ mice, almost no K82, a HF cuticle-specific keratin, was observed. Finally, we investigated K75 expression and localization, which is specific for the companion layer, and detected a decreased signal for this keratin after aPKCλ deletion (Fig. 2.8A). Decreased expression of K82 and K75 was confirmed by western blot (Fig. 2.8B).

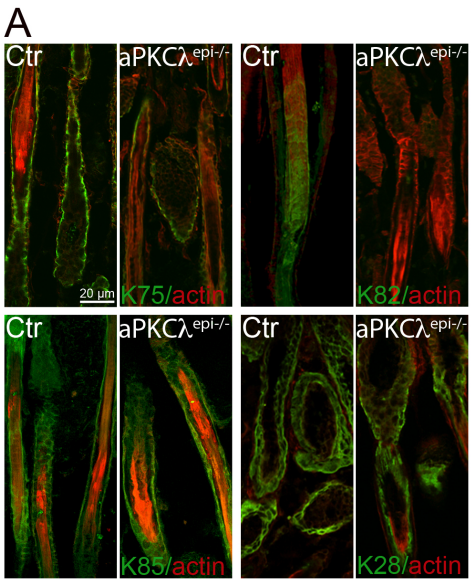

C

Name	*Gene*	*Fold regulation*	*Specificity*
K27	keratin complex-1, acidic, gene C29	-1,99	Medulla, IRS, Cuticule
K85	keratin complex 2, basic, gene 18	-2,32	Hair forming compartment
K35	keratin complex 1, acidic, gene 24	-2,67	Hair forming compartment
K82	keratin complex 2, basic, gene 20	-2,71	Cuticle
K71	keratin complex 2, basic, gene 6g	-2,77	IRS: Henle-, Huxley layer, cuticle
K32	keratin complex 1,acidic, gene 2	-3,39	Cuticle

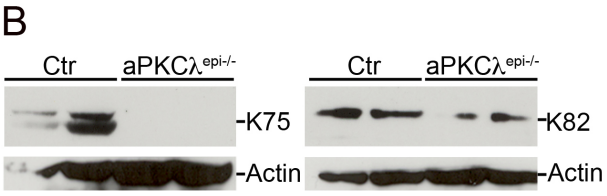

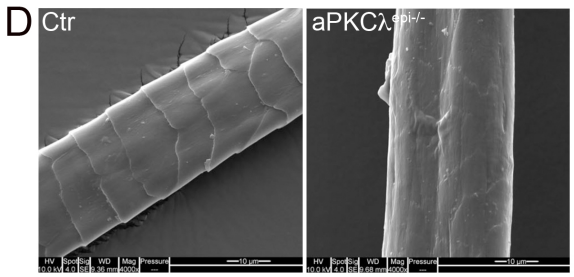

Figure 2. 8: Hair follicle differentiation is impaired in aPKCλ$^{epi-/-}$ mice

(A) Cryo-preserved dorsal skin sections of 6 day old ctr and aPKCλ$^{epi-/-}$ mice were stained with antibodies against the keratins K28, K85, K82 and K75 using littermate pairs from n=3 independent litters. Actin cytoskeleton was counterstained with phalloidin. (B) Western blot analysis of K75 and K82 expression using fresh epidermal lysates from newborn control (ctr) and aPKCλ$^{epi\ -/-}$ mice. N= 3 independent lysates from different ctr and aPKCλ$^{epi\ -/-}$ mice. (C) Selected results of Affymetrix gene expression analysis of ctr and aPKCλ$^{epi-/-}$ newborn mice. The table shows a selection of downregulated hair specific keratins in aPKCλ$^{epi-/-}$ mice, the official name, the respective gene, the fold downregulation and the specific expression pattern of the genes. (D) Electron micrographs of single hairs from of adult (P60) aPKCλ$^{epi-/-}$ mice and ctr littermates (Carien Niessen).

A global RNA microarray expression analysis of newborn aPKCλ$^{epi-/-}$ mice compared to ctr epidermis further confirmed the observations of impaired HF differentiation, specifically pronounced in the HF cuticle. The analysis identified six keratin-genes expressed in the cuticle as 2-3.5 fold downregulated. These include K82 and K85, keratins we also studied in immunohistochemical experiments, as well as K27, K35, K71 and K32. All of these keratins are expressed in the HF cuticle (Fig. 2.8C). In addition, electron micrographs of hairs plucked from adult (P60) mice demonstrated that the defects in HF differentiation result in a loss of regular patterning and an uneven surface of aPKCλ$^{epi-/-}$ hair filaments (Fig. 2.8D) (in collaboration with Neil Smith, Southhampton).

2.4.4 Altered hair follicle cycling

Since quantification of HF length showed that aPKCλ$^{epi-/-}$ HFs were significantly longer, we examined whether this is accompanied by abnormalities in postnatal hair cycling. Histological analysis revealed that when ctr HFs were in 1st telogen, 60% of aPKCλ$^{-/-}$ HFs did not display morphological characteristics of telogen, which are shortening of HFs or the appearance of the secondary hair germ. During 2nd telogen, no aPKCλ-deficient HFs could be detected in resting phases, but 100% of the HFs displayed an “anagen-like” appearance characterized by lengthening of HFs and a proliferative hair bulb (Fig. 2.9). Moreover, we could not detect any HFs in telogen at later stages of development (P100, P230, P356), where the hair cycle becomes asynchronous. Importantly, aPKCλ$^{-/-}$ HFs showed degeneration of the hair bulb at several stages of postnatal development (1st and 2nd telogen), suggesting that the hair follicles might enter catagen stages.

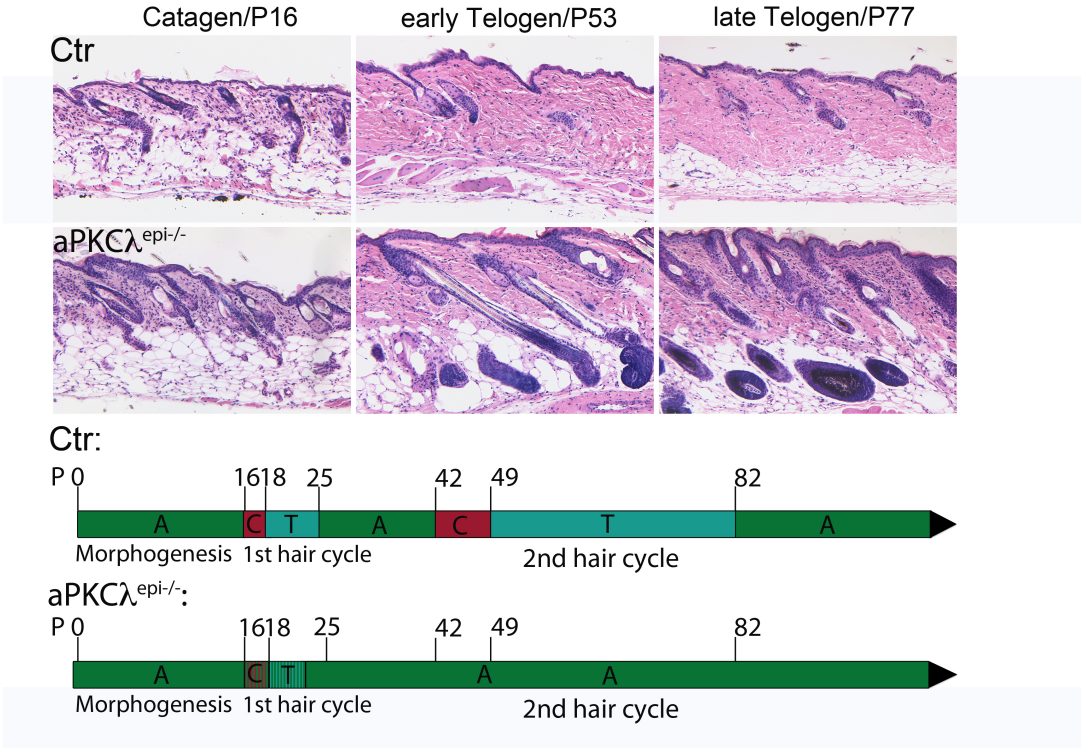

Figure 2. 9: **aPKCλ$^{-/-}$ hair follicles do not enter telogen phases of the hair cycle**

(A) H&E staining of paraffin sections of back skin from ctr and aPKCλ$^{epi-/-}$ mice from the indicated postnatal (P) days. (B) Schematic drawing of hair cycle stages at indicated postnatal time points (P). Anagen (A)= green; Catagen (C)= red; Telogen (T)= turquois. Timing is based upon C57/Bl6 mice.

Altogether, the aforementioned data demonstrate that the polarity protein aPKCλ is crucial for HF morphology, differentiation and cycling. The fact that differentiation of the SG and IFE is increased whereas HF differentiation is perturbed points towards a change in cellular fate toward IFE and SG on the expense of the HF lineage.

2.5 aPKCλ is crucial for HFSC homeostasis in the epidermis

HF cycling requires controlled proliferation and is tightly coupled to activation/quiescence of hair follicle stem cells (HFSC) (Watt and Jensen, 2009). The observation that aPKCλ$^{-/-}$ HFs did not enter telogen phases of the hair cycle suggests that aPKCλ influences HFSC behavior. Therefore, HFSC quiescence, identity and maintenance were analyzed.

2.5.1 Loss of stem cell quiescence in aPKCλ$^{epi-/-}$ HFSCs

To investigate the effect of aPKCλ- loss on the quiescent state of HFSCs, the ability of aPKCλ$^{-/-}$ keratinocytes to retain a BrdU label was analyzed. Bulge SCs of the HF are characterized by their slow-cycling nature and can thus be visualized as DNA-label retaining cells after a long (70 d) BrdU chase (Braun et al., 2003). Whereas ctr HFSCs retained a BrdU label, essentially no label was retained in aPKCλ$^{epi-/-}$ HFs (Fig. 2.10A). Next, we

analyzed the expression of NfatC1, a marker for quiescent HFSCs. Loss of NfatC1 in the HFSC compartment is associated with activation of bulge SCs and precocious entry into anagen stages. NfatC1 transcritionally represses the *cyclin dependent kinase 4* gene CDK4 specifically during HFSC quiescence (Horsley et al., 2008). A strong decrease in NfatC1 staining was observed in HFs of P58 aPKCλ$^{epi-/-}$ mice (Fig. 2.10B). NfatC1 downregulation in proliferating aPKCλ$^{epi-/-}$ HFSC was not reflected on the mRNA level (Fig. 2.10C). Moreover, we did not detect significant alterations in CDK4 expression by qRT-PCR analysis (Fig. 2.10C). Overall, these data provide evidence for a loss of slow cycling bulge SCs in aPKCλ$^{epi-/-}$ mice inferring that aPKCλ is important to maintain HFSCs in their quiescent state.

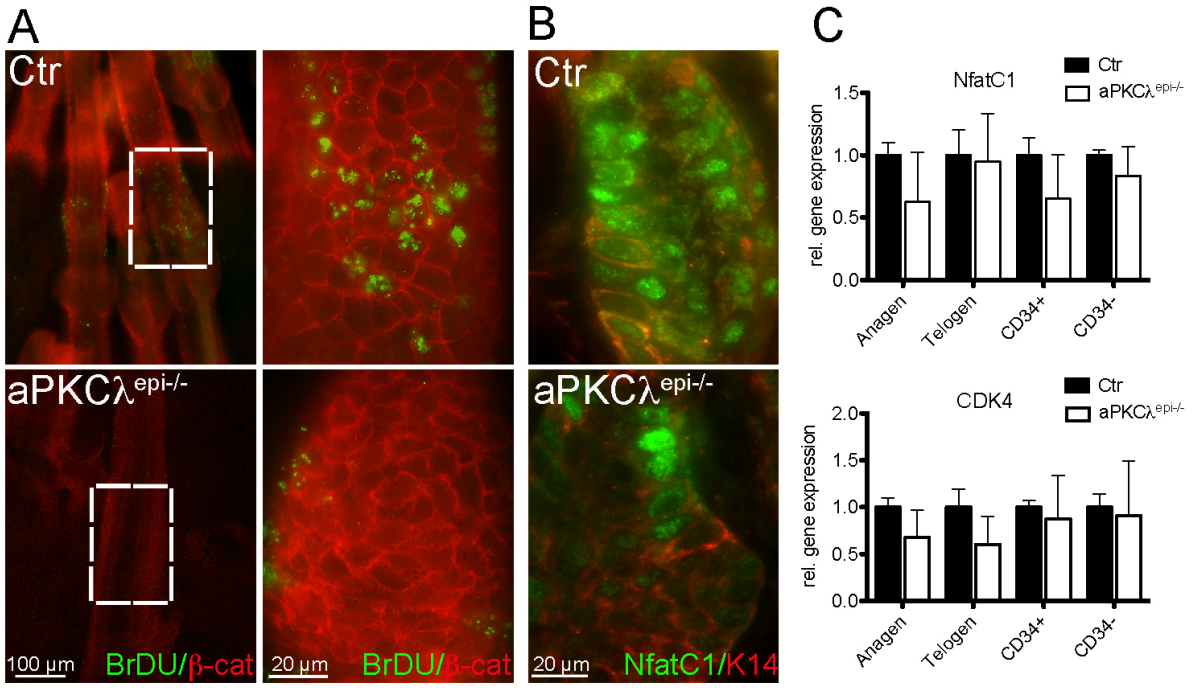

Figure 2. 10: Loss of quiescence in aPKCλ$^{-/-}$ hair follicles

(A) Whole-mount immunofluorescent staining of BrdU in tail epidermis of the indicated genotypes 70 days after BrdU labeling. Cell-cell borders were counterstained for β-catenin (β-cat). (B) Immunofluorescent staining of NfatC1 on paraffin sections of dorsal skin of 58 days old mice of the indicated genotypes. Basal keratinocytes were counterstained with K14. (C) QRT-PCR of NfatC1 and CDK4 expression using RNA isolated from epidermal preparations of anagen (P30), telogen (P19) skin and FACS-sorted keratinocytes isolated from adult (P30) ctr and aPKCλ$^{epi-/-}$ mice. N=5 independent experiments of independent epidermal preparations/ cell isolations. Data are presented in mean +/-SD.

2.5.2 Increased proliferation in aPKCλ$^{epi-/-}$ HFSCs

Due to loss of quiescence in aPKCλ$^{-/-}$ HFs we argued that aPKCλ-deficient HFSCs might be hyper-activated, leading to increased proliferation in the HF. To investigate whether proliferation is affected by aPKCλ-deletion, we performed short BrdU- pulse chase experiments and analyzed BrdU incorporation in tail skin whole-mounts (Braun et al., 2003). At all time points analyzed and all hair cycle stages (anagen, catagen, telogen), we detected an increase in the number of BrdU-positive cells in aPKCλ$^{-/-}$ compared to ctr HFs. This effect occurred throughout all follicular compartments (Fig. 2.11A). Quantification of the percentage of BrdU positive cells revealed an increased (0.5 fold) percentage of proliferating cells in the infundibulum of P33 and P100 aPKCλ$^{-/-}$ HFs (Fig. 2.11B). Strikingly, BrdU incorporation was approximately 3 fold increased in the K15 positive bulge region of aPKCλ$^{-/-}$ HFs at P33 and P100, which under normal conditions harbors slow-cycling progenitor cells. In anagen (P33) few HFSCs were detected reported to be actively cycling (BrdU positive) in ctr mice (0.9+/-0.6/HF), however the number of BrdU positive cells was significantly increased in aPKCλ$^{-/-}$ SCs (3.1+/-0.2/HF). This result further supports that aPKCλ$^{-/-}$ bulge SCs have lost their quiescent state (Fig. 2.11C). The data suggest that aPKCλ is important to balance proliferation of keratinocytes during epidermal homeostasis, especially in the HFSC compartment.

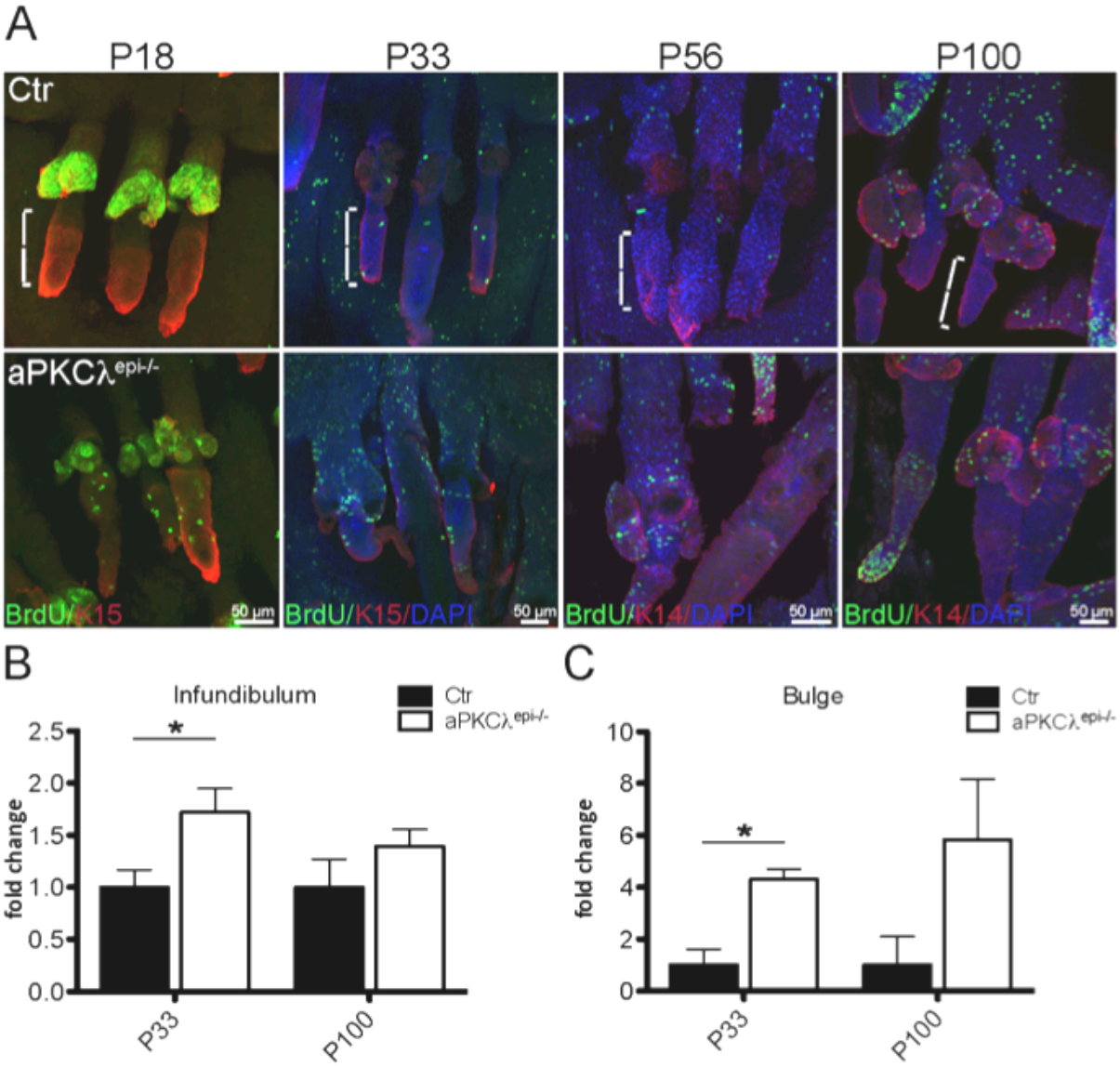

Figure 2. 11: Increased proliferation in the HFSC compartment of aPKCλ$^{epi-/-}$ mice

(A) Whole-mount immunofluorescent staining of BrdU and K14 of tail skin of the indicated genotypes and postnatal (P) days. Nuclei were counterstained with DAPI. White brackets mark HF bulge region. (B) Quantification of BrdU positive cells in the infundibulum of HFs from adult mice of the indicated genotypes and postnatal (P) days. BrdU positive cells were quantified after a short BrdU (100 mg/ml, 0.5 hrs) pulse before sacrifice. N > 4 mice for each genotype. Data are presented as mean +/-SD. *= P<0.05. (C) Quantification of BrdU positive cells in the HF bulge region of the indicated genotypes and postnatal (P) days. The bulge region was identified during the quantifications by co-staining with K15 (data not shown). BrdU positive cells were quantified after a short BrdU (100 mg/ml, 0.5 hrs) pulse before sacrifice. N > 4 mice for each genotype. Data are presented in mean +/-SD. *= P<0.05.

2.5.3 Loss of bulge SC homeostasis in aPKCλ$^{-/-}$HF

The observed changes of differentiation of all epidermal lineages in combination with altered HFSC activation raised the question if this was accompanied by changes in SC identity and function. To this end, HFSC marker expression and localization was analyzed in 2nd telogen HFs (P58) in detail (Jaks et al., 2010). Staining of the widely used bulge-specific surface marker CD34 was strongly decreased in aPKCλ$^{-/-}$ HFs. The loss of the CD34 positive cells correlated with aPKCλ$^{-/-}$ HF phenotypic severity. If, in rare cases, follicles were still detected to have a telogen-like appearance, a weak signal for CD34 was observed. However, when the HF displayed a striking aPKCλ$^{-/-}$ phenotype (anagen-like appearance, widened infundibulum), no CD34 expression could be detected (Fig. 2.12A). Next, HFSCs were quantified by FACS using antibodies to α6-integrin as marker for basal keratinocytes and to CD34 (Blanpain et al., 2004). These experiments further confirmed a significant reduction of CD34 positive bulge SCs in 2nd telogen (Fig. 2.12B).

Furthermore, we analyzed the expression of the transcription factor Sox9, whose expression is restricted to bulge SCs and is crucial for HFSC specification and HF differentiation (Nowak et al., 2008; Vidal et al., 2005). During telogen, Sox9 is described to localize to bulge HFSCs but not in P-cadherin positive cells of the secondary hair germ, whereas in anagen Sox9 is present abundantly throughout the HF region below the bulge. Sox9 is absent from the lower part of the HF and Infundibulum (Vidal et al., 2005). Immunohistochemical analysis showed that the hair germ, marked by expression of P-cadherin, seems to be expanded in aPKCλ$^{-/-}$ HFs. Strikingly, analysis of telogen (P58) aPKCλ$^{-/-}$ HFs revealed overlapping localization patterns of P-cadherin and Sox9. As expected, Sox9 positive cells were observed in K15 positive bulge SCs of both ctr and aPKCλ$^{-/-}$ HF, despite the K15 positive cell population being strongly reduced in aPKCλ$^{-/-}$ HFs. Notably, ectopic Sox9 expression in K15 negative cells was observed in aPKCλ$^{-/-}$ HFs (Fig. 2.12C). In addition, the bulge SC marker CD34 and K15 were analyzed by qRT-PCR. The mRNA levels of CD34 and K15 were significantly reduced P33 aPKCλ$^{epi-/-}$ mice compared to ctr mice (Fig. 2.12D).

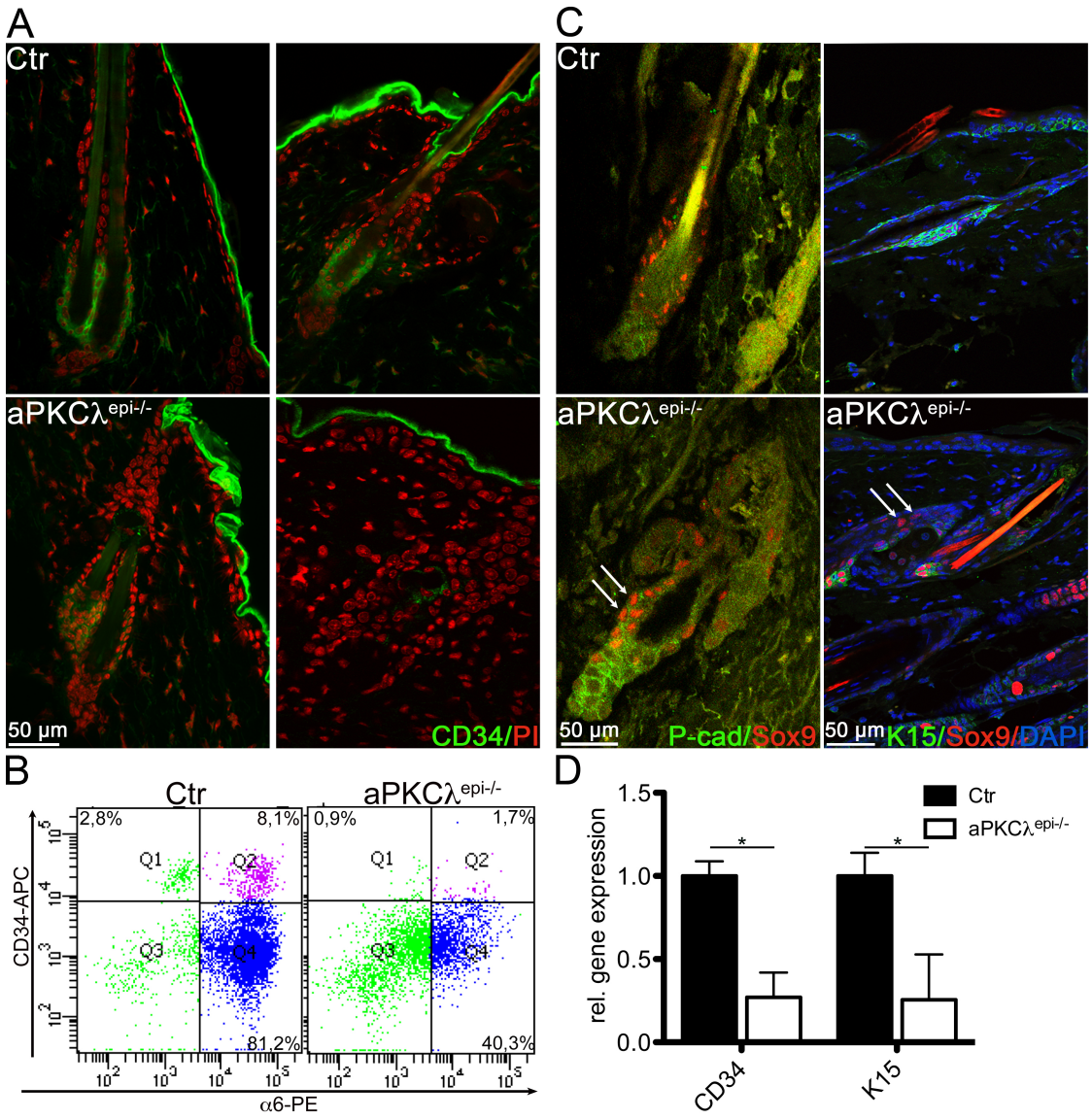

Figure 2. 12: Altered localization of stem cell markers after loss of aPKCλ

(A) Immunofluorescent staining of CD34 on paraffin sections of P58 ctr and aPKCλ$^{epi-/-}$ back skin. Nuclei were counterstained with prodidium iodide (PI). (B) FACS analysis of keratinocytes isolated from P58 ctr and aPKCλ$^{epi-/-}$ mice. FACS encompasses surface expression of α6-Integrin (α6-PE) and CD34 (CD34-APC). The percentage of the respective cell populations is noted in the borders of the plot. (C) Immunofluorescent staining of Sox9 and P-cadherin or Sox9 and K15 on cyro-preserved sections of dorsal skin from 58 day old mice. In the right panel, nuclei were counterstained with DAPI. (D) QRT-PCR analysis of either CD34 or K15 expression using RNA from epidermal splits isolated P33 mice of the indicated genotypes. N=5 RNA isolations from independent mice for each genotype. Data are presented as mean +/-SD. *= P<0.05.

Overall, these data demonstrate that localization and expression of HFSC markers is affected upon deletion of epidermal aPKCλ, suggesting that homeostasis of the bulge SC niche is perturbed.

2.5.4 Enhanced population of infundibulum-localized progenitor cells

Multipotent progenitors are described to reside between the IFE and the HF bulge adjacent to the SG and are characterized by the expression of the transmembrane protein Lrig1 or the epitope MTS24 (Jensen et al., 2009; Depreter et al., 2008). We next examined whether loss of HFSC marker expression in aPKCλ$^{-/-}$ HFs was accompanied by altered localization of more differentiated progenitor populations. Immunohistochemical analysis of Lrig1 localization revealed a strongly increased Lrig1 signal in aPKCλ$^{-/-}$ HF compared to ctr HFs (Fig. 2.13A). Lrig1 positive signal is described to occur in the ORS of the ctr anagen HF, below the SG extending toward the bulge (Jensen et al., 2009). This localization pattern was observed in aPKCλ-deficient HF irrespective of the hair cycle stage (P9, P18, P33, P58, P77, P100). Moreover, increased Lrig1 signal was observed in the upper infundibulum of aPKCλ$^{-/-}$ follicles, a region negative for Lrig1 in ctr follicles (Fig. 2.13A, white arrows). Quantification by FACS revealed a 2 fold increase in Lrig1 positive cells in P58 aPKCλ$^{-/-}$ HF (data not shown). Additionally, we used the MTS24 antibody to analyze a progenitor population residing in the upper isthmus zone. The epitope for MTS24 has recently been identified to correspond to Plet1, a protein also expressed in more differentiated keratinocytes in the HF (Raymond et al., 2010; Depreter et al., 2008). Consistent with stronger Lrig1 signals in aPKCλ-deficient follicles we also observed a striking increase in the MTS24 positive cell population throughout the hair shaft of aPKCλ$^{-/-}$ follicles. Moreover, MTS24 positive signal was detected in aPKCλ$^{-/-}$ SGs (Fig. 2.13B, white arrows). Interestingly, the enhanced signal for MTS24/Lrig1 in aPKCλ-deficient compared to ctr follicles was more pronounced in later telogen (P58) than in earlier anagen (P33) stages, suggesting a gradual enhancement of this population. In summary, the analysis suggests an expanded population of progenitor cell populations located in the upper part of the HF.

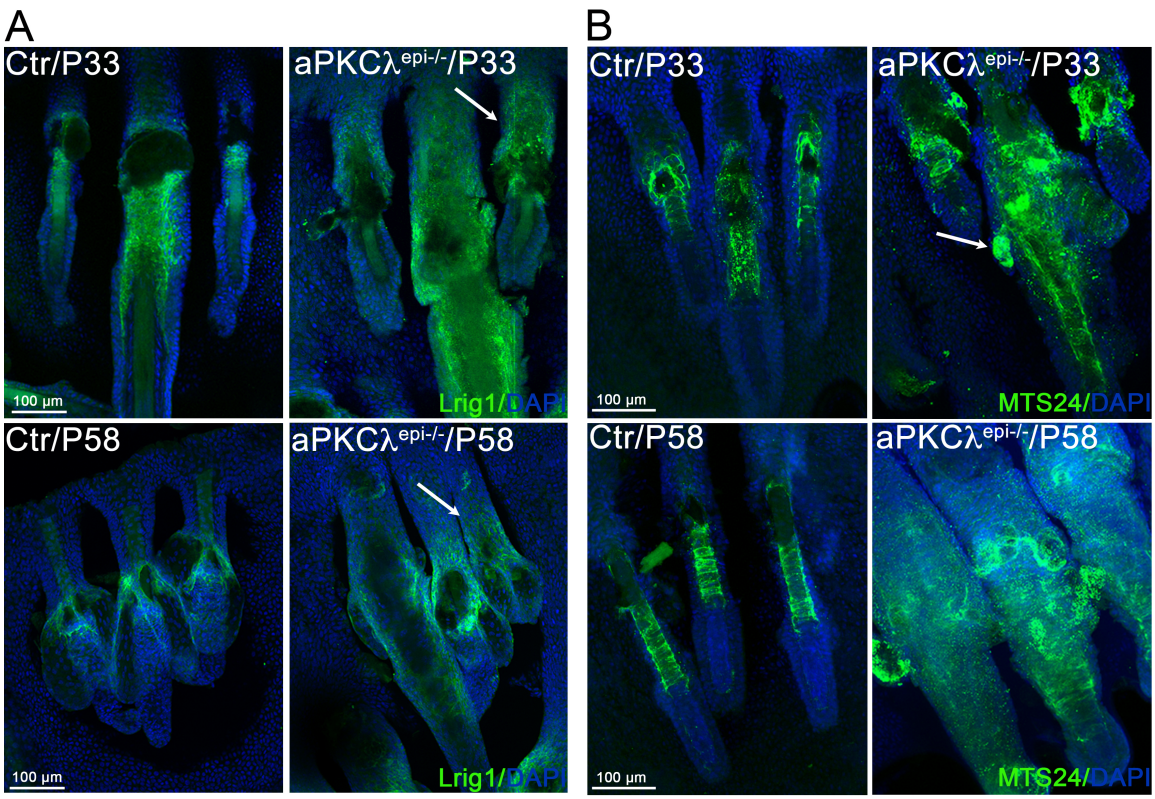

Figure 2. 13: Enhanced population of Lrig1/MTS24 positive progenitors in aPKCλ$^{epi-/-}$HF.

(A) Immunofluorescent staining of Lrig1 on whole-mounts of tail epidermis of P33 or P58 ctr and aPKCλ$^{epi-/-}$ mice. Nuclei were counterstained with DAPI. White arrows indicate ectopic Lrig1 localization in the infundibulum zone of aPKCλ$^{epi-/-}$ HFs. (B) Immunofluorescent staining of MTS24 on whole-mounts of tail epidermis of P33 or P58 ctr and aPKCλ$^{epi-/-}$ mice. Nuclei were counterstained with DAPI. White arrow indicates MTS24/Plet1 positive SGs in aPKCλ$^{epi-/-}$ HFs.

aPKCλ$^{epi-/-}$ HFs display a loss of bulge SC marker expression together with expanded Lrig1 or MTS24 populations. These findings suggest that cell fate of quiescent aPKCλ$^{-/-}$ bulge SCs is altered towards the MTS24 and Lrig1 expressing fate in the infundibulum zone.

2.5.5 Unaltered progenitor cell population in embryonic aPKCλ$^{-/-}$ skin

Bulge niche architecture is not defined until 3 weeks of postnatal life of the mice, however during embryogenesis several HFSC marker, as for example Sox9 and Lrig1, are co-expressed and referred to as early progenitor markers (Nowak et al., 2008; Jensen et al., 2009). To analyze whether the aPKCλ$^{-/-}$ phenotype of altered SC homeostasis is already pronounced during embryonic morphogenesis, we investigated the expression of prenatal SC markers. Analysis of Sox9 localization revealed no major differences in embryonic epidermis (E16.5) and the quantification of Sox9 positive cells supported no significant differences between ctr and aPKCλ$^{epi-/-}$ mice (Fig. 2.14A+B). In line with these findings, the localization and amount of Lrig1 positive cells were not majorly altered at E16.5 (Fig. 2.14C). These findings suggest that the homeostasis of embryonic progenitor cell compartments is not affected by epidermal aPKCλ deletion.

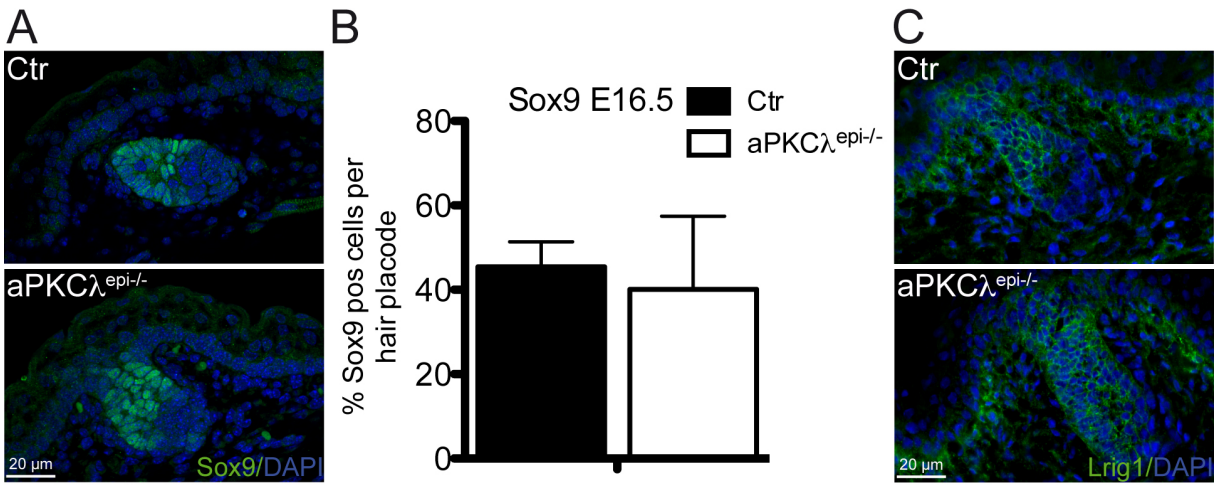

Figure 2. 14: Embryonic SC marker expression is not affected by aPKCλ deletion

(A) Immunofluorescent staining of Sox9 on paraffin sections of E16.5 dorsal skin of the indicated genotypes. Nuclei were counterstained with DAPI. (B) Quantification of Sox9 positive cells in back skin of E16.5 ctr and aPKCλ$^{epi-/-}$ embryos. N=4 mice for each genotype. Data are presented in mean +/-SD. (C) Immunofluorescent staining of Lrig1 on cryo-preserved sections of E16.5 dorsal skin of the indicated genotypes. Nuclei were counterstained with DAPI.

2.6 Gradual development of the HFSC phenotype in ageing mice

2.6.1 Gradual loss of aPKCλ$^{-/-}$ bulge stem cells with ageing

The phenotype of aPKCλ$^{epi-/-}$ mice gradually develops through postnatal life. To investigate in more detail at which time-point the phenotype of altered SC homeostasis arises in aPKCλ$^{-/-}$ mice, the expression of the bulge SC markers K15 and S100a6 was analyzed during first anagen (P33) and at several earlier time-points (data not shown). For both SC markers, no major differences in signal intensity or number of positive cells was observed during these early time points, showing that niche identity was maintained until P33 (Fig. 2.15A). As opposed to the findings at P33, in 2nd telogen (P58), no distinct bulge structure could be identified after staining for K15 or S100a6 (Fig. 2.15B). These data suggest that loss of SCs after aPKCλ deletion occurs either hair cycle-dependently or develops gradually during ageing.

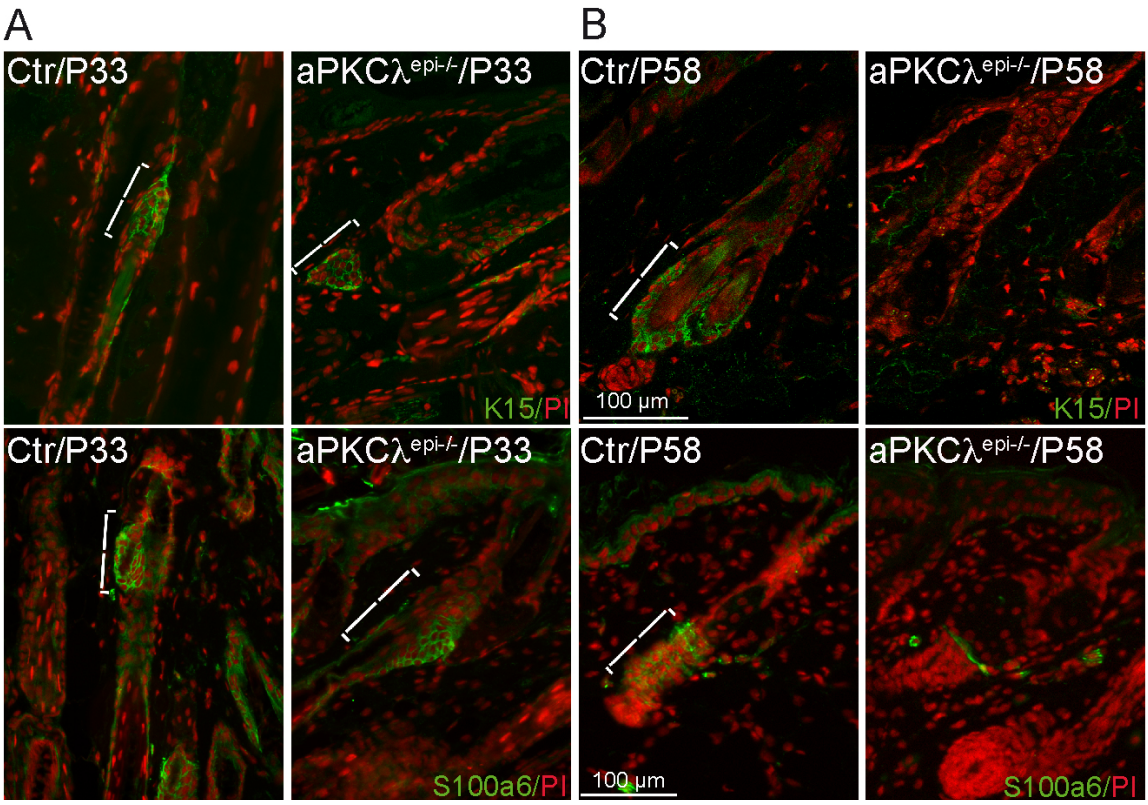

Figure 2. 15: Loss of bulge SC marker espression in aPKCλ$^{epi-/-}$ mice with ageing

(A) Immunofluorescent staining of K15 (upper panel) or S100a6 (bottom panel) on anagen ctr and aPKCλ$^{epi-/-}$ dorsal skin. Nuclei were counterstained with propidium iodide (PI). White brackets mark the bulge region of the HFs. (B) Immunofluorescent staining of K15 or S100a6 on telogen ctr and aPKCλ$^{epi-/-}$ dorsal skin. Nuclei were counterstained with propidium iodide (PI). White brackets mark the bulge region of HFs.

Next, the number of bulge-SCs was quantified on the basis of cell surface markers α6-integrin and CD34 by FACS at several postnatal time-points (Fig. 2.16A). This study clearly revealed that the percentage of α6-Integrin+/CD34+ (α6-Int+/CD34+) double positive bulge SC gradually decreased during ageing of aPKCλ$^{epi-/-}$ mice, whereas the number of this cell population remained relatively constant in ctr mice (Fig. 2.16B).

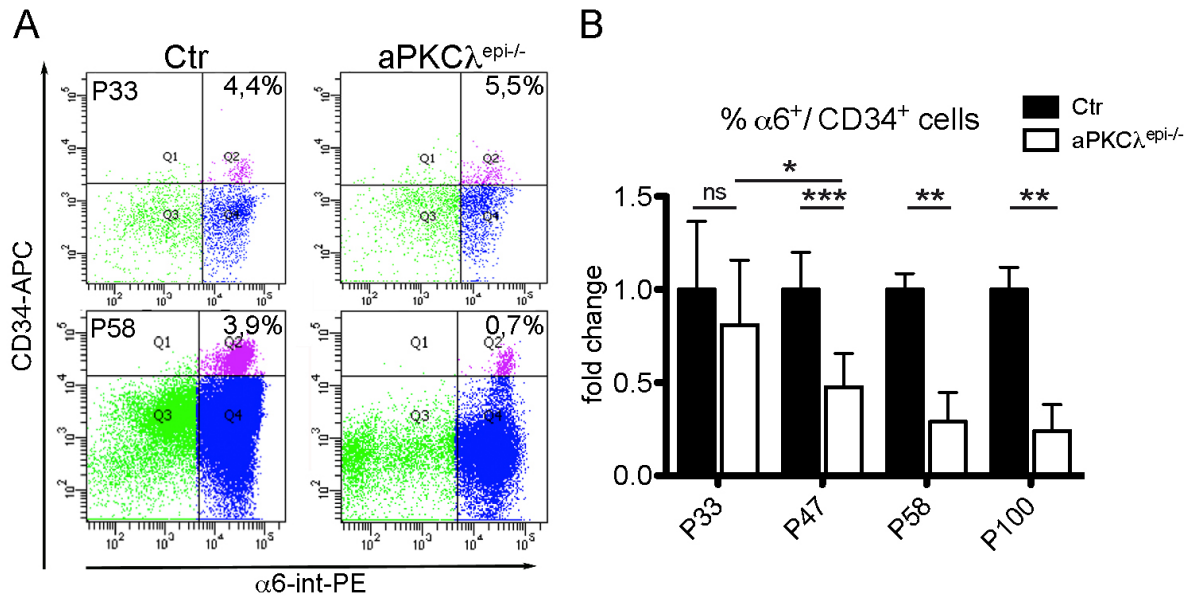

Figure 2. 16: Gradual decrease of CD34 positive cells after aPKCλ deletion

(A) FACS analysis of keratinocytes isolated from P33 versus P58 ctr and aPKCλ$^{epi-/-}$ mice. FACS encompasses surface expression of α6-Integrin (α6-PE) and CD34 (CD34-APC). The percentage of the respective cell populations is noted in the borders of the plot. (B) Quantification of the percentage of α6Integrin and CD34 positive (α6Int^{+}/CD34^{+}) cells by FACS at several postnatal (P) days. The percentage of α6Int^{+}/CD34^{+} cells in the matched ctr animals was set as 100%. N >5 independent cell isolations for each genotype. Data are presented in mean +/-SD. ns= p>0,5;*= p<0.05; **= p<0.01; ***=p<0.001.

aPKCλ- deficient mice regrew their hair faster than ctr mice when shaved at first telogen (P18). This result suggests that aPKCλ$^{-/-}$ HFSC maintain their proliferating, activated state However, P58 aPKCλ$^{-/-}$ mice were not able to grow hair back as efficient as ctr mice after shaving, suggesting that perturbed SC homeostasis overcomes the effect of increased proliferation in older age (data not shown). The above-presented data demonstrate that aPKCλ is crucial for maintenance of the CD34 positive bulge HFSC compartment throughout postnatal life.

2.6.2 Gradually increased progenitor cells in the infundibulum during ageing

If bulge SCs change their cell fate towards progenitors expressing the marker MTS24 and Lrig1, then the gradual loss of α6-Int+/CD34+ double positive bulge should be accompanied by an increase in MTS24 and Lrig1 expression over time. Immunohistochemical analysis of Lrig1 localization in 100 days old mice revealed an even more pronounced enlargement of the Lrig1-positive cell population when compared to P58 or P33 mice (Fig. 2.17A, compare Fig. 2.13A). Since FACS quantification of Lrig1 did not offer reproducible results, we focused on the quantification of MTS24 positive cells by FACS analysis at several postnatal time points. Determining of the percentage of MTS24 positive cells revealed a significantly 2.5 fold increase of MTS24 positive cells in P58 aPKCλ$^{epi-/-}$ compared to P33 aPKCλ$^{epi-/-}$ HF.

However, this increase in the percentage of MTS24 positive cells may be temporary as the effect was less pronounced in aPKCλ$^{epi-/-}$ HF from 100 day old mice (Fig. 2.17B).

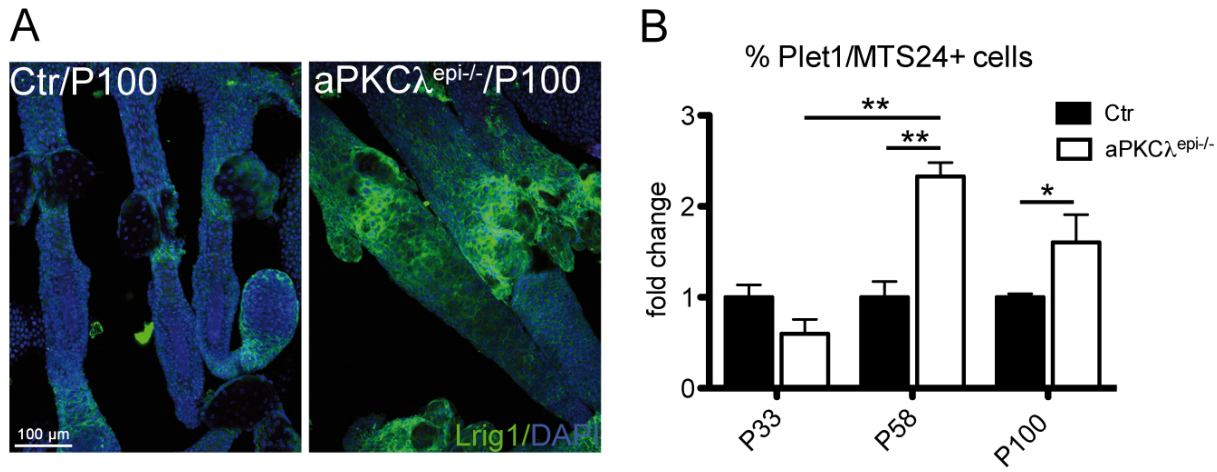

Figure 2. 17: Gradual increase of Plet1/MTS24 positive cells in aPKCλ$^{epi-/-}$ HF

(A) Immunofluorescent staining of Lrig1 on whole-mounts of tail epidermis of P100 ctr and aPKCλ$^{epi-/-}$ mice. Nuclei were counterstained with DAPI. (C) Quantification of the expression of the cell surface marker MTS24 by FACS at several postnatal (P) days. The percentage of Plet1/MTS24 positive cells in respective ctr animals was set as 100%. N =3 cell isolations from independent mice for each genotype. Data are presented in mean +/-SD. *= p<0.05; **= p<0.01.

These data indicate that aPKCλ$^{-/-}$ progenitors gradually change their cellular fate from quiescent bulge SCs towards more committed progenitor cells residing above the bulge region.

2.6.3 Altered growth behavior and morphology in aPKCλ$^{-/-}$ keratinocytes

To investigate whether aPKCλ-deficient keratinocytes show a cell autonomous phenotype *in vitro*, primary keratinocytes from newborn (P0) and adult (P30) mice were compared regarding growth behavior und morphology. Due to the gradual development of the aPKCλ$^{epi-/-}$ phenotype, we hypothesized that adult aPKCλ$^{-/-}$ keratinocytes would exhibit a more pronounced phenotype compared to newborn aPKCλ$^{-/-}$ keratinocytes. Newborn aPKCλ$^{-/-}$ keratinocytes exhibited a slightly more differentiated but overall comparable morphology and size as cells isolated from ctr littermates. In contrast, in line with the increased expression of differentiation markers *in vivo*, aPKCλ$^{-/-}$ keratinocytes isolated from adult mice displayed, a much more differentiated appearance and a larger cell size than ctr keratinocytes (Fig. 2.18A). Fitting with increased BrdU incorporation *in vivo*, newborn aPKCλ$^{-/-}$ keratinocytes reached confluency much faster than ctr keratinocytes when plated at the same density. Moreover, newborn aPKCλ$^{-/-}$ keratinocytes displayed increased BrdU incorporation *in vitro* (Fig. 2.18B, upper panel). In contrast, adult aPKCλ$^{-/-}$ keratinocytes showed the opposite behavior: these cells grew much slower than ctr keratinocytes and incorporated significantly

less BrdU *in vitro* (Fig. 2.18B, bottom panel). Keratinocytes isolated from even older aPKCλ$^{-/-}$ mice (P58, P100) could not be cultured with the herein applied protocol, suggesting that these cells had lost the ability to proliferate (data not shown). These *in vitro* data demonstrate that adult aPKCλ$^{-/-}$ keratinocytes show a different phenotype when compared to newborn aPKCλ$^{-/-}$ keratinocytes and supports that alterations in growth behavior in aPKCλ$^{epi-/-}$ epidermis are cell autonomous effects. The results underline that the aPKCλ$^{epi-/-}$ phenotype is developing during ageing of the mice.

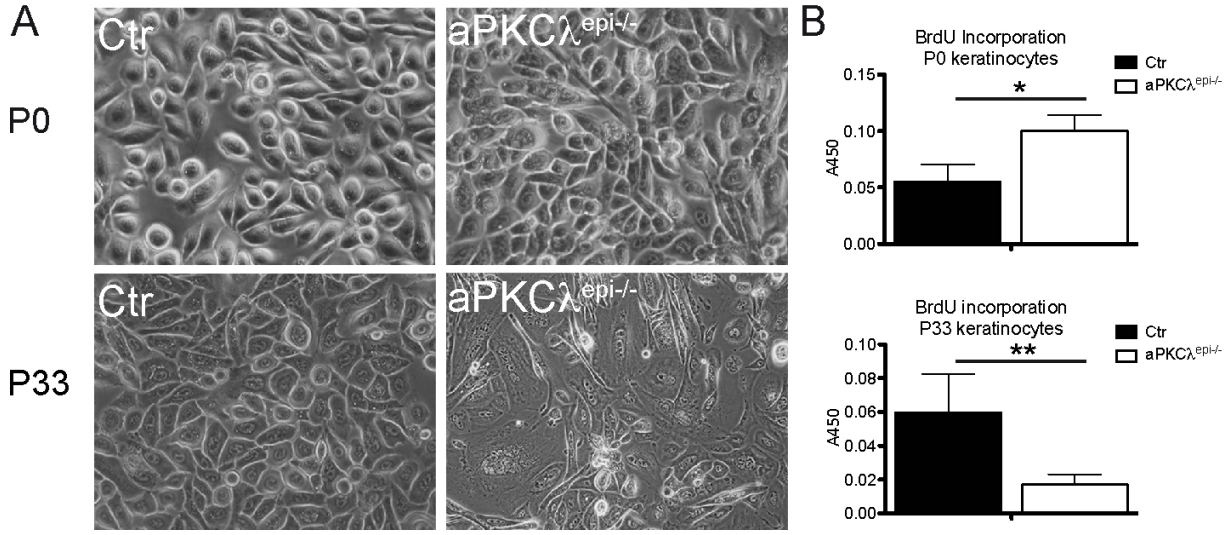

Figure 2. 18: Opposing behavior of aPKCλ$^{-/-}$ keratinocytes isolated from newborn vs. adult mice

(A) Primary ctr and aPKCλ$^{-/-}$ keratinocytes isolated from either newborn (P0) or adult (P33) mice. (B) Colorimetric BrdU incorporation assays using ctr and aPKCλ$^{epi-/-}$ P0 (upper panel) or P33 (bottom panel) primary keratinocytes. 3 independently isolated cell lines of passage 0-3 were compared for each genotype. Data are presented as mean +/- SED. *= p<0.05; **= p<0.01.

2.6.4 Loss of proliferative potential in aPKCλ$^{-/-}$ keratinocytes

Reduced proliferation of aPKCλ$^{-/-}$ keratinocytes *in vitro* (s. 2.6.3) may be due to a lack of progenitor cells in keratinocytes isolated from adult aPKCλ$^{epi-/-}$ mice. The ability of HFSCs to proliferate and differentiate can be tested *in vitro* by colony forming assays (CFAs). When primary keratinocytes are plated in low density in CFAs, multicompetent SCs give rise to large colonies, whereas more committed cells generate colonies of moderate size and cultivation of differentiated cells leads to formation of small abortive clones (Barrandon and Green, 1985; Morris and Potten, 1994). CFAs using keratinocytes isolated from newborn aPKCλ$^{epi-/-}$ mice were highly variable, but in most cases an increased number of colonies were counted. Interestingly, these colonies were smaller than colonies formed by ctr cells, indicating a reduced number of progenitor cells with high proliferative potential (Fig. 2.19A). The increased number of aPKCλ$^{-/-}$ colonies could be due to differing adhesive behavior of

the cells, however attachment and cell spreading of ctr and aPKCλ$^{-/-}$ cells was monitored *in vitro* and no differences were observed (data not shown). In adult mice, the result was much more dramatic: Colony-formation was nearly abolished in adult aPKCλ-deficient keratinocytes compared to ctr keratinocytes. A complete loss of colonies of a size > 1mm was observed, demonstrating that the progenitor cell population with high proliferative potential is strongly reduced (Fig. 2.19B).

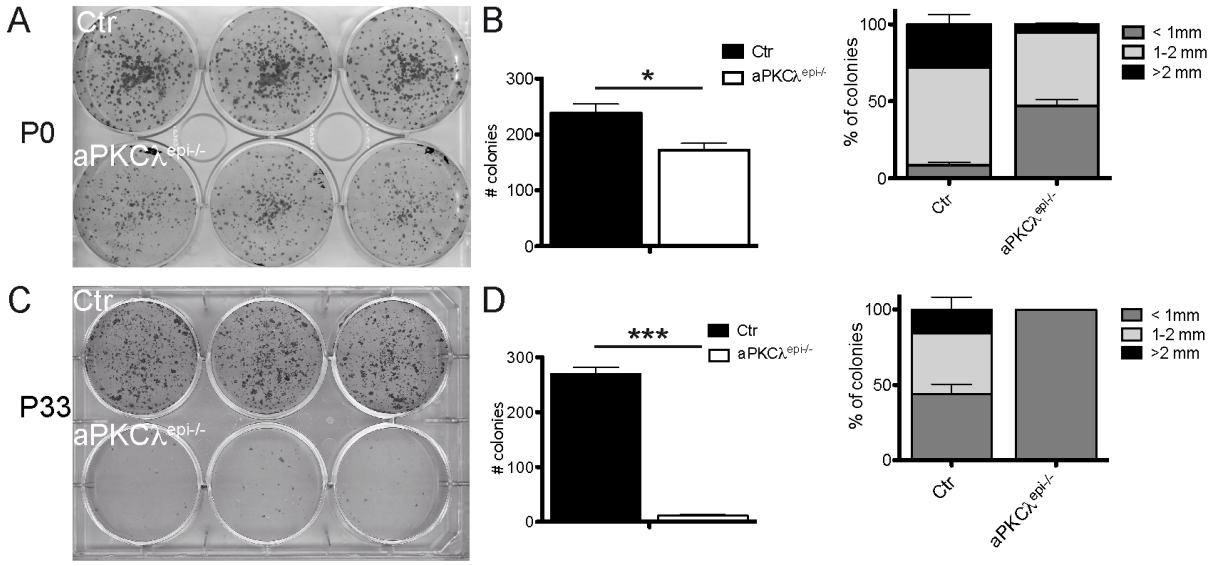

Figure 2. 19: aPKCλ affects the *in vitro* proliferative potential of keratinocytes

(A) Representative example of a colony-forming assay using primary keratinocytes from newborn (P0) ctr and aPKCλ$^{epi-/-}$ mice. (B) Quantification of the number of colonies and the size of colonies for (A). N=14 independent cell isolations for each genotype. Data are presented in mean +/-SD. *=P<0.05. (C) Right: Representative example of a colony-forming assay using primary keratinocytes isolated from adult (P33) ctr and aPKCλ$^{epi-/-}$ mice. (D) Quantification of the number of colonies and the size of colonies for (C). N=7 independent cell isolations for each genotype. Data are presented as mean +/-SD. ***=P<0.0005.

This result demonstrates that gradual decrease in the number of aPKCλ$^{-/-}$ bulge SCs is followed by loss of proliferative potential *in vitro*.

2.6.5 aPKCλ deletion leads to complete boldness and a striking epidermal phenotype

To examine how the gradually developing aPKCλ$^{epi-/-}$ phenotype is pronounced at later postnatal time-points, we analyzed 1-year-old mice. These older aPKCλ$^{epi-/-}$ mice showed an even more pronounced macroscopic phenotype than younger animals and harbored characteristics of a premature ageing phenotype (compare to 2.3). For example, aPKCλ$^{epi-/-}$ mice exhibited complete alopecia (in rare cases, sparse fur was still detectable in the facial region). Moreover, all mice showed an even more pronounced eye phenotype and 100% of aPKCλ-depleted mice displayed clouded lenses (cataract) (Sugiyama et al., 2009). Strikingly, several skin lesions were detectable across the whole body (Fig. 2.20A). Histological analysis revealed a noticeable epidermal phenotype. The IFE was thicker and the Infundibulum widened in aPKCλ$^{-/-}$ epidermis as compared to ctr epidermis. Whereas ctr HFs seemed to be in catagen or telogen, aPKCλ$^{epi-/-}$ HF displayed such striking morphological changes that hair cycle stages could not be classified. Importantly, 75% of HFs exhibited degeneration of the lower part of the HF. If the HFs were not degenerated, they showed a significant increase in length and volume (Fig. 2.20B/C). The aPKCλ$^{-/-}$ SG compartment has even enlarged further as compared to younger mice. The histological analysis of later stage enlarged SGs is strongly suggestive of ectopic SG formation (Fig. 2.20B, upper panel). Finally, many richly dendritic melanocyte-like cells were detectable in the dermal compartment near the HFs of aPKCλ$^{epi-/-}$ skin (Fig. 2.22B middle and lower panel). In ctr skin, cells of this morphology are mainly detected in the bulb of HFs.

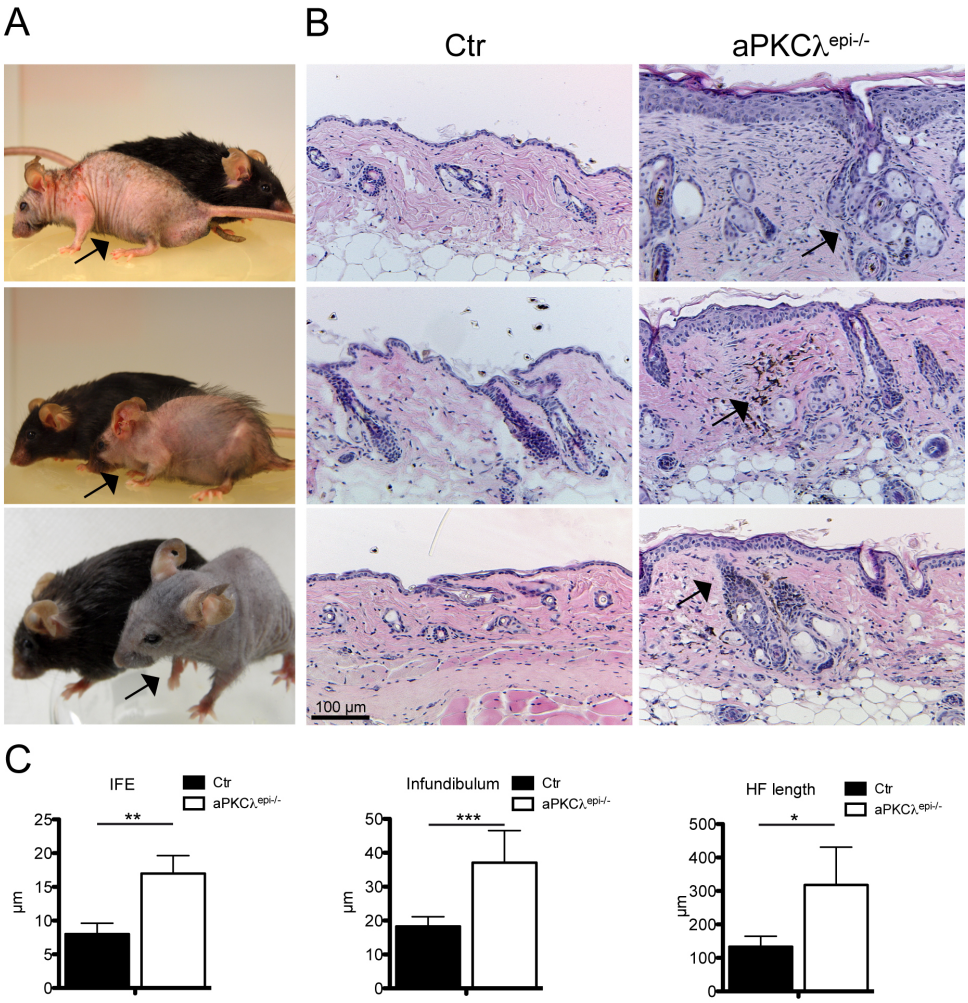

Figure 2. 20: One year old aPKCλ$^{epi-/-}$ mice show degenerated HFs and enlarged SGs

(A) Macroscopic appearance of 365 days old aPKCλ$^{epi-/-}$ mice (black arrows) and ctr littermates. (B) H&E staining of paraffin sections of back skin from mice from the one year old ctr and aPKCλ$^{epi-/-}$ mice. Arrows indicate ectopic SGs and melanocytes. (C) Quantification of the thickness of the IFE, width of the infundibulum and length of HF from one year old mice using H&E stainings of dorsal skin paraffin sections for measurements. N=4 different mice for each genotype. Data are presented as mean +/- SD. *= p<0.05; **= p<0.01; ***=p<0.001.

2.6.6 aPKCλ$^{epi-/-}$ mice exhaust their bulge SC compartment eventually

To better characterize the SC compartment in aged aPKCλ$^{epi-/-}$ and ctr mice, FACS analysis to quantify the percentage of α6-Int+/CD34+ versus α6-Int+/CD34- keratinocytes was performed. As expected, the CD34-expressing bulge SC population was significantly diminished in one year old aPKCλ$^{epi-/-}$ HFs (Fig. 2.21A). We detected a decreased percentage of MTS24 positive cells in one year old mice compared to earlier time points (Fig. 2.21B). However, the population of Lrig1 expressing progenitors seemed, as judged by immunohistochemistry, enlarged in aPKCλ$^{epi-/-}$ compared to ctr mice suggesting the populations of Lrig1 and MTS24 are differentially affected by the loss of bulge SCs (Fig. 2.21C).

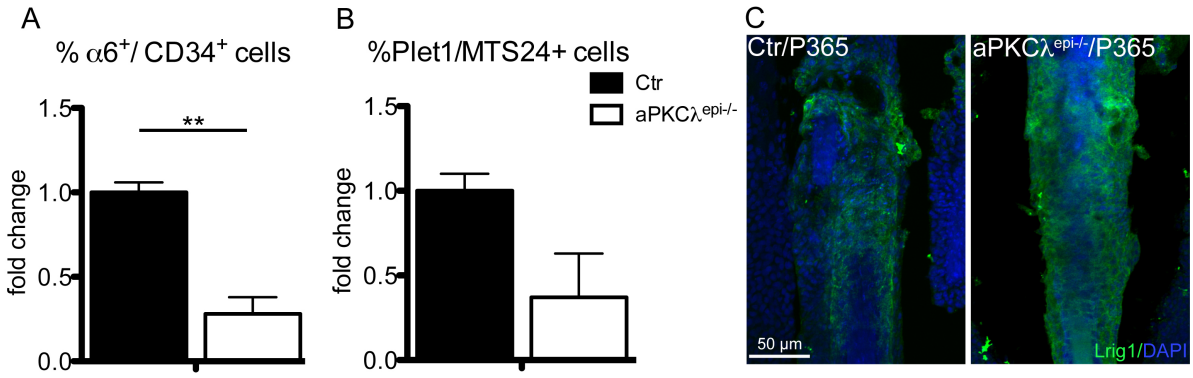

Figure 2. 21: Bulge SC exhaustion in one year old aPKCλ$^{epi-/-}$ mice

(A) Quantification of cells expressing α6-Intergin (α6) and CD34 by FACS at P365. The percentage of α6-Int^{+}/CD34^{+} cells in the respective ctr animals was normalized to 100%. N=4 independent cell isolations for each genotype. Data are presented as mean +/-SD. **= p<0.01 (B) Quantification of cells expressing MTS24 by FACS at P365. The percentage of Plet1/MTS24 positive cells in ctr animals was normalized to 100%. N =3 independent cell isolations for each genotype. Data are presented in mean +/-SD. (C) Immunofluorescent staining of Lrig1 on whole-mounts of tail epidermis of P365 ctr and aPKCλ$^{epi-/-}$ mice. Nuclei were counterstained with DAPI.

2.7 The SC phenotype is a morphogenetic phenotype

To investigate, whether aPKCλs role in SC maintenance is important during development or if aPKCλ is exclusively required for adult SC homeostasis, aPKCλ$^{fl/fl}$ mice were crossed to K14CRE^{ERT2} mice. The K14-Cre^{ERT2} allele encodes the Cre recombinase fused to a murine estrogen receptor with a mutant hormone binding domain (ERT2), which fails to bind estrogen but instead responds to the synthetic ligand 4-hydroxytamoxifen (Tam) (Stratis et al., 2006; Littlewood et al., 1995). aPKCλ deletion was tested by genotyping PCRs for the aPKCλ gene. The mice showed, as previously reported (Stratis et al., 2006), a spontaneous deletion of aPKCλ in some non-treated K14CRE^{ERT2},aPKCλ$^{fl/fl}$ mice. However, when fed for 3 weeks with Tam, a strong deletion band was observed in K14CRE^{ERT2},aPKCλ$^{fl/fl}$ mice (aPKCλ$^{indepi-/-}$), which was significantly stronger than the deletion band detected in non-Tam-fed mice (Fig. 2.22A, right lane). To test, if postnatal loss of aPKCλ is sufficient to recapitulate the aPKCλ$^{epi-/-}$ phenotype, two feeding protocols were established. The mice were fed for three weeks with Tam-food, and sacrificed either three weeks (35 days chase period), or five weeks (65 days chase period) after switching to normal food. Regardless of the latency period, aPKCλ$^{indepi-/-}$ mice did not develop a specific macroscopic phenotype comparable to aPKCλ$^{epi-/-}$ mice, which is characterized by alopecia. Analysis of skin histology showed that mice with postnatal deletion of aPKCλ developed a hyperkeratized epidermis. Tam treatment in mice not expressing K14Cre^{ERT2} also showed a slight thickening of the IFE, suggesting that Tam treatment alone might be sufficient to induce epidermal proliferation. Nevertheless, the epidermis of aPKCλ$^{indepi-/-}$ was consistently thicker than ctr epidermis.

Moreover, aPKCλ$^{indepi-/-}$ showed a tendency towards increased HF and SG size similar to aPKCλ$^{epi-/-}$ mice (Fig. 2.22B), though detailed quantification would aid the interpretation of the obtained data.

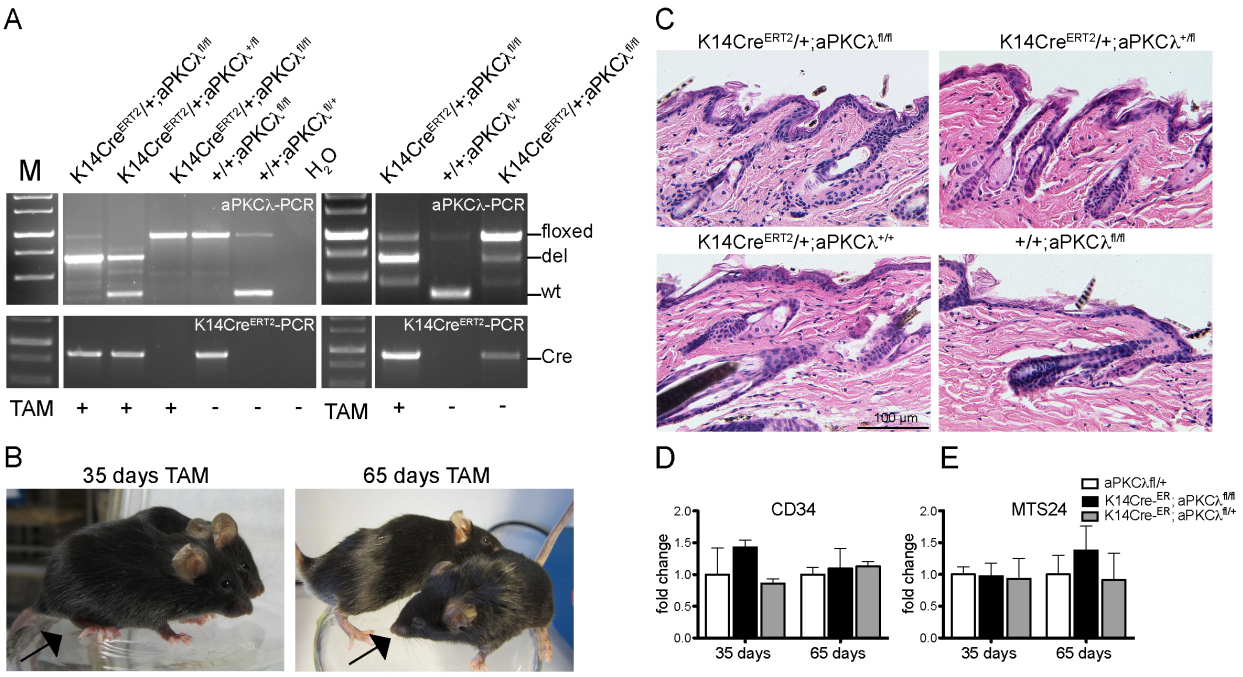

Figure 2. 22: Inducible deletion of aPKCλ does not result in a macroscopic or SC phenotype

(A) PCR genotyping using aPKCλ-specific and K14-Cre-specific primers on genomic DNA isolated from tail biopsies showing the different genotypes of the mice. Feeding for 21 days with (+) or without (-) Tam is denoted below each lane. += wildtype; fl= floxed (B) Macroscopic appearance of mice is shown 35 days or 65 days after start of Tam feeding. In each picture, aPKCλ$^{indepi-/-}$ mice (marked by black arrows) and ctr littermates are shown. (C) H&E staining of paraffin sections of back skin from adult (P58) mice of the indicated genotypes sacrificed 35 days after start of Tam feeding. (D) Quantification of expression of α6-Intergin and CD34 by FACS 35 or 65 days after Tam feeding. The percentage of α6Int^{+}/CD34^{+} cells in the respective ctr animal was set as 100%. N=3 for each genotype. Data are presented as mean +/-SD. (E) Quantification of expression of the cell surface marker MTS24 by FACS 35 or 65 days after Tam feeding. The percentage of MTS24 positive cells in respective ctr animals was set as 100%. N=3 for each genotype. Data are presented as mean +/-SD. For (B)-(E): K14-CreERT2, aPKCλ$^{fl/fl}$ animals, fed with normal food were analyzed in each experiment and showed no differences in phenotype or SC marker expression from ctr animals (data not shown).

To analyze the impact of the postnatal deletion of aPKCλ on the SC compartment, the percentage of α6Int/+CD34+ bulge HFSCs as well as of MTS24 expressing progenitor cells of the isthmus zone were determined. However, after 35 days or 65 chase period, no significant changes in the size of either the CD34 or MTS24 positive cell population was observed, indicating that induced deletion of aPKCλ did not strikingly impact the HFSC compartment (Fig. 2.22 D+E). These data suggest, that aPKCλ deletion during embryonic development is a prerequisite for the formation of the aPKCλ$^{epi-/-}$ phenotype.

2.8 Increased aymmetric cell division in aPKCλ$^{-/-}$ HFs

The above-presented data point towards cell fate changes of HFSCs in aPKCλ$^{epi-/-}$ mice. Since we detected increased ACD in adult IFE, we speculated that aPKCλ might regulate cell fate decisions of HF progenitors by balancing the ratio of ACD vs. SCD. Cells being in late anaphase/metaphase were identified by a condensed DAPI-appearance and a positive signal for Survivin. The axis of division was determined by measuring the angle between the plane transecting two dividing nuclei relative to the outer root sheath. Divisions were classified as asymmetric (45°-90°) or symmetric (0°-45°) (Fig.2.23A). Moreover, a "random" (30°-60°) angle was defined, however taking this parameter into account did not impact the outcome of the data and was therefore excluded in the final results (data not shown). The orientation of cell division in HF from newborn (P0), 6 days old (P6) and 33 days old (P33) mice was determined, since HFs of ctr vs. aPKCλ$^{epi-/-}$ mice are in comparable morphogenesis/anagen-like stages at these time-points. Quantification of divisions oriented in perpendicular to the ORS revealed a significantly increased percentage of ACD in all compartments of aPKCλ$^{-/-}$ HF compared to ctr HFs. In P0, P6 and P33 ctr follicles, 41(+/-10)% of divisions were oriented perpendicular to the ORS, whereas in HF from aPKCλ$^{epi-/-}$ mice, the percentage was enhanced to 60(+/-13)%. When the overall percentage of SCD in HFs was normalized to 1, a 0.5 fold reduction of ACDs towards SCDs was measured at all time points in ctr mice. In contrast, when SCDs were normalized to 1 in aPKCλ$^{epi-/-}$ HFs, a 1.5 fold increase of ACD towards SCDs was observed in aPKCλ$^{epi-/-}$ HFs at all time points investigated (Fig. 2.23B). We next asked whether increased ACD was specific for the bulge, the infundibulum or the cycling region of the HF between bulge and bulb of anagen follicles (herein referred to as hair shaft (HS)). At P33, where the bulge region was already formed, co-stainings for K15 were performed (data not shown) to distinguish between the HF sub-compartments bulge (K15 positive), infundibulum (above the K15 positive compartment) and hair shaft (HS; below the K15 positive compartment, above the hair bulb). In aPKCλ-deficient HFs, the effect of increased ACD was most pronounced and significantly increased 1.3 fold specifically in the infundibulum zone. When SCDs were normalized to 1, a tendency towards increased ACD (1 fold increase) was observable in the bulge region of both ctr and aPKCλ$^{epi-/-}$ HF. In contrast, in the HS and infundibulum of aPKCλ$^{epi-/-}$ HFs, the percentage of ACD was enhanced at least 1.5 fold, whereas it was reduced towards 0.5 fold in HSs and infundibula of ctr mice (Fig. 2.23C).

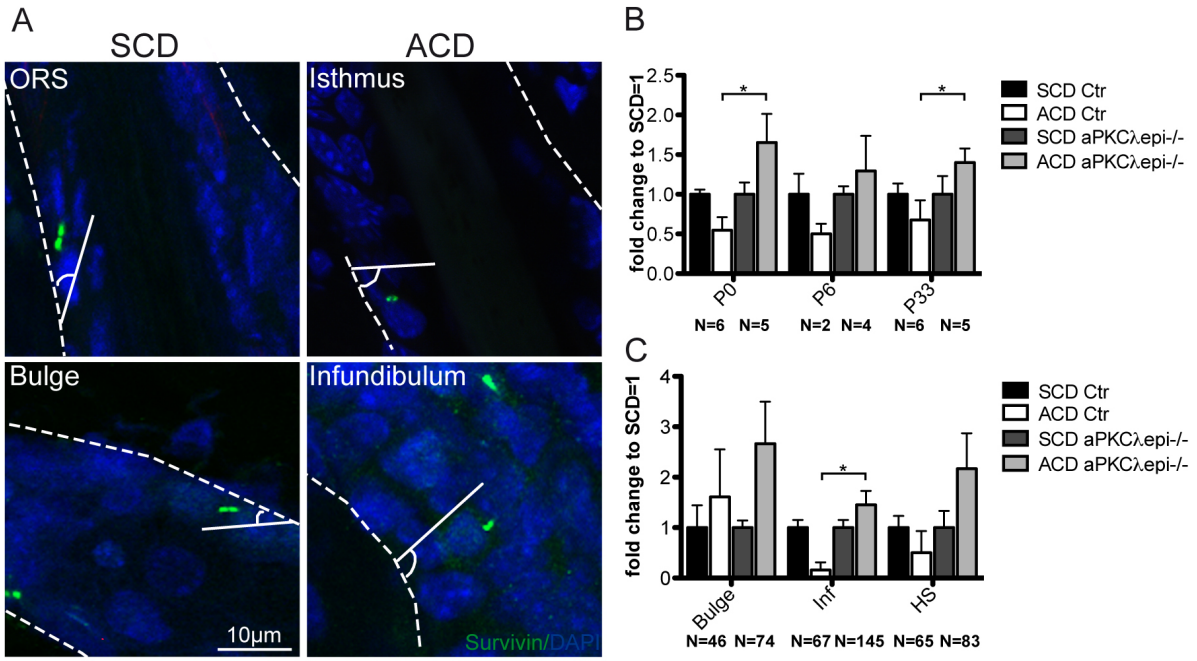

Figure 2. 23: aPKCλ controls spindle orientation in hair follicles

(A) Representative pictures of immunohistochemical staining of Survivin on dorsal skin sections of P33 ctr mice as used for the quantifications depicted in (B) and (C). Shown are examples of divisions classified to be symmetric cell divisions (SCD; left panel, angel between ORS and axis of Survivin doublet 0°-45°) and asymmetric cell divisions (ACD, right panel, angel between ORS and axis of Survivin doublet 45°-90°). The HF-subcompartments where divisions were detected are indicated (outer root sheath=ORS, isthmus (included in infundibulum quantification), infundibulum, bulge). Nuclei were counterstained with DAPI. (B) Quantification of ACD vs. SCD at several postnatal (P) days using skin sections from ctr and aPKCλ$^{epi-/-}$ mice. N= depicts the number of mice analyzed for each data point. 3 paraffin sections were counted for each mouse. Data are represented as mean +/- SD. SCD was set as 100%. *= P<0.05. (C) Quantification of ACD and SCD in different HF sub-compartments at P33 using skin sections from ctr and aPKCλ$^{epi-/-}$ mice. Inf=infundibulum, HS=hair shaft. N>5 different mice and 3 paraffin sections per mouse for each genotype. Data are represented in mean +/-SD. SCD was set as 100%. *= P<0.05. Numbers of analyzed divisions are denoted below the graph.

Overall, the data indicate that aPKCλ is crucial to maintain balanced spindle orientation in HFs, thereby controlling cell fate decisions and thus maintenance of HFSCs.

2.9 Increased asymmetric cell division in embryonic aPKCλ$^{-/-}$ epidermis

2.9.1 aPKCλ$^{-/-}$ controls spindle orientation in the embryonic epidermis

Adult aPKCλ$^{epi-/-}$ mice show increased ACD associated with altered differentiation. Inducible deletion of aPKCλ in adult mice suggests that aPKCλ is important during embryogenesis. To determine, whether spindle orientation was already affected by the aPKCλ$^{epi-/-}$ deletion during embryonic development, the angle of division in mitotic basal cells was measured at E16.5 (Fig. 2.24A). In line with previously reported numbers (Lechler and Fuchs, 2005), 61% of divisions were asymmetric in ctr basal cells. Basal divisions of aPKCλ$^{epi-/-}$ mice were biased towards asymmetric divisions: 80% of divisions were oriented perpendicular to the basement membrane. The fraction of divisions as classified to be random was slightly (3%), but not significantly increased in aPKCλ$^{epi-/-}$ mice compared to ctr mice. Interestingly, in accordance with the observations in aPKCλ- deficient adult IFE and HFs, the ratio of ACD versus SCD increased around 20% (Fig. 2.24B/C). This result implicates aPKCλ in the regulation of ACD also in the developing epidermis.

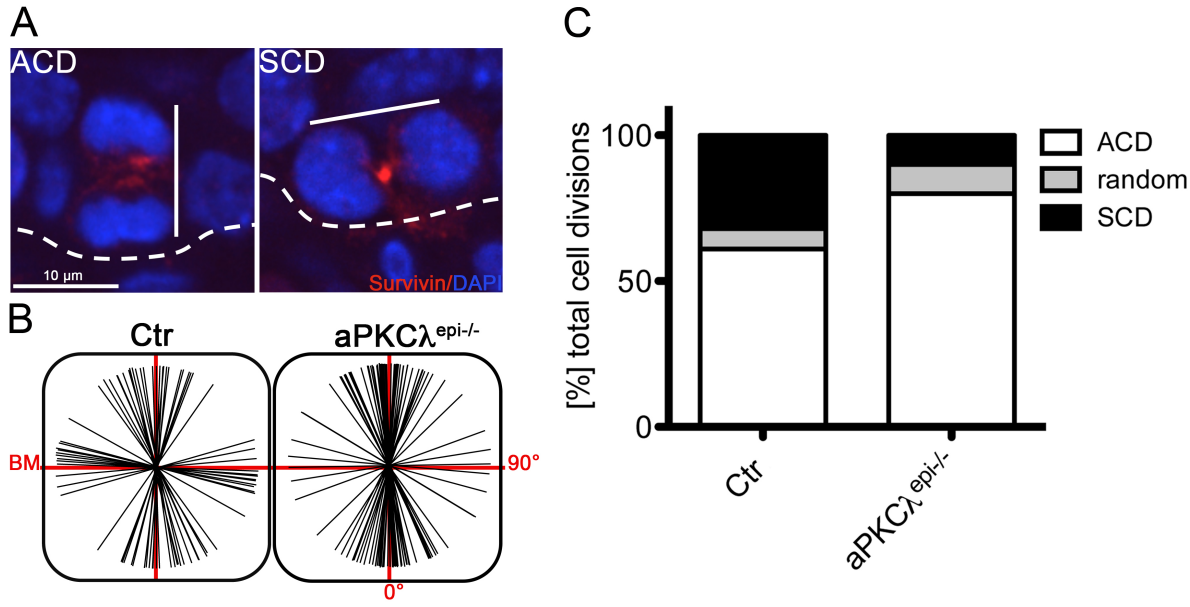

Figure 2. 24: Increased asymmetric cell division in aPKCλ$^{-/-}$ embryonic IFE

(A) Co-staining of Survivin and DAPI to visualize dividing cells in the basal layer of E16.5 embryonic skin. ACD: asymmetric cell division, perpendicular basement membrane (broken line). SCD: symmetric cell division, in parallel to basement membrane. (B) Schematic of spindle orientation in embryonic skin of ctr and aPKCλ$^{epi-/-}$ mice. (C) Quantification of the percentage of asymmetric (60-90°C), symmetric (0-30°C) or random (30-60°) divisions in regard to the basal layer. N=5 embryos per genotype, data are presented in mean values. Data obtained by Susanne Vorhagen.

2.9.2 Normal differentiation in embryonic aPKCλ$^{-/-}$ skin

To test whether increased percentage of ACD directly impacts on stratification and cell fate decisions during morphogenesis, we characterized stratification and differentiation in the embryonic aPKCλ-deficient epidermis. Histological analysis revealed no major differences between ctr and aPKCλ-deficient epidermis at either E16.5 or E19.5 (Fig. 2.25A). In line with this, quantification of the epidermal thickness did not show significant differences and quantification of Ki67 positive cells did not suggest changes in cell proliferation (Fig. 2.25B). Localization of the differentiation markers K14 (*str. basale*), K10 (*str. spinosum*) and Loricrin (*str. granulosum*) was comparable in ctr and aPKCλ$^{-/-}$ embryonic skin. Moreover, γ-tubublin staining visualized the majority of dividing keratinocytes in the K14 and K10 positive compartment in both ctr and aPKCλ$^{epi-/-}$ epidermis (Fig. 2.25C). Collectively, these data suggest that aPKCλ is dispensable for interfollicular differentiation and stratification during morphogenesis. The observed shift towards increased ACD in aPKCλ$^{epi-/-}$ mice is not reflected in a differentiation phenotype at this developmental stage.

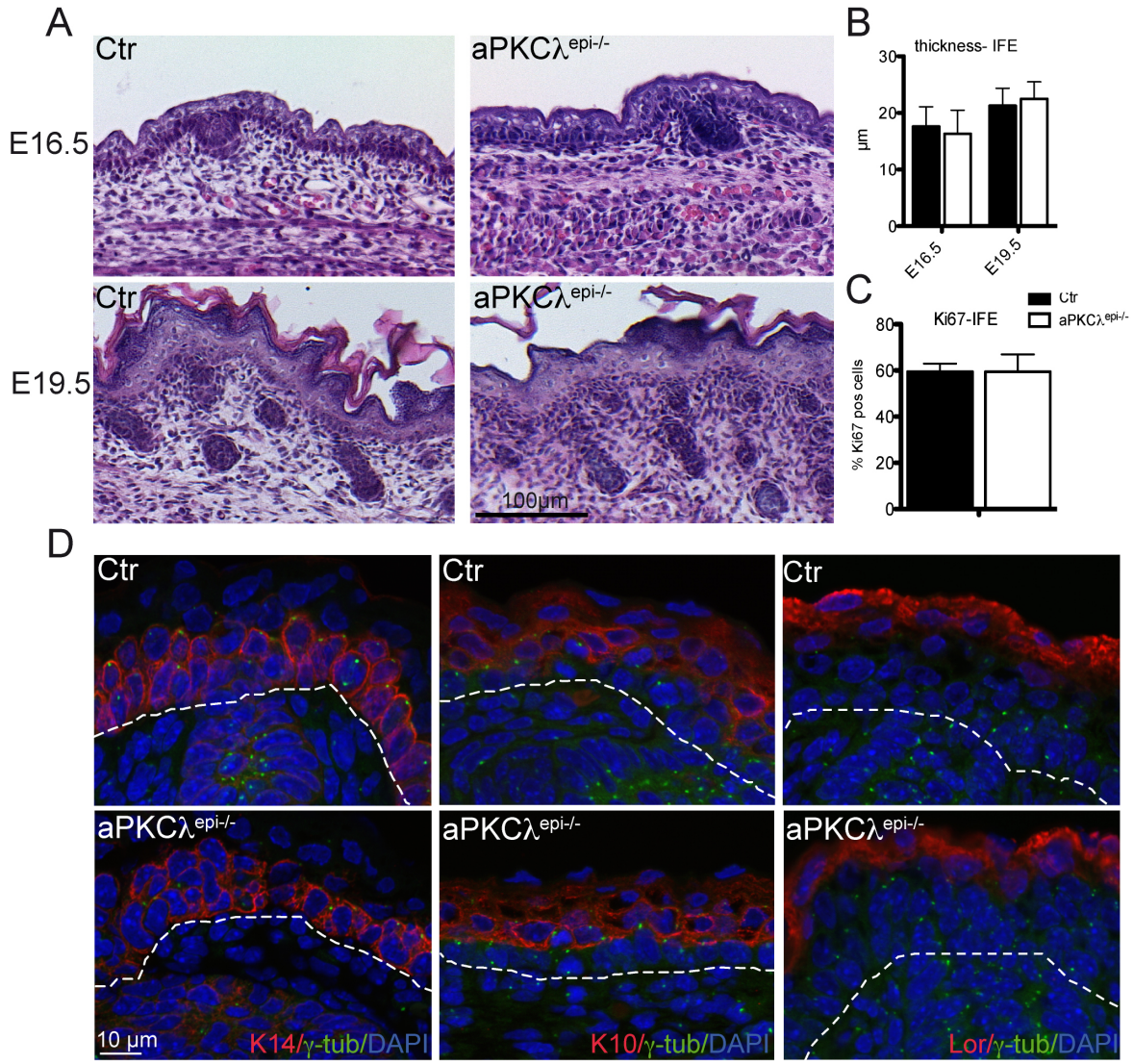

Figure 2. 25: Loss of aPKCλ does not affect embryonic proliferation and differentiation

(A) H&E staining of paraffin sections of back skin from ctr and aPKCλ$^{epi-/-}$ mice of the indicated embryonic (E) days. (B) Quantification of epidermal thickness (without the *str. corneum*) using H&E stained sections from E16.5 and E19.5 back skin. N=4 different mice for each genotype. Data are presented as mean +/-SD. (C) Quantification of Ki67 positive cells in the basal layer of ctr and aPKCλ$^{epi-/-}$ E16.5 IFE. Data are presented as mean +/-SD. N=4 different mice for each genotype. (D) K10, K14 and Loricrin staining of paraffin sections from E16.5 ctr and aPKCλ$^{epi-/-}$ mice. Dividing cells were visualized by γ-tubulin staining. Nuclei were visualized with DAPI.

2.10 Establishment of a lineage tracing system to investigate SC fate *in vivo*

The data presented in this thesis suggest that epidermal aPKCλ deletion causes over-activation, cell fate changes and a gradual exhaustion of HFSCs, possibly via an altered ration of ACD vs SCD in epidermal progenitors.

To analyze migration behavior and trace the fate of single HFSCs *in vivo* under homeostatic conditions, homozygous aPKCλ$^{fl/fl}$ mice were crossed to K14CRE^{ERT2}; EYFP$^{TG/TG}$ mice. Next to the allel coding for the Tam-inducible Cre recombinase under the control of the K14 promoter (Stratis et al., 2006; Littlewood et al., 1995), these mice express the reporter gene EYFP. EYFP is located downstream of a STOP codon which prohibits the production of the reporter protein (Srinivas et al., 2001). In double transgenics in the presence of Tam, Cre is imported into the nucleus, the STOP codon is excised and the reporter gene is expressed. In theory, a cell that undergoes such a recombination event during will continue to permanently express EYFP (Fuchs and Horsley, 2011; Hayashi and McMahon, 2002). This system enables genetic labeling of single epidermal cells to trace their behavior and progeny over time.

As the K14 promotor well known to drive expression of the Cre-recombinase in all basal proliferative cells of the IFE and ORS of the HF (s. 2.1), a low Tam dose was needed to label single cells. Several Tam- doses were tested and a single intraperitoneal injection between 1 and 3 mg Tam was observed to label single cells in the HFs after 7 days of chase. Moreover, heterozygous expression of the EYFP reporter gene was detected to be sufficient to induce several EYFP positive cells by a single Tam injection. An injection protocol was established and labeled cells were visualized by immunochistochemical staining using a GFP antibody for the analysis of the localization of single cells (Fig. 2.26). Oil was injected as a negative control to rule out Tam-specific effects. The analysis of several Tam-injections revealed a high variation in the number of EYFP positive cells. Moreover, mice injected with oil exhibited, in approximately 40 % of experiments, a substantial number of positive cells. Furthermore, a deletion of the aPKCλ gene was detected in 40-50 % of oil-injected K14CRE^{ERT2}; aPKCλ$^{fl/fl}$ mice by PCR. Therefore this system is unpredictable and we chose not to further utilize it.

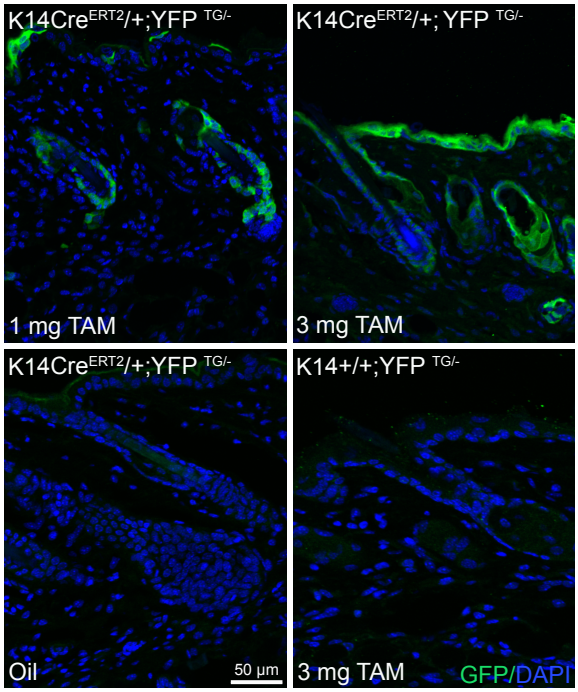

Figure 2. 26: Establishment of a lineage tracing system to trace cell fate *in vivo*

Immunofluorescent staining of GFP on cryo-preserved dorsal skin sections mice of the indicated genotypes (all mice were aPKCλ$^{+/+}$). Dose of Tamoxifen injection is depicted in the left bottom corner of each picture. All animals were subjected to a chase of 1 week after TAM/oil injection. Nuclei were counterstained with DAPI.

2.11 aPKCλ expression is increased in the HFSC compartment

Many proteins essential for homeostasis of the HFSC compartment are upregulated on the mRNA level particularly in bulge SCs (Tumbar et al., 2004). To test, whether the expression of aPKCλ is increased in HFSC, HFSCs were isolated using FACS with a6-integrin (α6-Int) and CD34 antibodies (Blanpain et al., 2004). Analysis of aPKCλ and aPKCζ expression in FACS-sorted HFSCs by qRT-PCR revealed a statistically significant 5 fold increased expression of aPKCλ in α6-Int+/CD34+ compared to α6-Int+/CD34- keratinocytes from ctr mice. This effect was specific for the aPKCλ isoform. Expression of aPKCζ was not specifically upregulated in HFSCs (Fig. 2.27A). In contrast, only a very mild enrichment of aPKCλ could be detected in the P33 K15 positive bulge cells by immunofluorescence using an antibody against aPKCλ (Fig. 2.27B). Since aPKC exists in a dynamic complex with the polarity protein Par3, we asked whether localization of Par3 in HFs is affected by the aPKCλ deletion. By usage of an antibody that recognizes all three mammalian isoforms (180, 150, 100 kDA) of Par3, Par3 was detected at sites of cell-cell contacts in both the IFE and the entire HF. However, no differences in Par3 localization were observed in aPKCλ$^{epi-/-}$ compared to ctr epidermis (Fig. 2.27C).

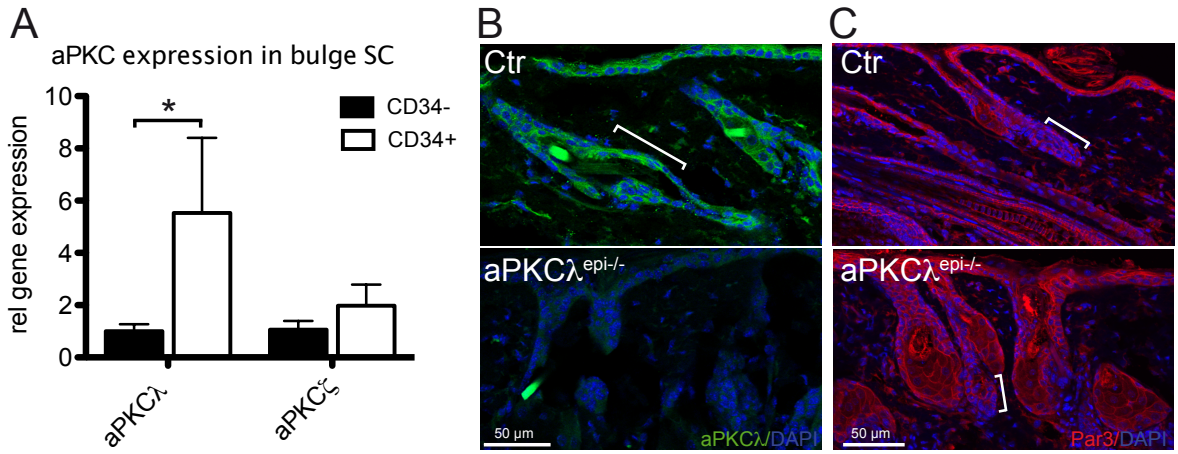

Figure 2. 27: Increased expression of aPKCλ in CD34 positive HFSCs

(A) QRT-PCR analysis of FACS-sorted α6-Int+/CD34+ versus α6-Int-/CD34- keratinocytes from adult ctr mice (P33) for either aPKCλ or aPKCζ. N=7 RNA preparations from independently isolated cells for each target gene. Data are presented as mean +/-SD. *= P<0.05. (B) Immunofluorescent staining of aPKCλ on dorsal skin of mice of ctr and aPKCλ$^{epi-/-}$ mice. Nuclei were counterstained with DAPI. White brackets mark the bulge region of the HFs. (C) Immunofluorescent staining of Par3 on dorsal skin of ctr and aPKCλ$^{epi-/-}$ mice. Nuclei were counterstained with DAPI. White brackets mark the bulge region of the HFs.

2.12 Enhanced Wnt/β-catenin signaling in aPKCλ$^{epi-/-}$ mice?

aPKCλ is crucial for HFSC maintenance cellular fate in postnatal life. We next asked which signaling pathway might be mediating the development of the aPKCλ$^{epi-/-}$ phenotype. A crucial signaling pathway controlling HF differentiation, SC function and fate is the canonical Wnt/β-catenin pathway (Wend et al., 2010).

2.12.1 aPKCλ represses β- catenin signaling in vitro

β-catenin transcriptional activity was assessed *in vitro* by transient TOP/FOP-Flash reporter assays using keratinocytes isolated from newborn (P0) and adult (P33) mice. The TOP-Flash plasmid is activated in response to binding by TCF/LEF transcription factors, which lie downstream of Wnt/β-catenin (Korinek et al., 1997). Transfection with FOP-Flash vector, a vector with mutated copies of Tcf/Lef binding sites, yielded minimal activity. In newborn (P0) and adult (P33) aPKCλ$^{-/-}$ keratinocytes, significantly elevated TOP-Flash activity was detected suggesting increased endogenous Wnt/β-catenin signaling *in vitro* (Fig. 2.28A). To test whether aPKCλ directly suppresses β-catenin signaling, aPKCλ-deficient keratinocytes (P0 or P33) were co-transfected with constructs expressing TOP/FOP-Flash reporter constructs and aPKCλ-wild type or aPKCλ-kinase-dead (KD) mutants. Strikingly, increased β-catenin signaling in aPKCλ$^{-/-}$ keratinocytes could be reversed to levels comparable to ctr cells by co-expression of both aPKCλ constructs (Fig. 2.28B). When the highly transfectable

CHO cell line (Chinese hamster cells) was co- transfected with TOP/FOP-Flash reporter and a stable β-catenin mutant, β-catenin transcriptional activity was increased. In contrast, when CHO- cells where transfected with aPKCλ or aPKCλ-KD constructs, TOP/FOP-Flash co-transfection indicated that β-catenin transcriptional activity was reduced compared to ctr cells. Importantly, when stable β-catenin and aPKCλ constructs were co-transfected into CHO cells, the enhanced β-catenin transcriptional activity induced by stable β-catenin expression was suppressed by aPKCλ, suggesting that also in CHO cells, aPKCλ is able to suppress β-catenin signaling (Fig. 2.28C). These results provide evidence that aPKCλ may inhibit β-catenin signaling *in vitro*. The kinase activity of aPKCλ does not seem to be necessary for β-catenin inhibition.

β-catenin is found in two cellular pools: First, membrane localized β-catenin binds to E cadherin and is an essential part of adherens junctions (Niessen and Gottardi, 2008). Second, nuclear β-catenin is crucial the canonical Wnt/β-catenin signaling pathway, where it acts together with TCF/Lef transcription factors to activate the expression of various target genes, as for example Cyclin D1 (Shtutman et al., 1999). We asked if the membrane-associated fraction of β-catenin is reduced at the expense of increased nuclear, transcriptionally active β-catenin. A method for purifying membrane-bound glycoproteins is by lectin affinity chromatography using concanavalin-A (Con-A) sepharose (Poliquin and Shore, 1980). However, in undifferentiated and 2 hrs Ca^{2+}-differentiated keratinocytes, Con-A precipitations followed by western blot did not reveal any differences in overall protein levels (as judged by the input fraction) or in the amount of membrane-bound proteins (Con-A fractions) (Fig. 2.28D). In line with findings of increased transcriptional activity of β-catenin, an increased level of CyclinD1, one of the major target genes of β-catenin was detected in Ca^{2+}-stimulated aPKCλ$^{-/-}$ keratinocytes (Fig. 2.28E).

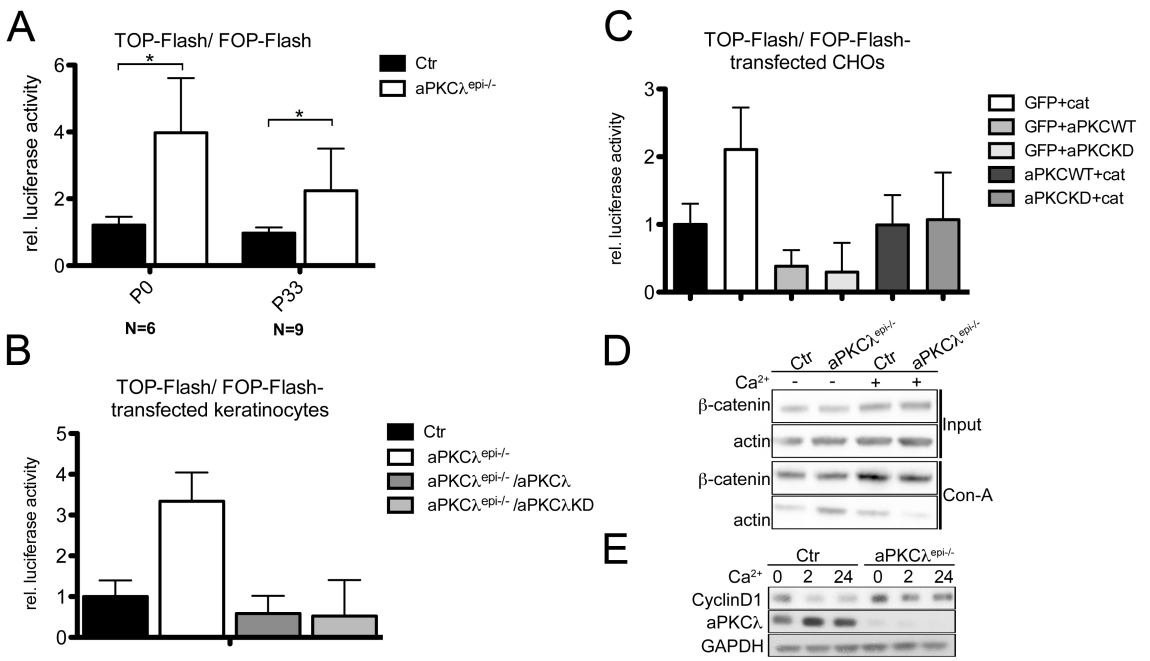

Figure 2. 28: Increased Wnt/β-catenin signaling in aPKCλ$^{-/-}$ keratinocytes

(A) Measurement of transcriptional activity of β-catenin by TOP /FOP-Flash assays *in vitro* in passage 1-3 keratinocytes isolated from newborn (P0) or adult (P33) mice. N=6 independent experiments for P0 keratinocytes, N=9 independent experiments with different lines of P33 keratinocytes. (B) Measurement of transcriptional activity of β-catenin *in vitro* (TOP/FOP-Flash assay) in passage 1-3 keratinocytes isolated from P0 mice after transfection with aPKCλ or aPKCλ kinase-dead (aPKCλ-KD) constructs. N=3 independent measurements. (C) Measurement of transcriptional activity of β-catenin *in vitro* (TOP/FOP-Flash assay) in CHO cells after transfection with aPKCλ or aPKCλ kinase-dead (aPKCλ-KD) constructs. N=4 independent experiments. For (A)-(C): Results are expressed as the ratio of TOP-Flash over FOP-flash activity. Luciferase activity from TOP/Flash or FOP/Flash vectors was normalized to Renilla luciferase. Data are presented as mean +/-SD. (D) Concavalin-A precipitation assay using ctr and aPKCλ$^{-/-}$ keratinocytes followed by western blot for β-catenin. Immunoblot using the pulled-down fraction (Con-A) and Input fraction is shown. Immunoblot using α-actin served as loading control. N=3 independent experiments. (E) Western blot of ctr and aPKCλ$^{-/-}$ keratinocytes after Ca^{2+}-induced differentiation for CyclinD1. Immunoblot using α-actin served as loading control. N= 4 independent experiments with different cell lines.

2.12.2 β- catenin localization is altered in aPKCλ$^{epi-/-}$ HFs

To investigate whether β-catenin signaling is also affected by aPKCλ deletion *in vivo*, localization of β-catenin was examined in ctr and aPKCλ$^{epi-/-}$ HFs. Staining of β-catenin in whole-mounts revealed differences in β-catenin localization: In ctr HFs, β-catenin was present at intercellular junctions and appeared to be highly organized within cell borders. In aPKCλ-deficient HFs this regular pattern was perturbed, the staining was enhanced and a much more diffuse, disorganized pattern was observable (Fig. 2.29A). When we focused on the bulge region of the aPKCλ$^{-/-}$ HFs, where aPKCλ is important for SC maintenance, β-catenin seems to be recruited less to intercellular junctions but rather exhibits a disorganized staining. The staining demonstrated alterations in cellular shape that might be due to perturbed cell polarity in aPKCλ$^{epi-/-}$ mice (Fig. 2.29B + 2.10A). No differences in β-catenin localization were observed in the hair bulbs of ctr and aPKCλ$^{epi-/-}$ HFs. Here, some faint

nuclear staining of β-catenin could be detected as described, in some inner matrix cells and in the precortex of the HF (Fig. 2.29B). The antibody used for this study as well as several additional antibodies tested did not reveal nuclear β-catenin staining in the permanent parts of the HF, and therefore gave no indication of altered nuclear β-catenin activity. These findings suggest that aPKCλ deletion affects recruitment of β-catenin to intercellular junctions, indicating a role of aPKCλ via β-catenin in junction formation.

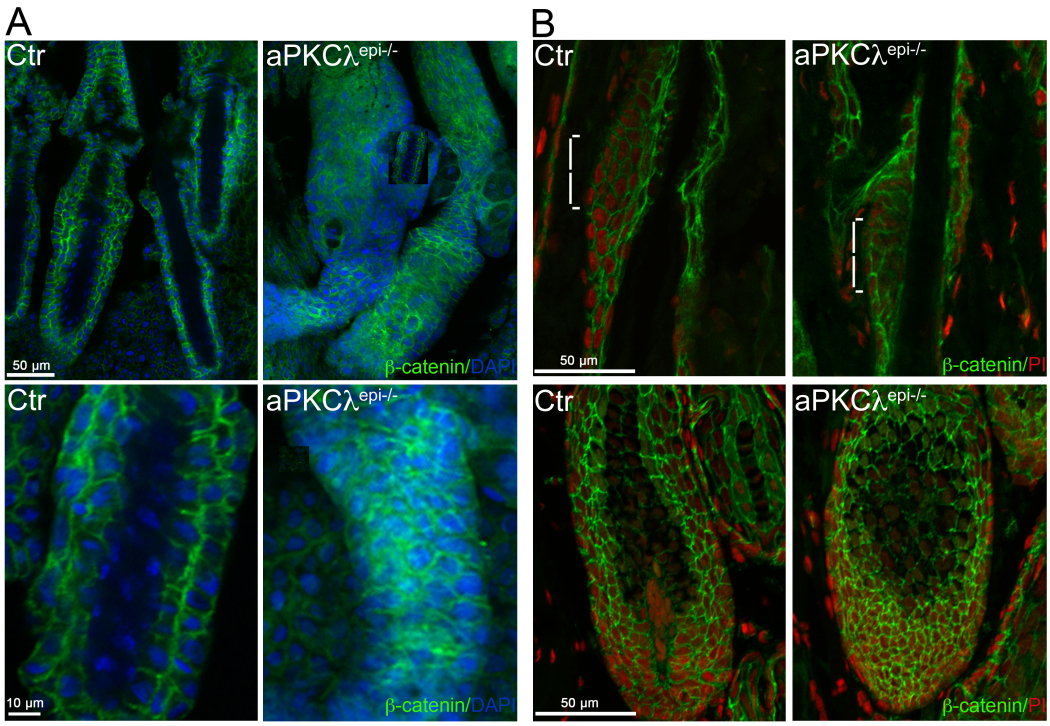

Figure 2. 29: Altered localization of β-catenin aPKCλ$^{-/-}$ HF

(A) Immunofluorescent staining of β-catenin on whole-mounts of P33 tail epidermis of ctr and aPKCλ$^{epi-/-}$ mice. Nuclei were counterstained with DAPI. (B) Immunofluorescent staining of β-catenin on paraffin sections of P33 dorsal skin of the indicated genotypes. Nuclei were counterstained with propidium iodide (PI).

The transcription factors Tcf/Lef1 are important mediators of Wnt/β-catenin signaling in bulge SC activation for hair renewal and HF differentiation (Haegebarth and Clevers, 2009). To study if aPKCλ activated the transcription factor Lef1, Lef1 staining at several stages of HF morphogenesis and cycling were performed. The immunofluorescent signal for nuclear Lef1 is restricted to the hair germ during telogen and to the inner matrix/precortex cells oh the bulb in anagen and HF morphogenesis. Analysis of Lef1 localization in aPKCλ-deficient HFs did not display dramatic differences, however, Lef1 signal seemed to be less restricted compared to ctr HFs. For example in telogen stages, weak Lef1 positive cells were detected in ORS cells near the bulge region of the HF (Fig. 2.30A).

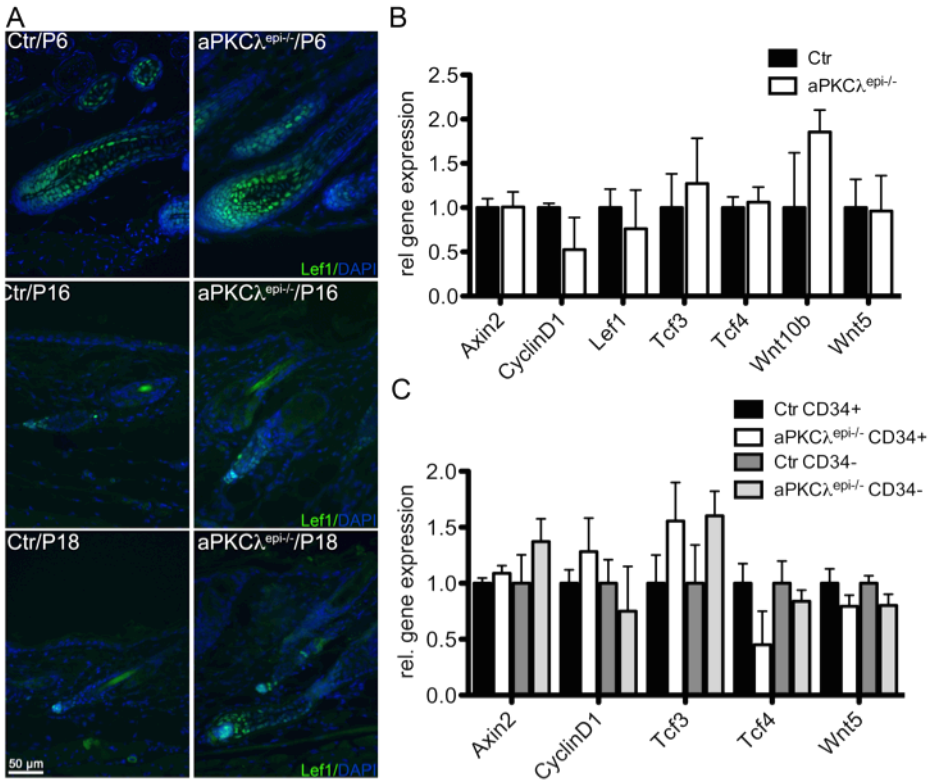

Figure 2. 30: No differences in Lef1 localization or β-catenin target gene expression in aPKCλ$^{-/-}$ HFs

(A) Immunofluorescent staining of Lef1 on paraffin sections of dorsal skin of ctr and aPKCλ$^{epi-/-}$ mice at the indicated postnatal (P) days. Nuclei were counterstained with DAPI. (B) QRT-PCR to analyze expression of genes involved in β-catenin signaling using epidermal RNA of P33 ctr and aPKCλ$^{epi-/-}$ mice. N=5 independent RNA samples for each genotype. Data are presented as mean +/-SD. (C) QRT-PCR of expression of genes involved in β-catenin signaling using epidermal RNA of FACS-sorted keratinocytes (CD34+/α6-Int+ vs CD34-/α6-Int+) isolated from P33 ctr and aPKCλ$^{epi-/-}$ mice. Data are presented in mean +/-SD. N=5 independent cell isolations for each genotype.

2.12.3 aPKCλ does not impact the expression of β-catenin target genes

To define whether altered β-catenin signaling impacts the expression of β-catenin target genes or mediators of the Wnt signaling pathway in aPKCλ$^{epi-/-}$ mice, qRT-PCR analyis of the expression of several candidates was performed. However, no significant alteration in target gene expression was observed in aPKCλ$^{epi-/-}$ epidermis compared to ctr epidermis (Fig. 2.30B). To assess SC-specific effects, RNA isolated from cells sorted for expression of the bulge SC marker CD34 and α6-Intergin (CD34+/α6-Int+ vs CD34-/α6-Int+) was used. The expression of all tested genes appeared not to be significantly altered by deletion of aPKCλ in the HFSC compartment (Fig. 2.30C). These data suggest that, if β-catenin signaling is increased *in vivo*, this does not influence the expression of β-catenin target genes, and thus are in conflict with our findings of increased transcriptional activity in aPKCλ$^{-/-}$ keratinocytes *in vitro*.

2.13 Decreased BMP signaling aPKCλ$^{epi-/-}$ epidermis.

BMP signaling is crucial to maintain SCs in their quiescent state during telogen phases of the hair cycle and directly antagonizes β-catenin signaling (Horsley et al., 2008; Kobielak et al., 2007). Hence, we assessed whether BMP signaling is affected by the deletion of aPKCλ. We detected a significant reduction of BMP4 transcript levels in aPKCλ$^{epi-/-}$ anagen HFs and in CD34+/α6-Int+ bulge SCs from telogen aPKCλ$^{epi-/-}$ HFs by qRT-PCR (Fig. 2.31A). Additionally, localization studies of the activated downstream mediators of BMP signaling, p-SMAD-1/5/8, were performed. The antibody produced a strong signal exclusively in the bulb region and the IRS of the HF. Analysis p-SMAD-1/5/8 staining suggests a possibly reduced signal for p-SMAD-1/5/8 in aPKCλ$^{epi-/-}$ HFs (Fig. 2.31B). In summary, these data suggest that in aPKCλ$^{-/-}$ HFs BMP signaling might be reduced, however, additional studies are required to further support these findings.

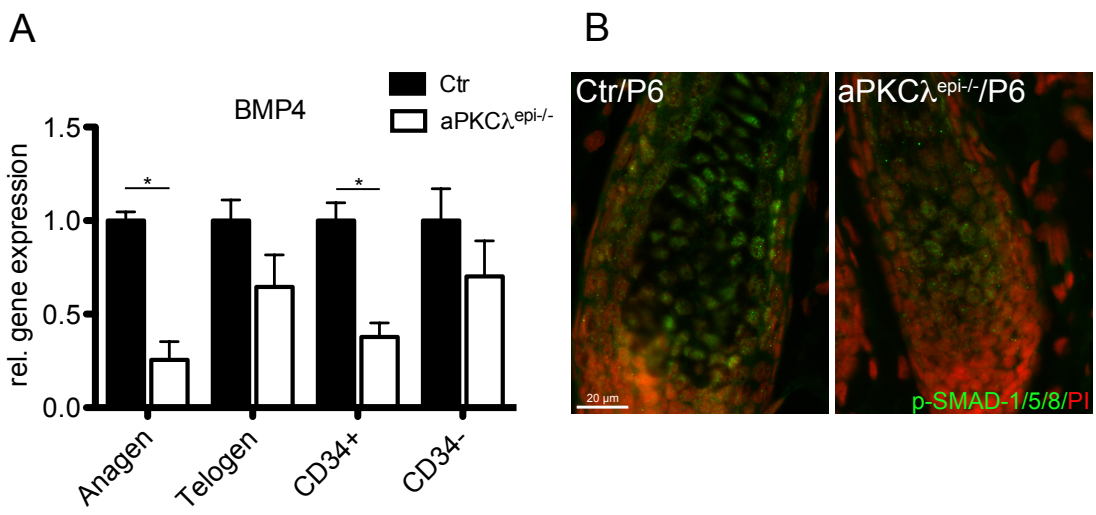

Figure 2. 31: Decreased expression of BMP4 in aPKCλ$^{-/-}$ HFs

(A) QRT-PCR of BMP4 expression using epidermal RNA isolated from P33 (anagen) or P20 (telogen) ctr and aPKCλ$^{epi-/-}$ mice or sorted keratinocytes (CD34+/α6-Int+ vs. CD34-/α6-Int+) from P30 mice. N=5 independent RNA isolations for each genotype. Data are presented as mean +/-SD. *= p<0.05. (B) Immunofluorescent staining of p-SMAD-1/5/8 on paraffin sections of P6 ctr and aPKCλ$^{epi-/-}$ dorsal skin. Nuclei were counterstained with PI.

2.13 Analysis of molecular mediators of ACD in aPKCλ$^{epi-/-}$ epidermis

The above-presented data demonstrate that aPKCλ is affecting spindle orientation in the murine epidermis. However, the molecular mechanism by which aPKCλ might control the balance of ACD and SCD is currently unknown.

2.14.1 Localization of cell fate determinants/ polarity proteins during ACD

We next asked whether the subcellular localization of polarity proteins or proteins implicated in the control of *Drosophila* spindle orientation was affected by aPKCλ-depletion during ACD. The polarity proteins and aPKC-substrates Lgl and Par3 showed no obvious differences in localization during embryonic ACD at E16.5. Lgl was found to be localized to both poles of the dividing cells whereas Par3 displayed, as previously reported, an apical localization (Lechler and Fuchs, 2005) (Fig. 2.32A).

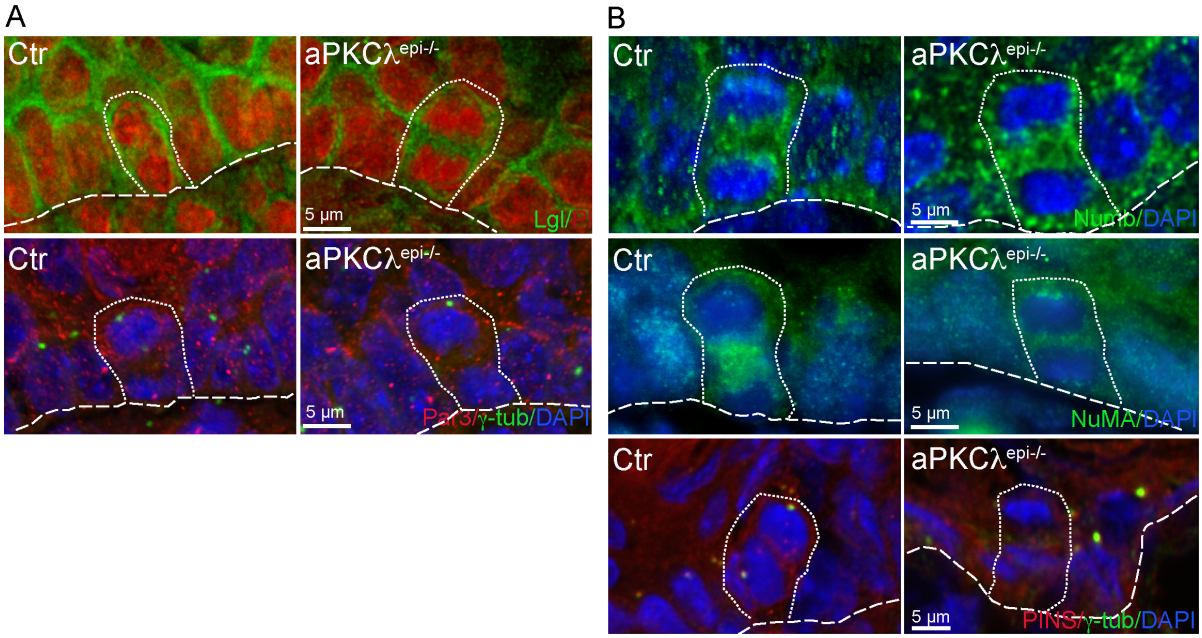

Figure 2. 32: Unchanged localization of polarity proteins and cell fate determinants during ACD in aPKCλ$^{epi-/-}$ mice

(A) Immunohistochemical staining of Lgl and Par3 in paraffin sections of E16.5 embryos. Nuclei were counterstained with propidium iodide (PI; Lgl) and DAPI (Par3). Pictures of Lgl staining were deconvolved. (B) Immunohistochemical staining of Numb, NuMA and PINS on paraffin sections (Numb, NuMA) or cryo-preserved sections (PINS) of E16.5 embryos. Nuclei were counterstained with DAPI. (A) and (B): broken line marks basement membrane, dotted line surrounds dividing cells.

Subsequently, we focused on proteins known to be important for spindle orientation in *Drosophila*. Analyzing the subcellular localization of the direct aPKC substrate Numb during embryonic ACD revealed a rather basal localization of Numb and no differences in localization were apparent after aPKCλ deletion. NuMA localized to both spindle poles in metaphase (data not shown) and formed an apical crescent in anaphase divisions, both in ctr

and aPKCλ$^{epi-/-}$ dividing cells. The LGN antibody only produces a positive signal using cryo-preserved skin sections and thus localization studies on single cell level were difficult due to the perturbed structural integrity of cryo sections. As far as we could judge, subcellular localization of LGN was not altered in aPKCλ$^{epi-/-}$ compared to ctr cell divisions (Fig. 2.32B). In summary, aPKCλ does not seem to control the subcellular localization of polarity proteins or cell fate determinanats during embryonic ACD in the epidermis.

2.14.2 aPKCλ influences expression and localization of Numb

Numb can be phosphorylated by aPKC, which may be a prerequisite of Numbs asymmetric distribution during ACD (Nishimura and Kaibuchi, 2007). In order to test the impact of aPKCλ deletion on Numb expression, immunoblot analysis was performed. The mammalian *NUMB* gene encodes at least four alternatively spliced transcripts producing four protein isoforms, ranging from 65 to 72 kDa and resulting in a doublet on Western blots (Smith et al., 2007). Western blot analysis revealed that total amount of Numb was reduced in aPKCλ$^{epi\ -/-}$ compared to ctr epidermis (Fig. 2.33A). After initiation of cell-cell contacts due to a Ca^{2+}-induced differentiation *in vitro*, the expression of Numb was upregulated in ctr cells, whereas in aPKCλ$^{-/-}$ keratinocytes, this upregulation did not occur (Fig. 2.33B). Treatment of cells with 0.1 µm Calyculin A, an inhibitor for serine-threonine phosphatases PP1 and PP2A, increased the stability of Numb, indicating that Numb regulation by aPKC is indeed phosphorylation-dependant (Fig. 2.33C). The downregulation of Numb observed *in vivo* and *in vitro* is suggestive of aPKCλ stabilizing Numb. As a side note, in all immunoblots performed using a polyclonal antibody against Numb (isoforms 1-4) we detected a predominant band around 100 kDa of unknown identity, however, decreased Numb expression in aPKCλ$^{-/-}$ keratinocytes was reproduced using a second Numb-specific antibody (data not shown).

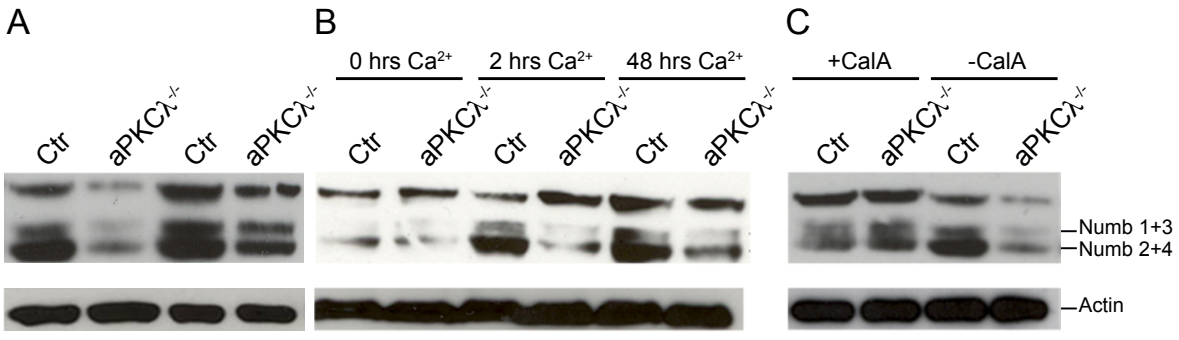

Figure 2. 33: Decreased expression of Numb in the absence of aPKCλ

(A) Western blot analysis of epidermal lysates of newborn ctr and aPKCλ$^{epi-/-}$ mice. (B) Western blot analysis of ctr and aPKCλ$^{-/-}$ keratinocyte lysates after 0 hrs, 2 hrs, and 48 hrs of Ca^{2+}-induced differentiation. (C) Western blot analysis of ctr and aPKCλ$^{-/-}$ cell lysates after treatment of the cells for 5 min with (+Cal) or without (-Cal) Calyculin A. (A) –(C): immunoblot using α-actin served as loading control. Data are representative for N=4 independent experiments showing same results. Numb 1+3 and Numb 2+4 refers to the respective Numb isoforms present in the bands.

We next analyzed the impact of the aPKCλ deletion on Numb distribution in primary dividing keratinocytes. Clayton et al. (2007) reported asymmetric partitioning of Numb in epidermal cells undergoing asymmetric cell division. After immunohistochemical staining for Numb, we monitored its distribution in late stage mitotic keratinocytes. If a crescent-like localization was observed in only one of the resulting daughter cells, these cells were scored as asymmetrically segregating Numb. After 2 hrs of Ca^{2+} induced differentiation, 47(+/-2.7)% of ctr keratinocytes and 72(+/-7.1)% of the aPKCλ$^{-/-}$ keratinocytes asymmetrically inherited Numb into daughter cells (Fig. 2.34A+B). This analysis indicates that *in vitro*, the deletion of aPKCλ leads to a significant increase of asymmetric distribution of Numb in dividing cells.

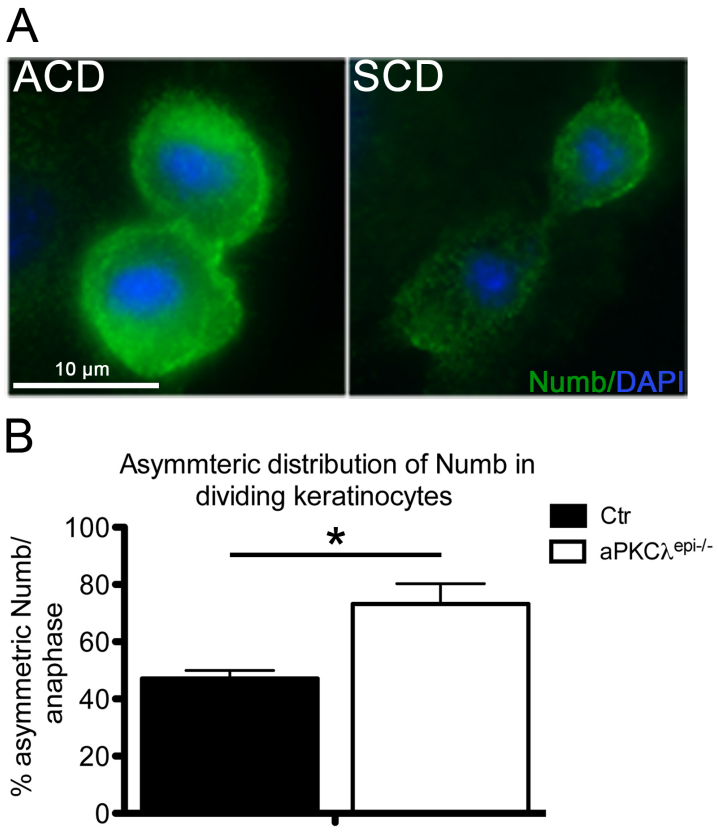

Figure 2. 34: Increased asymmetric distribution of Numb in aPKCλ$^{-/-}$ dividing cells

(A) Ctr and aPKCλ$^{-/-}$ keratinocytes were scored for asymmetric vs. symmetric Numb distribution using an antibody against Numb. (B) The percentage of divisions with asymmetric Numb distribution of overall anaphases was calculated; Approximately 150 cells in anaphase from 3 independent cell lines wer scored. Data are presented as mean +/-SD. *= p <0.05.

2.15 aPKCλ might regulate cell polarity in the epidermis

aPKCλ is crucial for the establishment of cell polarity in lower organisms and mammals (Niessen and Niessen, 2010), and β-catenin stainings visualized cell shape changes in HFs suggesting alterations in cell polarity in aPKCλ$^{epi-/-}$ mice.

2.15.1 Expression and activation of polarity proteins are affected by aPKCλ deletion

To characterize how establishment of cell polarity might be affected by epidermal loss of aPKCλ, we examined protein levels and activity of polarity proteins known to interact and/or to be phosphorylated by aPKCs. First, analyzing the protein level of the polarity protein Par4/LKB1 revealed elevated levels of this serine/threonine (ser/thr) kinase in aPKCλ$^{-/-}$ epidermal splits. Next, we investigated the expression of the ser/thr kinase Par1, a direct aPKC substrate (Hurov et al., 2004). Four Par1 isoforms exist in mammals, known as MARK1-4. The antibody used recognizes MARK3 (Par1A/ C-TAK1), the isoform reported to be critical for cell polarity (Göransson et al., 2006). In contrast to elevated Par4 levels, immunoblot analysis revealed a reduction in the amount of Par1 in aPKCλ$^{-/-}$ compared to ctr epidermal splits. In line with the data obtained by immunohistochemistry, an antibody recognizing all three mammalian isoforms (180, 150, 100 kDA) of Par3 showed no difference in Par3 protein levels in aPKCλ$^{-/-}$ compared to ctr skin (Fig. 2.35A). Finally, we assessed potential alterations in the activation of the small GTPases Cdc42 and Rac1. Rac1 and Cdc42 are generally involved in transmitting polarity cues to aPKC but can also be activated by aPKC (Iden and Collard, 2008). To precipitate active Rac1/Cdc42 from epidermal lysates, the biotin- CRIB-PAK peptide was used (Price et al., 2003). aPKCλ$^{-/-}$ samples showed no changes in total Rac1 expression, but a reduction in active Rac1 was detected in aPKCλ$^{-/-}$ compared to ctr lysates. In contrast, neither total levels nor the amount of active Cdc42 were changed in aPKCλ$^{-/-}$ deficient skin (Fig. 2.35B).

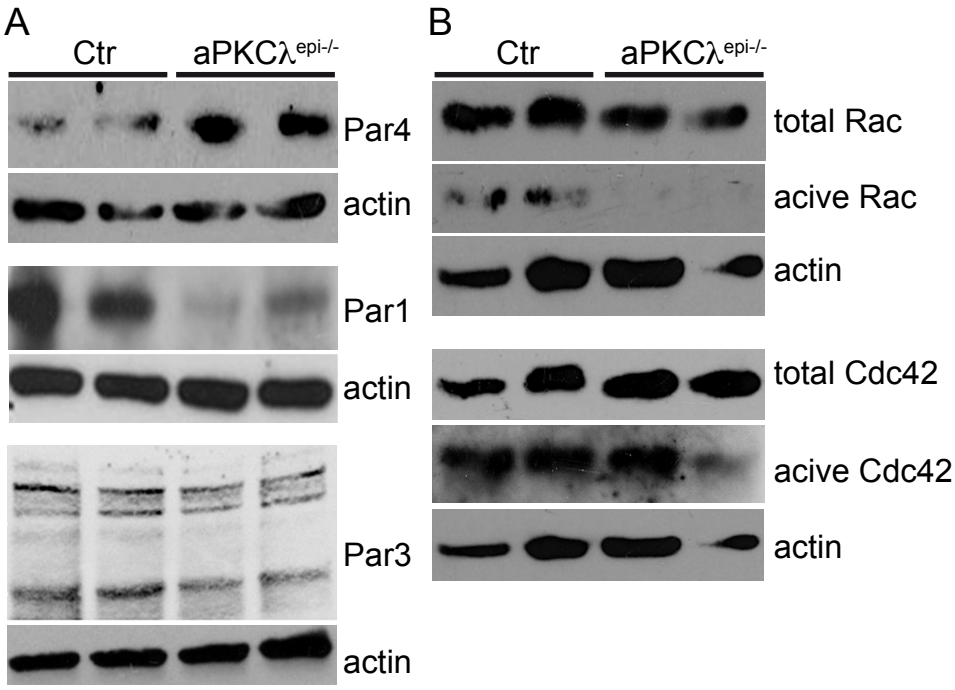

Figure 2. 35: Altered expression of polarity proteins and activation of the small GTPase Rac1 in the absence of aPKCλ

(A) Western blot analysis of Par4, Par3 and Par1 expression using epidermal lysates from newborn mice. Immunoblot using α-actin served as loading control. Data are representative for N=4 independent experiments showing same results. (B) Rac/Cdc42 activation assay using epidermal skin lysates from newborn mice. Immunoblot using α-actin served as loading control. Data are representative for N=3 independent experiments showing same results.

These experiments demonstrate that cell polarity is affected by aPKCλ depletion and imply that the aPKCλ$^{epi-/-}$ phenotype might be a result of altered expression or activity of polarity proteins.

2.15.2 Apico-basal polarity is not perturbed in aPKCλ$^{epi-/-}$ epidermis

Finally, we assessed if altered expression of polarity proteins is accompanied by differences in apico-basal (A/B) polarity or cell shape in aPKCλ$^{-/-}$ epidermis. Intercellular adhesion is a prerequisite of A/B-polarity, however, staining of E-cadherin, the major components of adherens junctions (Niessen and Gottardi, 2008) was indistinguishable between aPKCλ$^{-/-}$ and ctr epidermis. When area and height of basal cells was measured, aPKCλ$^{-/-}$ cells showed a more columnar morphology compared to ctr cells. The overall cell area was not altered, but aPKCλ-negative cells were slightly taller (9.4+/-1.4µm) than basal ctr keratinocytes (7.5+/-1.9)(Fig. 2.36A). Another feature of A/B polarity is the apical localization of centrosomes in the basal layer of E16.5 embryos (Luxenburg et al., 2011). Using γ-tubulin as a marker, centrosomal localization was examined revealing a regular apical localization of centrosomes in non-dividing ctr basal keratinocytes. The percentage of non-apical

centrosomes versus apical centrosomes was not significantly altered in aPKCλ-deficient compared to ctr skin (Fig. 2.36B). Finally, localization of Par3, important for the establishment of A/B polarity, was investigated. Par3 is known to of localize apically in basal keratinocytes (Lechler and Fuchs, 2005) and is recruited to cell-cell junctions in suprabasal layers. The overall localization pattern was not grossly altered in aPKCλ$^{-/-}$ skin compared to ctr epidermis (Fig. 2.36C). Overall, A/B polarity does not appear to be majorly affected by epidermal aPKCλ deletion.

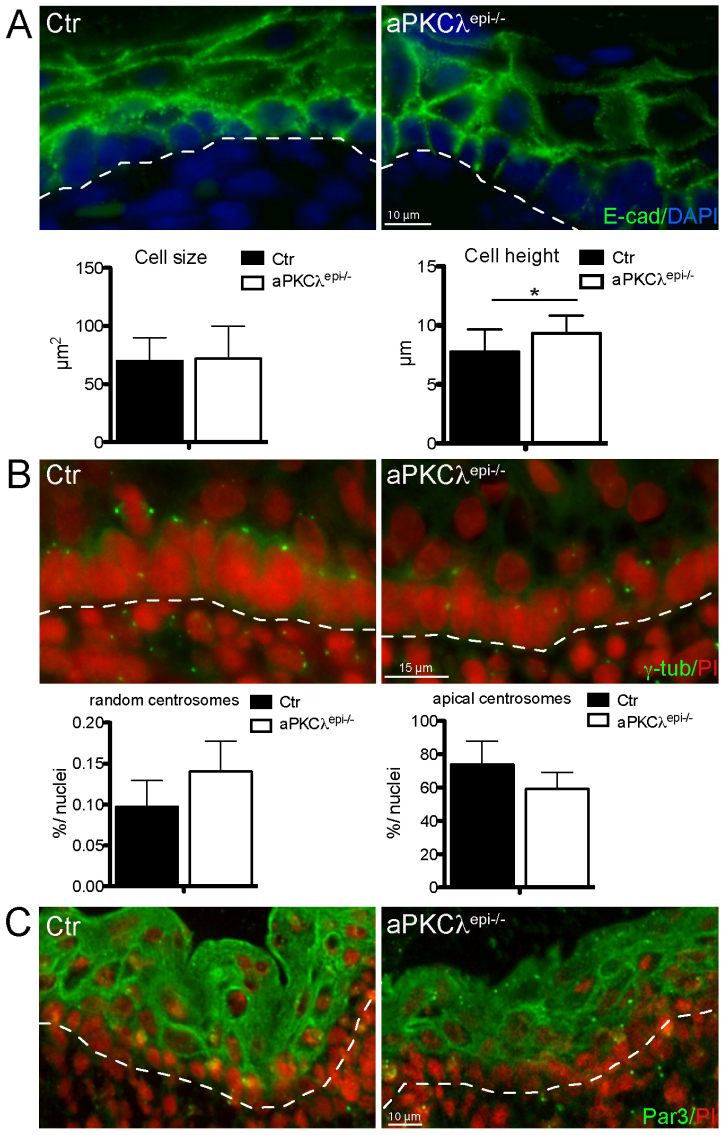

Figure 2. 36: Altered apico-basal polarity the absence of aPKCλ

(A) Upper panel: Immunohistochemical staining of E-cadherin on paraffin sections of P0 dorsal skin. Nuclei were counterstained with DAPI. Lower panel: quantification of measurement cell size and height in ctr and aPKCλ$^{epi-/-}$ mice in the basal layer of newborn skin. N= 3 paraffin sections of different mice for each genotype. *= P< 0.05. (B) Upper panel: immunohistochemical staining of γ-tubulin in the basal layer of E16.5 skin. Nuclei were counterstained with propidium iodide (PI). Lower panel: quantification of apical (right) and random (left) centrosomes in ctr and aPKCλ$^{epi-/-}$ mice in the basal layer of E16.5 skin. N= 3 paraffin sections of different mice for each genotype. (C) Immunohistochemical staining of Par3 on cryo-preserved skin sections of E16.5 embryos. Nuclei were counterstained with propidium iodide (PI).

3 Discussion

This study identifies the polarity protein aPKCλ as a crucial regulator for epidermal homeostasis throughout postnatal life. Using an epidermis-specific aPKCλ knock-out mouse model, aPKCλ was shown to be an essential regulator of epidermal polarity and cell fate decisions. The aPKCλ$^{epi-/-}$ phenotype is characterized by differentiation defects in all epidermal compartments associated with a gradual loss of HFSC quiescence and identity. In line with this, aged mice eventually loose all hair, indicating exhaustion of HFSCs. The loss of bulge HFSCs is accompanied by increased expression of more differentiated progenitor cell markers during ageing. Interestingly, closer analysis revealed that aPKCλ depletion increased the percentage of ACD vs. SCD providing a possible mechanism for how aPKCλ regulates cell fate decisions. Moreover, the data suggest increased Wnt/β-catenin signaling as one of the drivers of the aPKCλ$^{epi-/-}$ phenotype. Importantly, this study is the first work demonstrating that the aPKC isoform aPKCλ controls SC homeostasis and cell fate decisions in the murine epidermis.

3.1 aPKCλ is important for epidermal polarity

The mammalian epidermis is an excellent model to study several forms of cell polarity, as for example ACD, junction formation and apico-basal cell polarity. This thesis provides evidence that aPKCλ is important to balance ACDs vs. SCDs, a classical example of cell polarity, in the IFE and HFs (Fig. 2.3; 2.23; 2.24). Moreover, altered expression of the polarity proteins Par1 and 4 and a reduced activity of the small GTPase Rac1 strongly indicate that polarity signaling is affected in aPKCλ$^{epi-/-}$ mice (Fig. 2.35). Notably, these effects are detectable already in skin or keratinocytes isolated from newborn aPKCλ-deficient mice, whereas the aPKCλ$^{-/-}$ phenotype develops later during postnatal development. This suggests that changes in the establishment of polarity precede the development of the aPKCλ$^{-/-}$ phenotype and might be a prerequisite for the alterations in epidermal homeostasis observed in aPKCλ$^{epi-/-}$ mice. Furthermore, cell shape changes were detected by staining for β-catenin both *in vivo* (Fig. 2.10) and *in vitro* (data not shown), suggesting that aPKCλ impacts junction formation in the epidermis. Indeed, delayed barrier formation, measured as transepithelial resistance (TER) *in vitro*, was detected in primary aPKCλ$^{-/-}$ keratinocytes (data not shown). Overall epidermal integrity and apico-basal polarity in the basal layer seemed to be maintained in aPKCλ$^{epi-/-}$ skin (Fig. 2.36). Nevertheless, the stratified epidermis is not a classical apico-basal polarized epithelium, but apico-basal polarity is rather established over different layers, e.g. by layer-specific junction formation. Since we propose defects in junction formation in aPKCλ$^{epi-/-}$ mice, these findings point towards altered polarity over the different

layers of aPKCλ$^{-/-}$ epidermis. Several reports recently demonstrated a role of mammalian aPKCλ in adherens junction formation, whereas apico-basal polarity was maintained when aPKC was conditionally deleted (Dard et al., 2009; Imai et al., 2006). In contrast in *Drosophila* aPKC null mutants, loss of aPKC resulted in severe defects in apico-basal polarity (Rolls et al., 2003), suggesting that the role of aPKC in the establishment of polarity is not conserved, or that aPKCζ might compensate for the loss of aPKCλ in the establishment of apico-basal polarity in aPKCλ$^{epi-/-}$ mice. These data indicate, that even if apico-basal polarity in the basal epidermal layer is established, aPKCλ$^{epi-/-}$ epidermis exhibits an overall polarity defect already at birth, possibly accompanied by alterations in junction formation.

3.2 aPKCλ controls cell fate decisions in all epidermal compartments

Several results of this work implicate aPKCλ in the regulation of cell fate decisions within the epidermal lineage. First, increased differentiation was detected in the SGs and adult IFE, (Fig. 2.3; 2.6) whereas HF differentiation was perturbed (Fig. 2.8), suggesting altered cell fate of HF keratinocytes towards SG/IFE identity. In accordance, the IFE and SG compartment was thickened in aging mice (Fig. 2.2), whereas partial HF degeneration was observed in one year old mice (Fig. 2.20). The finding of altered cell fate is also manifested in the HFSC compartment, where loss of bulge SC identity (Fig. 2.15; 2.16) is accompanied by increased expression of more committed progenitor markers (Fig. 2.17).

This novel function of aPKC in cell fate regulation seems to be specific for the aPKCλ isoform. Expression of the aPKCζ gene was not significantly upregulated in aPKCλ negative epidermis, suggesting that aPKCζ does not compensate for the loss of aPKCλ (Fig. 2.1). Whereas aPKCζ$^{-/-}$ mice do not display an obvious epidermal phenotype, loss of both aPKC isoforms resulted in a different, more severe phenotype as detected in aPKCλ$^{epi-/-}$ mice: all aPKCλ$^{epi-/-}$;ζ$^{-/-}$ mice died at birth, showing a translucent skin and limb malformation (data not shown). These findings indicate that the aPKC isoforms are able to act compensatory for each other, e.g. in aPKCζ$^{-/-}$ mice. On the other hand, the aPKCλ$^{epi-/-}$;ζ$^{-/-}$ phenotype manifests that both isoforms have non-overlapping roles in the epidermis.

Similar to the role of epidermal aPKCλ to control murine epidermal SC identity, aPKC maintains undifferentiated progenitor cell fate in *Drosophila* neuroblasts (Lee et al., 2006; Rolls et al., 2003) and in the *Xenopus* neuronal system (Sabherwal et al., 2009). Opposing data were obtained in *Danio rerio*, where loss of both aPKC isoforms results in an increased progenitor cell pool (Baye and Link 2007). In contrast, studies on mammalian cell fate specification in the hematopoietic or neuronal system demonstrated that aPKCλ is dispensable for cell fate decisions of progenitor cells (Sengupta et al., 2011; Imai et al.,

2006), suggesting that aPKCs role in cell fate determination is not conserved in mammals. Nevertheless, aPKCζ was recently implicated in the control of stemness in mammalian neuronal SCs *in vitro*. aPKCζ interacts with the cell fate determinant Trim32 and thus excludes it from the nucleus to keep neuronal cultured SCs in a undifferentiated state (Hillje et al., 2011). However, whether this interaction is indeed a prerequisite to maintain progenitor identity *in vivo* in neuronal or epidermal SCs and if this also applies for the aPKCλ isoform remains elusive. Altogether, these data suggest that the role of aPKC in cell fate determination is not conserved among different species. Our observation of altered cell fate and a loss of 'stemness' after loss of aPKCλ are intriguing since this report is the first to show that aPKCλ is crucial for SC fate in a mammalian tissue *in vivo*.

3.3 aPKCλ negatively regulates the establishment of epidermal ACDs

This work shows that loss of aPKCλ alters polarity by affecting the balance of ACD/SCD. Importantly, ACDs were reported to control cell fate determination in several systems ranging from *C. elegans* to mammalian cells (Knoblich, 2008; Knoblich, 2010). Since the ratio of ACD vs. SCD is increased in all compartments where epidermal fate was altered after loss of aPKCλ (Fig. 2.3; 2.23; 2.24), we propose that balancing the ratio of ACDs vs. SCDs is the cellular mechanism by which aPKCλ regulates epidermal cell fate. Notably, aPKCλ$^{-/-}$ keratinocytes were still able to divide symmetrically and rather a shift towards increased ACD was observed. Moreover, the fraction of divisions as classified to be random was not drastically increased in aPKCλ$^{epi-/-}$ mice compared to ctr mice. This suggests that the overall machinery which is crucial for spindle orientation is not lost. Moreover, the aPKCζ isoform might compensate for the depletion of aPKCλ in ACD. Future analyis of the ratio of ACD vs. SCD aPKCλ$^{epi-/-}$;ζ$^{-/-}$ and aPKCζ$^{-/-}$ mice will elucidate a possible function of aPKCζ in balancing ACDs/SCDs. If the Par3/Par6/aPKC complex is mislocalized in *Drosophila,* the "telophase-pathway" has been proposed to act as a rescue mechanism to ensure proper spindle formation. This microtubule-dependent pathway accumulates Pins and Gα to one cell pole and thus ensures asymmetric cell fate determinant segregation and cell cleavage (Knoblich, 2008; Knoblich, 2010). A related backup mechanism may exist in the murine epidermis, explaining why aPKCλ$^{epi-/-}$ epidermis does not completely loose spindle orientation. In line with this, epidermal overexpression of mInsc promotes ACD but upon prolonged mInsc expression this effect is reversed, suggesting that epidermal progenitors, like *Drosophila* neuroblasts, can sense and correct disturbances in the balance of ACDs vs. SCDs (Fig.3.1) (Poulson and Lechler, 2010).

Recent publications demonstrated that orientation of basal divisions is tightly coupled to interfollicular differentiation (Williams et al., 2011; Poulson and Lechler 2010). Since no differentiation defect was observed in embryonic epidermis, a counter-acting mechanism, for example increased apoptosis in the suprabasal layers, might balance the impact of perturbed spindle orientation on differentiation. Indeed, a slight but significant increase in apoptosis was observed in aPKCλ$^{epi-/-}$ IFE and HFs at several postnatal days (P0, P6, P16, data not shown). Furthermore, the observed shift of only 20 % towards more ACDs vs. SCDs might explain that differentiation defects become apparent gradually later during postnatal life.

Our data support a model in which epidermal aPKCλ is not crucial for establishment of ACD but rather promotes symmetric spindle orientation. In line with this observation, Par3/Par6/aPKCs are crucial for spindle positioning in SCDs, as recently demonstrated in 3D cell culture and in *Drosophila* larval wing discs (Durgan et al., 2011; Hao et al., 2010; Guilgur et al., 2012). In *Drosophila*, polarized aPKC/Par3 will be inherited to the non-differentiated neuroblast daughter cell after ACD (Knoblich, 2008)(Fig. 1.4). In the epidermis, Par3/aPKC are apically localized not only in asymmetrically but also in symmetrically dividing cells and the aPKC/Par3-enriched domain will segregate into the more differentiated suprabasal daughter cell (Fig. 1.9)(Lechler and Fuchs, 2005). This infers that the role of polarized aPKC localization is non-conserved between species and suggests that aPKC/Par3 localization might be uncoupled from spindle orientation in the epidermis. The role of mammalian aPKCs in the regulation of spindle orientation *in vivo* is not clear. In accordance with increased ACD in aPKCλ$^{epi-/-}$ epidermis mice, loss of aPKCλ in cultured mouse embryos altered spindle orientation towards more divisions scored as asymmetric (Dard et al., 2009). However, in chicken neuroepithelial cells, mammalian developing neurons or the hematopoietic system, aPKC is not required for *in vivo* spindle orientation during symmetric cell division (Peyre et al., 2011; Imai et al., 2006; Sengupta et al., 2011). These data suggest that aPKCλs role in balancing SCDs vs. ACDs in the epidermis is not transferable to all mammalian tissues.

3.3.1 Which molecular mediators control epidermal ACD?

The molecular players by which aPKC controls ACD in *Drosophila* may mediate aPKC dependent regulation of spindle orientation in the murine epidermis. However, upon loss of aPKCλ, neither polarity proteins (Par3, LGL) nor mediators crucial for spindle orientation and cell fate determination (NuMA, Numb, LGN) showed obvious differences in intracellular localization during epidermal cell division. Par3 appeared to be localized normally both in dividing cells (Fig. 2.32) and in adult skin (Fig. 2.27). In the establishment of polarity, Par3 has been described to activate/recruit aPKC in mammalian cells (Macara, 2004), and Par3 localizes independently from aPKC in *Drosophila* (Rolls et al., 2003; Guilgur et al., 2012). Together, these and our results suggest that aPKCs role in the regulation of epidermal

SCD/ACD is either independent of Par3, or that Par3 acts upstream of aPKC. In *Drosophila* neuroblasts, Lgl is essential for recruiting cell fate determinants, e.g. Numb, to the cell cortex and for their asymmetric localization during mitosis. Lgl is phosphorylated by aPKC and competes with Par3 for binding to the aPKC complex (Betschinger et al., 2003; Wirtz-Peitz et al., 2008). However, no qualitative (Fig. 2.32) and quantitative (data not shown) differences in Lgl localization were observed in aPKC$\lambda^{-/-}$ asymmetrically dividing cells. Next to polarity processes, cell adhesive cues were reported to balance spindle orientation (Lechler and Fuchs 2005). Since membrane staining for the adherens junction protein β-catenin was affected in aPKC$\lambda^{-/-}$ keratinocytes (Fig. 2.10), altered spindle orientation in aPKC$\lambda^{-/-}$ epidermis might also be triggered by changes in cell adhesion composition.

The function of molecules controlling ACD in *Drosophila* might be conserved in the murine epidermis. For example the expression of mInsc is sufficient to drive ACD in the epidermis (Fig. 3.2) (Poulson and Lechler 2010). Additionally, Gαi, LGN and NuMA were reported to be fundamental to establish epidermal ACD (Williams et al., 2011). However, how these mediators interact in molecular detail and how polarity cues, as for example by aPKCλ, are integrated in the regulation of epidermal ACD is not yet understood. aPKC/Par3 were still localized apically in the NuMA/LGN knock-down epidermis (Williams et al., 2011), suggesting that, like in neuroblasts, aPKC/Par3 are either upstream of LGN/NuMA or the apical localization of these two complexes serve different functions. The fact that epidermal LGN/NuMA knock-down or mInsc overexpression result in the opposite outcome than aPKCλ-deletion (Fig.3.2) argues for either independent or mutually inhibitory roles of these proteins. In *Drosophila* and mammalian cells, aPKC is responsible for apical exclusion of Pins (mammalian LGN) and thus planar orientation of the mitotic spindle (Durgan et al., 2011; Hao et al., 2010; Guilgur et al., 2012). Additionally, phosphorylation of the NuMA homologue LIN-5 in the *C. elegans* embryo is crucial for Lin-5 localization and spindle orientation (Galli et al., 2011). Hence, aPKCλ might establish epidermal SCDs through controlling the subcellular localization of LGN or NuMA by excluding them from the apical pole. In aPKC$\lambda^{-/-}$ dividing cells, ectopic apical LGN/NuMA localization might cause a shift towards more ACDs compared to SCDs. Decreased ACD after LGN/NuMA knock-down in the epidermis is in line with the hypothesis that apical LGN/NuMA localization is crucial for ACDs (Williams et al., 2011). However, LGN was detected to localize apically in both symmetrically and asymmetrically dividing cells (Poulson and Lechler 2010), and examination of LGNs or NuMAs subcellular localization did not reveal any obvious differences in aPKC$\lambda^{epi-/-}$ as compared to ctr ACD (Fig. 2.32), arguing against this hypothesis. On the other hand, since the ratio of ACD/SCD is shifted and not switched towards one form of cell division, aPKCλ might rather modulate than control LGN/NuMAs localization to an

extent not detectable by immunofluorescent studies. Importantly, immunofluorescent analyses provide insight into static protein localization at a certain time point in a dividing cell, but no information about dynamic localization of molecular mediators throughout cell divisions can be gained. Lentiviral constructs to overexpress or knock-down specific proteins (LGN/Numb/NuMA/Insc) *in vitro* in combination with live cell imaging to monitor cells undergoing cell division will provide dynamic insight into the role of these proteins in the establishment of ACD.

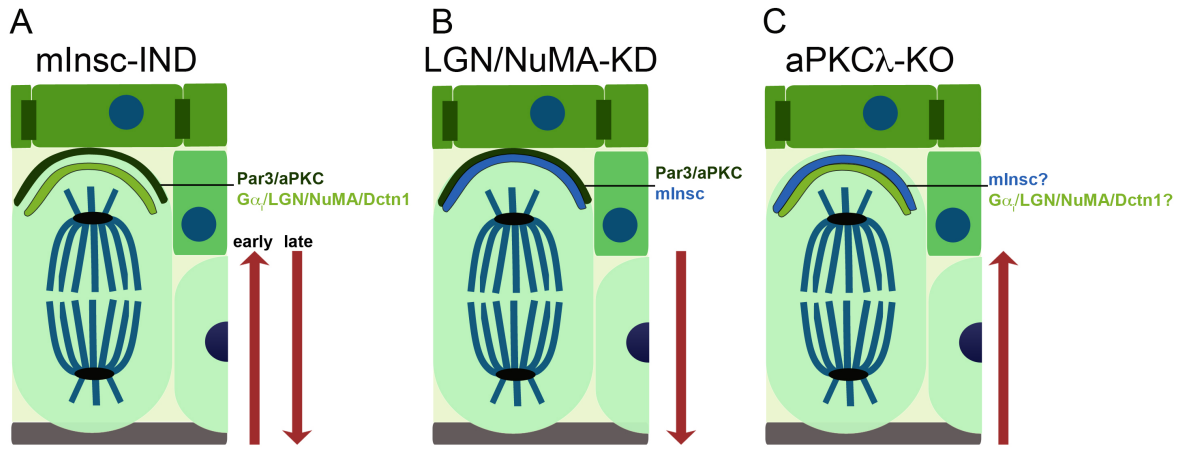

Figure 3. 1: aPKCλ negatively regulates ACD, whereas Insc, LGN or NuMA promote ACD

Effects of deletion/induction of molecular mediators in the murine epidermis on the ratio of asymmetric vs. symmetric cell division. (A) Forced expression of mInsc induces increased asymmetric spindle orientation in the epidermis shortly after induction (early), whereas 3 days after induction, this effect is reversed (late) (Poulson and Lechler, 2010). (B) Epidermal basal cells were biased towards symmetric spindle orientation after transfection with shRNAs targeting either LGN or NuMA (Williams et al., 2011). (C) aPKCλ$^{epi-/-}$ mice display an increased amount of ACD. KO: Knock-out, IND: inducible, KD: Knock-down.

3.3.2 Altered localization and expression of the cell fate determinant Numb

One possible candidate to mediate cell fate changes caused by epidermal loss of aPKCλ is the cell fate determinant Numb. Although no differences in Numb localization were detected in asymmetrically dividing embryonic basal cells (Fig. 2.32), a significant increase in asymmetric Numb segregation in aPKCλ$^{-/-}$ keratinocytes was discovered *in vitro* (Fig. 2.34). In *Drosophila*, Numb is a direct substrate of aPKC and its asymmetric segregation has been reported to be a prerequisite for ACD (Smith et al., 2007; Wirtz-Peitz et al., 2008). In mammalian hematopoietic SCs, Numb is essential to maintain hematopoietic SCs in their undifferentiated state (Duncan et al., 2005). Increased asymmetric segregation of Numb in aPKCλ$^{-/-}$ keratinocytes, which display increased ACD *in vivo,* suggests that Numb might execute a similar function in mammalian keratinocytes as in *Drosophila* neuroblasts. Moreover, we report a phosphorylation-dependent downregulation of protein levels of Numb

in aPKCλ$^{-/-}$ epidermis and differentiated aPKCλ$^{-/-}$ keratinocytes (Fig. 2.33). Since Numb levels are only downregulated in aPKCλ$^{-/-}$ keratinocytes after Ca^{2+}-induced differentiation, this effect might rather be attributed to an essential role of mammalian Numb in adherens junction formation, as described in murine neuronal progenitors (Rasin et al., 2007). The decreased number of progenitor-like cells and downregulation of Numb in aPKCλ-deficient mice are consistent with the reports on Numbs function in the mouse brain: Loss of Numb function results in precocious neuronal differentiation at the expense of neuronal progenitors in the central nervous system (Verdi et al., 1999). However, if Numb is removed conditionally, neural progenitors overproliferate and show impaired neuronal differentiation (Li et al., 2003). How the reduced number of progenitor cells in aPKCλ$^{epi-/-}$ mice and increased proliferation in aPKCλ$^{-/-}$ cells might be linked to Numb downregulation is under investigation (Susanne Vorhagen, PhD thesis).

3.4 aPKCλ is crucial for postnatal HFSC maintenance and cell fate

Altered cellular fate, possibly mediated by increased ACD, was also manifested in the HFSC compartment of aPKCλ$^{epi-/-}$ mice. We observed a loss of BrdU label retention in HFSCs (Fig. 2.10), a gradual decrease in bulge SC marker expression (Fig. 2.12) and a loss of colony formation *in vitro* (Fig. 2.16+2.19) after aPKCλ depletion, demonstrating that aPKCλ is necessary to maintain bulge SC quiescence, identity and proliferative potential. The gradual exhaustion of quiescent bulge SCs was accompanied by an expansion of a population of progenitor cells located above the bulge in the infundibulum/junctional zone (Fig. 2.13), strongly suggesting that cell fate of bulge progenitor cells is altered towards more committed progenitor cell populations residing in the infundibulum zone of the HF (s. 2.8.2; Fig. 3.1). Several reports couple HFs being continuously in a proliferative state to decreased expression of SC markers (Castilho et al., 2009; Yang et al., 2009). Similar to aPKCλ$^{epi-/-}$ mice, these findings are generally accompanied by epidermal hypertrophy and either perturbed BMP signaling or elevated β- catenin signaling (Benitah et al., 2005; Kobielak et al., 2007; Romano et al., 2010).

In mammalian SCs, as for example hematopoietic SCs, a balance between SCD and ACD needs to be maintained. Here, SCDs expand the SC pool by resulting in two daughter SCs, whereas ACDs simultaneously maintain their own SC pool and give rise to differentiating progeny (Duncan et al., 2005). Thus, since ACDs promote cell fate of differentiated cells, the loss of bulge HFSCs is in accordance with the observation of increased ACD in aPKCλ$^{epi-/-}$ mice. So far, these studies have not deciphered which exact cellular behavior leads to the loss of bulge SC identity over time. Bulge HFSCs and hair germ cells have been reported to divide asymmetrically in late telogen and at the onset of anagen (Zhang et al., 2010). How these dynamics are altered by the aPKCλ deletion is not yet clear. Spindle orientation is

affected in bulge SCs and proliferation is increased in the bulge region. On the other hand, specifically the infundibula are significantly widened (Fig. 2.7) and the shift towards more asymmetrically dividing cells is most pronounced in the infundibulum zone of aPKCλ$^{-/-}$ HFs (Fig. 2.23). This suggests, that quiescent bulge SCs might be activated and migrate towards the infundibulum zone prior to cell division. Analysis of *in vitro* migration behavior indeed revealed that nonpolarized aPKCλ$^{-/-}$ keratinocytes do migrate with a reduced directionality and an increased velocity (data obtained by Oana Persa). How dynamics of ACD/SCDs and migratory behavior throughout the hair cycle are specifically altered in aPKCλ$^{-/-}$ bulge HFSC *in vivo*, will be subject of further studies (s. 3.8).

Lrig1-expressing cells of the infundibulum zone are more actively cycling as compared to quiescent bulge SCs and were demonstrated to mainly replenish cells of the IFE and the SG in a bipotent manner (Zhang et al., 2010; Jensen et al., 2009). Recently, progeny of quiescent bulge SCs was shown to migrate upward of the bulge to transit through the MTS24 positive and Lrig1 positive compartment towards the SG to adopt sebocyte cell fate, indicating a hierarchy in marker expression of bulge HFSCs (Petersson et al., 2011). This suggests, that the increased population of Lrig1/MTS24 positive cells indeed originates from aPKCλ$^{-/-}$ bulge SC, and supports this model of a hierarchy of progenitor cells in the HF. Cell clones expanding from the bulge towards the HF bulb are observed in a cyclic fashion during anagen phases of the hair cycle (Zhang et al., 2010). On the other hand, bulge SC were recently demonstrated to continuously fuel the infundibulum and SG, independent from the hair cycle (Petersson et al., 2011). Thus, aPKCλ$^{-/-}$ bulge SC might be lost simultaneously in two directions: whereas hair bulb replenishing progenitors are constantly targeted towards the lower part of anagen-like aPKCλ$^{epi-/-}$ HFs, an increased amount of activated bulge SCs fuel into the infundibulum/SG region of aPKCλ$^{-/-}$ HFs. This dual constant replenishment of cells ultimately leads to exhaustion of the aPKCλ$^{epi-/-}$ HFSC compartment. The fact that aPKCλ$^{epi-/-}$ SGs seem to be MTS24 positive suggests that MTS24 expressing cells did inappropriately adopt sebocyte cell fate (Fig. 2.13) and histological analysis of one year old aPKCλ$^{epi-/-}$ epidermis suggested ectopic SG formation (Fig. 2.20). Moreover, ectopically localized cells of a melanocytic appearance were detectable in aPKCλ$^{epi-/-}$ skin (Fig. 2.20). These phenotypic observations further underline the detected alterations in cellular fate of aPKCλ$^{epi-/-}$ HFSCs towards progenitor cells of the SG and IFE. In accordance with the aPKCλ$^{epi-/-}$ phenotype, aPKCλ expression is specifically upregulated in the bulge HFSC compartment. Since aPKCζ expression is not altered in HFSCs (Fig. 2.27), aPKCλs role in maintaining the bulge HFSC compartment might be isoform-specific. Staining for markers of early HFSCs did not reveal any obvious change suggesting that loss of aPKCλ did not affect HFSC specification (Fig. 2.14). On the other hand, ACDs are already increased at E16.5

pointing towards altered cell fate already at this stage (Fig. 2.24). Moreover, mRNA expression of CD34 and K15 was already reduced in newborn mice (data not shown). Overall, our data demonstrate that aPKCλ is required to maintain the bulge HFSC compartment throughout postnatal life and to prevent HFSC fate changes leading to progression of aPKCλ$^{-/-}$ SCs into the more differentiated infundibulum or hair bulb compartments.

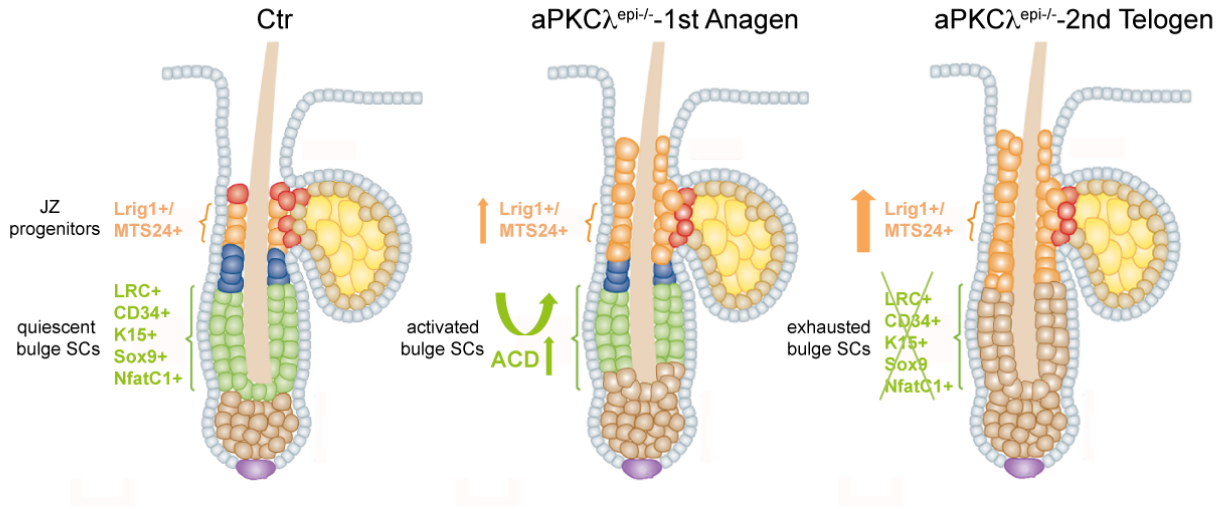

Figure 3. 2: Loss of aPKCλ leads to a gradual exhaustion of the SC compartment and cell fate changes in HFSCs

In ctr HFs, bulge SCs are largely quiescent (LRC=label retaining cells) and express a set of specific bulge SC markers (CD34, K15, Sox9, NfatC1). Loss of aPKCλ (panel 2, 1st anagen) leads to a loss of quiescence, concomitant with increased asymmetric cell division (ACD) in the bulge SC compartment. This leads to a decrease of SC marker expression and cell fate changes in aPKCλ$^{epi-/-}$ progenitors, followed by an increase in the expression of markers of junctional zone progenitors (Lrig1, MTS24). Gradually, the HFSC compartment is exhausted and the cell population residing in the upper part of the HF is expanded (panel 3, 2nd telogen). Modified from (Horsley 2011).

3.5 Altered progenitor cell marker expression in aPKCλ$^{epi-/-}$ mice

Reduced transcription of CD34 and K15 was already observed in first anagen aPKCλ$^{epi-/-}$ HFs, even though no obvious changes in K15 and CD34 staining were observed yet at this stage (Fig. 2.12). This suggests that loss of HFSC identity is first noticeable on the gene transcription level and these studies are more sensitive compared to immunohistochemical localization analyzes. Sox9 has been implicated in HF differentiation and activation of HFSCs towards HF fate (Fig. 2.12) (Vidal et al., 2005; Nowak et al., 2008). Ectopic expression of Sox9 in other HF regions than the bulge in aPKCλ$^{-/-}$ HFs may thus explain the observed defects in hair follicle differentiation and hair cycle upon loss of aPKCλ. In line with a loss of quiescence of aPKCλ$^{-/-}$ HFSCs is the reduced number of NfatC1-positive keratinocytes in aPKCλ$^{epi-/-}$ HFs (Fig. 2.10). NfatC1 is crucial to retain HFSCs in their quiescent state (Horsley

et al., 2008). In summary, altered expression of the above-mentioned SC markers indeed demonstrates perturbed HFSC homeostasis after loss of aPKCλ.

Whereas the aPKCλ$^{-/-}$ HFSCs were gradually depleted, MTS24 and Lrig1-positive cells significantly increased in aPKCλ$^{-/-}$ HFs (Fig. 3.1). Since replenishing bulge cells are lost over time, we expected a corresponding drop of the percentage of proliferating Plet1/MTS24 and Lrig1 expressing progenitor cells in older mice. Indeed, the effect of an increased population of MTS24 positive cells was no longer pronounced in one year old aPKCλ$^{epi-/-}$ mice compared to ctr mice. In contrast, the Lrig1 positive population was still enlarged at this stage. SCs have been shown to migrate successively through both (MTS24 followed by Lrig1 positive) compartments (Petersson et al., 2011). Perhaps, some progenitors originating from the bulge region end their trail in the Lrig1 positive compartment, or Lrig1 positive progenitors are depleted even later than we have analyzed in this study. In combination, these data support, that the MTS24 and Lrig1 positive cell populations might have independent functions.

In vitro colony formation assays (CFA) demonstrated a loss of proliferative potential in keratinocytes isolated from adult but not newborn aPKCλ$^{epi-/-}$ mice (Fig. 2.19). Notably, the HFSC niche integrity was not yet obviously affected in immunofluorescence studies using several SC markers at this stage. This indicates that CFAs are more sensitive as compared to immunofluorescence studies, and may thus be used in combination with transcriptional profiling to assay SC behavior and identity. Lrig1 and MTS24 positive keratinocytes should be present in ctr as well as aPKCλ$^{-/-}$ overall keratinocyte isolations. Since keratinocytes expressing Lrig1 and Plet1/MTS24 were shown to be clonogenic (Depreter et al., 2008; Jensen et al., 2009), one might hypothesize that the increased pool of Lrig1 and Plet1/MTS24 positive aPKCλ$^{-/-}$ keratinocytes would be able to rescue the loss of proliferative potential *in vitro*. However, aPKCλ$^{-/-}$ keratinocytes also display a more differentiated morphology and this might overcome the ability of Lrig1 or MTS24 positive cells to proliferate. Whether aPKCλ$^{-/-}$ keratinocytes expressing Lrig1 or MTS24 are still able to proliferate and form colonies may be analyzed after FACS sorting for these cell populations prior to CFAs. These results demonstrate that despite the increased expression of progenitor cells of the infundibulum *in vivo*, aPKCλ$^{-/-}$ keratinocytes have lost their potential to proliferate and form large colonies *in vitro*, confirming the *in vivo* observation of a loss of stemness over time.

3.6 aPKCλ is required for balanced proliferation in the HF

Loss of aPKCλ was associated with increased proliferation in all epidermal compartments, most pronounced in the HF bulge region (Fig. 2.11). Increased proliferation and a loss of BrdU-label retention in the bulge HFSC compartment suggests that the phenotype of increased proliferation is at least in part caused by an over-activation of SCs. If a gradually exhausting SC pool causes increased proliferation in aPKCλ$^{epi-/-}$ mice, we hypothesize that the amount of over-proliferating aPKCλ$^{-/-}$ cells might decline with ageing. Quantification of BrdU incorporation in one year old mice will provide more insight on how proliferation is affected by the exhaustion of bulge SCs.

The proliferation phenotype observed in aPKCλ$^{epi-/-}$ mice may be explained by the fact that aPKC has been implicated into proliferation/growth/survival pathways. For example, aPKC is known to activate Raf-1/MAPK signaling. At least the aPKCζ isoform interacts with the kinase MEK5, leading to mitogenic activation of the MAPK signaling cascade (Diaz-Meco and Moscat 2001). Moreover, aPKCζ phosphorylates and thus inhibits the MAPK signaling inhibitor RKIP (Corbit et al., 2003). However, if aPKCλ would mainly function to activate MAPK signaling in the skin, one would expect the opposite phenotype as observed for aPKCλ$^{epi-/-}$ mice, namely decreased proliferation. Moreover, phosphorylation of ERK1/2 was not altered in aPKCλ$^{epi-/-}$ keratinocytes after EGF stimulation (data not shown). This suggests, that a different signaling pathway must account for increased proliferation in aPKCλ$^{epi-/-}$ mice. The observed increase in Wnt/β-cat signaling may also be responsible for enhanced proliferation by transcriptionally activating proliferation-associated target genes, especially in activated HFSCs (Huelsken et al., 2001; Lo Celso et al., 2004). The fact that proliferation is especially increased in aPKCλ$^{-/-}$ bulge SCs promotes this hypothesis. Nevertheless, aPKC binds to a multitude of downstream mediators and for this reason, an unknown role of aPKC may account for the phenotype of increased proliferation. For example, aPKC has been demonstrated to modulate Insulin/IGF signaling in many tissues (Farese and Sajan 2010). This classical growth pathway is crucial for proliferative potential (Stachelscheid et al., 2008) and the balance of ACD/SCD (unpublished results Heike Stachelscheid) in the epidermis. In *Drosophila*, aPKC has been implicated in the regulation of proliferation by regulating the Salvador/Warts/Hippo pathway (Parsons et al., 2010) and this pathways is essential to control epidermal proliferation (Schlegelmilch et al., 2011). However, analysis of expression and localization of Yap1, the transcriptional effector in the Hippo pathway, did not reveal any differences (data not shown), suggesting that the function of aPKC in Hippo signaling is not conserved in murine skin. Overall, the data demonstrate that aPKCλ is important to balance proliferative behavior of keratinocytes, possibly due to increased Wnt/β-cat signaling.

3.7 aPKCλ controls epidermal differentiation

The aPKCλ$^{epi-/-}$ phenotype is characterized by altered differentiation in all epidermal compartments where ACD is increased. Reduced expression of HF-specific keratins (s. 2.4.3) that serve as markers for different HF layers indicated differentiation defects in aPKCλ$^{epi-/-}$ HFs (Fig. 2.8). The HF-specific keratins affected by the aPKCλ deletion are crucial for proper HF formation, differentiation and integrity (Chen et al., 2008; Kiso et al., 2009). Global RNA expression analysis on newborn epidermis revealed downregulation of several HF differentiation-specific genes in the absence of aPKCλ (Fig. 2.8; s. 2.4.3). Although most of these keratins are used to identify several layers within the HF, the only layer that expresses all affected keratin mRNAs is the cuticle, suggesting that aPKCλ specifically regulates cuticle differentiation. In contrast to HF-specific keratins, only one gene important for IFE differentiation (K2, specific for the *str. corneum*) and none specific for SG differentiation were affected by aPKCλ deletion, however SGs are not yet developed at this age. It is highly interesting that the effect of perturbed HF differentiation is already detectable on the gene expression level in newborn mice, even before a phenotypic defect becomes apparent later in postnatal development. This suggests that perturbed HF differentiation is a direct consequence of the aPKCλ deletion.

Alterations in several pathways might explain altered HF differentiation in aPKCλ$^{epi-/-}$ mice. For example, perturbed HF differentiation was reported in mice where Wnt/β-catenin was elevated (Van Mater et al., 2003). β-catenin and the transcriptional activator Lef1 promote hair cell fate and HF differentiation in response to Wnt signaling. Lef1 binds directly to HF-specific keratin genes (Huelsken et al., 2001; Merrill et al., 2001). Thus, the observations that HF differentiation and β-catenin localization are affected by the loss of aPKCλ might be connected. Another effector of IFE and HF differentiation as well as lineage commitment is the Notch signaling pathway (Blanpain et al., 2006; Watt et al., 2008; Demehri and Kopan 2009; Lin et al., 2011). However, preliminary qRT-PCR analyses of expression of the Notch ligand Jagged 1 or Notch target genes Hes1/2 and Hey1/2 in adult aPKCλ-deficient epidermis did not reveal any significant differences (data not shown). Shh signaling plays an important role for HF differentiation as well (L. C. Wang u. a. 2000), but qRT-PCRs did also not reveal major alterations in Shh target gene expression (data not shown). The role of polarity proteins in HF differentiation has not yet been studied in great detail. Nevertheless, it has been reported that epidermis-specific inactivation of the small GTPases Rac1 and Cdc42 cause perturbed HF differentiation associated with reduced expression of keratins specific for the IRS, HS and companion layer, similar to aPKCλ$^{epi-/-}$ mice (Benitah et al., 2005; Wu et al., 2006; Castilho et al., 2007). No differences were observed in Cdc42 activation after loss of aPKCλ, but Rac1 is less activated in aPKCλ$^{-/-}$ epidermis (s. 2.15), suggesting that aPKCλ

may act upstream of Rac1 in HF differentiation. Overall, the data shows that aPKCλ, likely in its capacity as a polarity protein, is important for HF differentiation.

3.8 Which signaling pathway might mediate the aPKCλ$^{epi-/-}$ phenotype?

It is not clear if aPKCλ may be altering signaling directly to cause the aPKCλ$^{epi-/-}$ phenotype and if so, through which signaling processes this would occur.

3.8.1 Enhanced β-catenin signaling

After loss of aPKCλ we report enhanced transcriptional activity of endogenous β-catenin (Fig. 2.28), which has been implicated in HF differentiation, HFSC activation and function (Watt and Jensen 2009). Increased Wnt/β-catenin signaling was not reflected in altered target gene expression *in vivo* (Fig. 2.30). One reason might be that aPKCλ does not act as a key determinant of β-catenin signaling but rather as a modulator setting thresholds in individual cells, e.g. at specific time points in the hair cycle. Constitutive activation of β-catenin (ΔN87-β-cat mice) results in *de novo* hair morphogenesis (Gat et al., 1998). Upon induction of low levels of β-catenin signaling (K5/S33y-β-catenin mice) HFs enter anagen phases, and with prolonged activation HF become hyperplastic, show increased proliferation and altered HF differentiation (Van Mater et al., 2003). Intriguingly, as we have shown for aPKCλ$^{epi-/-}$ mice, elevated Wnt/β-catenin signaling increases the Lrig1 positive cell population of the junctional zone (Jensen u. a. 2009). These phenotypes strongly resemble the main characteristics of the aPKCλ$^{epi-/-}$ phenotype therefore supporting that aPKCλ$^{epi-/-}$ mice may require activated β-catenin for the development of the phenotype. On the other hand, low levels of β-catenin signaling are also associated with increased SG and infundibulum fate (Huelsken et al., 2001). This is in contrast to the aPKCλ$^{epi-/-}$ phenotype, where elevated Wnt/β-catenin signaling is not only associated with promotion of anagen but also enlargement of the SG and infundibulum compartment. Moreover, in mice expressing stabilized β-catenin, neither development nor biochemistry of the bulge region is affected, whereas bulge SC identity is lost when β-catenin expression is diminished (Lowry et al., 2005). These findings suggest that aPKCλ mediated regulation of HFSCs might be independent of β-catenin signaling. The small GTPase Cdc42 may provide a direct link of aPKC to Wnt/β-catenin signaling in the epidermis. Binding of Cdc42 to Par6/aPKCζ activates aPKCζ, which phosphorylates GSK3β kinase thereby lowering its activity resulting in increased β-catenin stabilization (Wu et al., 2006). This would thus predict that loss of aPKC reduces β-catenin activity, which is in contrast to what is observed in aPKCλ$^{epi-/-}$ mice. However, the mechanism proposed by Wu et al. (2006) may be specific to the aPKCζ isoform. In addition, our findings indicate that aPKCλ dependent regulation of β-catenin signaling is independent of its kinase function (Fig. 2.28), thus also suggesting that aPKCλ

affects β-catenin via a different mechanism. *In vivo*, β-catenin did appear to be less recruited to sites of cell-cell junctions. A barrier defect was observed in aPKCλ$^{epi-/-}$ keratinocytes, indicating that mislocalized β-catenin might be indeed attributed to alterations in junction formation. In line with these findings, β-catenin has been reported to mediate the interaction of aPKC with cadherins in *Xenopus*, thus connecting the adherens junction complex to polarity (Seifert et al., 2009). To functionally test whether increased β-catenin signaling is indeed causative for the aPKCλ$^{epi-/-}$ phenotype, aPKCλ$^{epi-/-}$ mice might be crossed to mice expressing dominant-negative versions of β-catenin or Lef1 (Niemann et al., 2003). Moreover, it will be interesting to investigate whether the aPKCλ$^{epi-/-}$ phenotype can be rescued by the application of Wnt inhibitors *in vitro*.

3.8.2 Perturbed BMP signaling

Gene expression of BMP4 was significantly reduced during anagen and telogen in aPKCλ$^{epi-/-}$ HFs (Fig. 2.31). Inhibition of BMP (bone morphogenic protein) signaling is essential for the activation of HFSCs and entry of HFs into anagen phases of the cell cycle (Zhang et al., 2006). In accordance with the aPKCλ$^{epi-/-}$ phenotype, blocking BMP signaling by deletion of the BMP type 1a receptor results in precocious activation of HFSCs, induction of anagen and a loss of characteristics of the bulge SC niche (Kobielak et al., 2007). The finding that BMP4 expression was specifically reduced in CD34 positive SCs is of high interest since it mirrors the loss of quiescence detected in aPKCλ$^{-/-}$ HFs. BMP4 signaling was shown to maintain expression and activity of NfatC1, a transcription factor demonstrated to be crucial for HFSC quiescence via repression of CDK4 gene expression (Horsley et al., 2008). Since we did not observe significant differences in the expression of NfatC1 or CDK4 (Fig. 2.10), the effect of decreased BMP signaling is likely to be transduced via a differential pathway, for example by Smad transcriptional factors (Zhang et al., 2006). Whether perturbed BMP signaling is responsible for the development of the aPKCλ$^{epi-/-}$ phenotype or rather a consequence of it, and how Wnt/β-catenin and BMP signaling influence each other in aPKCλ$^{epi-/-}$ mice will be investigated in the future.

3.8.3 Decreased activity of the small GTPase Rac1

Since a decreased activity of the small GTPase Rac1 was detected in aPKCλ$^{epi-/-}$ epidermis (Fig. 2.35), studies on the role of Rac in HFSC maintenance are of great interest. Rac1 deletion led to an exhaustion of the HFSC compartment followed by HF degeneration, similar to the phenotype of one year old aPKCλ$^{epi-/-}$ mice (Benitah et al., 2005; Castilho et al., 2007). To test the significance of reduced Rac1 activation in aPKCλ$^{epi-/-}$ epidermis, aPKCλ$^{floxed/floxed}$ mice might be crossed to mice expressing an activating mutant of Rac (L61Rac1)(Behrendt et al., 2012; Stachelscheid et al., 2008).

3.9 Future directions

This work demonstrates that aPKCλ is crucial for the identity and maintenance of HFSC by affecting the ratio of asymmetric vs. symmetric cell divisions and thus cell fate decisions. Several important open questions remain:

1. Is altered behavior of progenitor cells specifically in the HFSC compartment sufficient to cause the aPKCλ$^{epi-/-}$ phenotype?
2. How exactly is cell fate affected in bulge SCs on a single cell level?
3. To which extend is the phenotype of aPKCλ$^{epi-/-}$ mice caused by increased ACD or different migratory behavior of SCs in the HFSC compartment?
4. Which exact molecular mechanism is causative to the aPKCλ$^{epi-/-}$ phenotype?
5. How do aPKCλ$^{epi-/-}$ SCs behave after being challenged, as for example by transplantation experiments?

First experiments were performed to establish a lineage-tracing system in aPKCλ$^{epi-/-}$ mice to analyze the fate of aPKCλ$^{epi-/-}$ keratinocytes *in vivo,* however the system harbored several technical challenges (s. 2.10). To specifically answer the questions stated above *in vivo* using a different system, aPKCλ$^{floxed/floxed}$ mice were crossed to two mouse models, where a Tamoxifen-inducible version of the Cre recombinase (Cre^{ERT2}) is expressed under the control of a SC-specific promotor (for explanation of the Cre^{ERT2} lineage tracing system, see 2.7). First, in Lgr5-EGFP-IRES-Cre^{ERT2} "knock-in" mice, the endogenous Lgr5 promotor controls the expression of enhanced green fluorescent protein (EGFP) and the Cre^{ERT2} fusion protein. The Lgr5 promotor marks a SC subpopulation located in the lower bulge, the secondary hair germ of telogen HFs, and the ORS of anagen HFs. Lgr5 positive SCs are actively cycling and maintain all HF lineages over long periods of time (Jaks et al., 2008). Induction of Cre^{ERT2} expression in Lgr5-EGFP-IRES-Cre^{ERT2};aPKCλ$^{floxed/floxed}$ mice by Tamoxifen application will enable us to specifically delete aPKCλ in the Lgr5 positive progenitor cell compartment. After induction of Cre^{ERT2} exclusively in the SC compartment, we can examine whether SC-specific loss of aPKCλ is sufficient to recapitulate the aPKCλ$^{epi-/-}$ phenotype. Since cells expressing an active Cre^{ERT2} recombinase are marked by EGFP expression, we will be able to monitor the behavior of single Lgr5-EGFP-IRES-Cre^{ERT2};aPKCλ$^{-/-}$ (aPKCλ$^{Lgr5-/-}$) progenitors over time. Isolation of EGFP-positive cells by FACS sorting will allow us to functionally analyze aPKCλ$^{Lgr5-/-}$ cells, as for example in transplantation experiments and CFAs or to assess possible signaling pathways by qRT-PCR. To study the cellular mechanisms of tissue renewal (e.g. orientation of division) in aPKCλ$^{Lgr5-/-}$ mice more precisely, live cell imaging techniques will we established (Petersson u. a. 2011).

Second, aPKCλ$^{floxed/floxed}$ mice were crossed to K15Cre^{ERT2} mice, which express Cre^{ERT2} under control of the K15 regulatory promotor sequence (Petersson et al., 2011). Furthermore, to perform lineage-tracing experiments, these mice were crossed to R26RYFP reporter mice (Srinivas et al., 2001). In these mice, the CreERT2 recombinase will be active in a subpopulation of the bulge, which harbors under homeostatic conditions largely quiescent and multipotent SCs repopulating all epidermal lineages (Jaks et al., 2010). After establishment of an induction protocol, the experimental set up will be similar as stated for aPKCλ$^{Lgr5-/-}$ mice. Finally, in cooperation with the laboratory of Valentina Greco (Yale University, New Haven), an *in vivo* imaging system using a 2-photon approach will be established. To monitor niche-intrinsic dynamics in aPKCλ$^{epi-/-}$ mice over time, K14Cre^{ERT2};aPKCλ$^{floxed/floxed}$ mice will be crossed to inducible K14H2BGFP mice (Greco et al., 2009; Tumbar et al., 2004). Together, these inducible mouse models will allow us to learn about the cellular mechanisms by which aPKCλ regulates asymmetric divisions, cell fate decisions and thus epidermal homeostasis.

4 Material and Methods

4.1. Mice

Deletion of aPKCλ was achieved by crossing aPKCλ$^{floxed/floxed}$ mice (collaboration with M. Leitges, Oslo) with a K14-Cre recombinase line (Hafner et al., 2004). To achieve an epidermis-specific, conditional aPKCλ deletion, female aPKCλ$^{floxed/floxed}$ mice were crossed to K14-Cre/+; aPKCλ$^{floxed/+}$ males on a C57 BL/6 background.

To achieve a Tamoxifen-inducible, conditional deletion, K14-Cre^{ERT2}/+; aPKCλ$^{floxed/+}$ males (Stratis et al., 2006) were crossed to female aPKCλ$^{floxed/floxed}$ mice. To perform lineage tracing experiments, mice were crossed to R26REYFP reporter mice (Srinivas et al., 2001). The K14-Cre^{ERT2}/+; aPKCλ$^{floxed/+}$ males were crossed to aPKCλ$^{floxed/+}$;EYFP$^{TG/TG}$ mice. Mice were housed was in the animal facilities of the Pharmacology or Center for Molecular Medicine, Cologne. Experimental procedures were performed according to institutional guidelines and animal license given by the State Office North Rhine-Westphalia.

4.1.2 PCR Genotyping

A small piece of the tip of the tail of 3 weeks old mice was clipped for DNA isolation and incubated in lysis buffer containing 0,2M NaCl, 0,1 M Tris/HCl, pH8,5; 5 µm EDTA; 0,2% SD and 100 µg/ml Proteinase K (Sigma Aldrich, 39 U/mg) for 4 hrs at 55°C. The DNA was extracted using a standard DNA-isolation protocol using the phenol-chloroform method and precipitated using isopropanol. Genotyping was performed with customized primers (table 3) in a standard Red-Taq DNA polymerase (Sigma Aldrich) reaction. PCR reactions were carried out in a Personal Thermocycler (Biometra) using a standard PCR program (table 4). The PCR product was run on a 1 % agarose gel with 1 kb ladder (Invitrogen).

Table 3: Primer used for genotyping PCRs.

Name	Sequence	Genotyping
PKCwt1	ttgtgaaagcgactggattg	aPKCλ flox
PKC355bp	aattgttcatgttcaacactgct	aPKCλ flox
PKCdel	actaagcattgcctggcatc	aPKCλ flox
PKC1kb	cttgggtggagaggctattc	aPKCλ flox
CreSL2as	catcactcgttgcatcgacc	K14Cre
K14-2202snew	gatgaaagccaaggggaatg	K14-Cre

Table 4: PCR programs for genotyping PCRs for aPKCλ or K14Cre.

aPKCλ			K14		
94 °C	5 min		94 °C	1 min	
94 °C	45 sec	40 x	94 °C	30 sec	35 x
55 °C	30 sec		58 °C	30 sec	
72 °C	1 min		72 °C	40 sec	
72°C	10 min		72 °C	5 min	

4.1.3 Tamoxifen treatment

Tamoxifen-food (Harlan Laboratories BV) was placed in cages instead of normal food for a feeding period of 3 weeks. After three weeks, Tamoxifen food was replaced by normal food.

Tamoxifen (Sigma Aldrich) was dissolved in 200 µl sun flower oil for 1 hr under vigorous shaking. Tamoxifen was injected intraperitoneally according to experimental injection protocol. To apply the Tamoxifen in the appropriate phase of the hair cycle, animals were shaved and the current hair cycle phase was determined according to (Müller-Röver et al., 2001).

4.2 Cell biology

4.2.1. Histological analysis and tissue collection

Mice were collected and dissected at several embryonic and postnatal days. Mice were weighed and exact age and sex was recorded. For proliferation analyis, 50 mg/kb Brom-desoxyuridine (BrdU), (Sigma Aldrich) was injected for 0,5 hr. For skin phenotypic analysis, back skin was, if necessary, shaved and mice were photographed. Segments of the skin were removed from the dorsal section of the mouse back and were either snap-frozen in TRIZOL (Invitrogen) for subsequent RNA isolation, embedded in Optimal Cutting Temperature (OCT) Compound (Tissue Tek) for cryo sections, fixed in 0,2 % glutaraldehyde for whole-mount staining or fixed in 4 % PFA for 12 hrs for paraffin sections. After fixation in 4 % PFA, samples were perfused with Xylene followed by Paraffin to enable paraffin embedding. Cryo or Paraffin sections were sectioned for immunohistochemistry (4-8 µm) and dried on glass coverslips for histological staining.

4.2.2 Histological staining

For histological analysis of 4-8 µm paraffin-embedded skin section, Hematoxylin and Eosin stainings were performed. Slides were deparaffinized with two Xylene washes followed by rehydration through an ethanol series. Slides were washed 3 minutes in Hematoxylin, washed twice in H_2O and 30 sec in 0.2 % (v/v) HCL. Subsequently, slides were washed

through increasing Ethanol series and stained using EosinY for 30 sec. After Ethanol washes, slides were mounted in Entellan. Stainings were analyszed and photographed by light microscopy using a BX51 Olympus light microscope.

4.2.3 Immunohistochemistry

Fluorescent stainings were analyzed using an Olympus IX71, a confocal microscope Zeiss Meta 510 or with a confocal Olympus FV1000 microscope. Pictures were processed with Adobe Photoshop and Illustrator. Statistical analyses were done using Microsoft Exel and GraphPad Prism 5.

4.2.3.1 Paraffin embedded skin sections

Slides were deparaffinized with two Xylene washes followed by rehydration through an ethanol series and washed twice in PBS. Antigens were unmasked with the recommended retrival buffer in the 2100 Retriever (Proteogenix) using high temperature >120 °C and pressure. Subsequently, the sections were blocked with 10 % serum derived from the species from which the secondary antibody was taken and incubated for 1hr at room temperature in a humified chamber. After washing with PBS, the slides were incubated in a humified chamber 1 hr or overnight with the primary antibody diluted in blocking solution. After washing with PBS, the slides were incubated with the secondary antibody according to manufactures instructions. Nuclei were counterstained using propidium iodide or DAPI (Sigma Aldrich). After a final washing, the slides were mounted in gelvatol and stored at 4 °C in the dark.

4.2.3.2 Frozen skin sections

Cryosections (6µm) were fixed in ice-cold methanol or aceton for 10 min at room temperature. Tissue were blocked in PBS containing 1 % BSA and in case of PFA fixation 0.02 % Tween 20 for 1 hr in a humified chamber. After washing with blocking solution the slides were incubated with the primary antibody diluted in blocking solution 1 hr or overnight at 4 °C in a humified chamber. After washing in PBS the slides were incubated with the secondary antibody coupled to Alexa 488 or Alexa 594 for 1hr diluted in blocking solution according to manufactures instructions. Nuclei were counterstained using propidium iodide or DAPI (Sigma Aldrich). After a final washing, the slides were mounted in gelvatol and stored at 4 °C in the dark.

4.2.3.3 Whole-mounts of tail skin

Whole-mounts of mouse tail epidermis were prepared as previously described (Müller-Röver u. a. 2001). Briefly, whole skin was removed from the tail of mice and incubated for 3 hrs at 37 ^{o}C in 5 mM EDTA/PBS. The epidermis was then separated from the dermis and fixed in 4% formal saline or 0,2 % glutaraldehyde for 2 hrs at room temperature (Braun et al., 2003).

Fixed epidermal sheets were blocked for 1 hr in TBS buffer (20 mM HEPES, pH 7.2, 0.9 % NaCl) containing 0.5 % milk powder, 0.25 % fish gelatine and 0.5 % TritonX-100. After incubation over night with primary antibodies at RT, whole-mounts were washed in PBS-0.2 % Tween-20 for 4 hrs. Secondary antibodies were then applied o/n at RT and washing steps were repeated for 4 hrs. Finally, the whole-mounts were washed and stored at 4 °C in the dark.

4.2.4 BrdU labeling

Bromodioxyuridine (BrdU) is a thymidine analogue that when present, incorporates into newly synthesized DNA during cell division. To compare populations of quiescent label-retaining cells (LRC) te-days-old mice were injected with 50 mg/kg bodyweight BrdU every 24 hrs for 3 injections. Following a 15, 40 or 70 day chase period the mice were sacrificed and dorsal skin (day15) and tail skin whole-mounts (day 40 and day 70) were isolated for immuno-histochemical staining and analysis (Braun et al., 2003)

4.2.5 quantitative Real-Time PCR

Gene expression was analyzed using qRT-PCR. RNA was extracted from isolated epidermis using RNeasy Minikit (Qiagen) according to the manufacturers instructions. After FACS sorting of α6-integrin/CD34+ or α6-integrin/CD34- keratinocytes from adult mice, RNA was isolated by TRIZOL isolation according to the TRIZOL manufactures' instructions (Invitrogen). In both cases, RNA was cleaned up after isolation by on-column DNase Digestion (Quiagen). Quality of the RNA was checked on a 1 % agarose gel and RNA concentration was determined usig a Nanospec Spectrometer (Thermo Scientific). cDNA was prepared using at least 500 ng of RNA by a reverse transcription reaction using either Superscript III Reverse Transcriptase (Invitrogen) or Quantitect Reverse Transcriptase (Quiagen) according to manufactures instructions. cDNA quality was checked by GAPDH and actin PCR. Taqman inventoried assays were purchased from applied biosystems (Table 5). To analyze gene expression of target genes, cDNA amplified using TaqMan Universal PCR Master Mix. Quantitative PCR was performed on an ABI-PRISM 7700 Sequence Detector (Applied Biosystems). Assays were linear over 4 orders of magnitude. Calculations were performed by a comparative cycle threshold (Ct) method: the starting copy number of test samples was determined in comparison with the known copy number of the calibrator sample (ddCt). The relative gene copy number was calculated as 2–ddCt. Probes for target genes were from TaqMan Assay-on-Demand kits (Applied Biosystems). Samples were adjusted for total RNA content by expression of HPRT or 18S protein and values of aPKC$\lambda^{-/-}$ RNA were normalized to ctr mice expression.

Table 5: Applied Biosystems (Taq Man) pre-made assays for qRT-PCR

Full name	Gene	Catalogue number
m 18S	18S	Mm03928990_g1
Axin 2	Axin2	Mm00443610_m1
bone morphogenetic protein 4	Bmp4	Mm00432087_m1
CD34 antigen	CD34	Mm00519283_m1
Cyclin-dependent kinase 4	CDK4	Mm00726334_s1*
cyclin D1	Ccnd1	Mm00432360_m1
keratin 15	Krt15	Mm01306866_m1
lymphoid enhancer binding factor 1	Lef1	Mm00550265_m1
nuclear factor of activated T-cells	Nfatc1	Mm00479445_m1
protein kinase C, iota	Prkci	Mm01293252_m1
protein kinase C, zeta	Prkcz	Mm00776345_g1
wingless-related MMTV integration site 5A	Wnt5a	Mm00437347_m1
wingless related MMTV integration site 10b	Wnt10b	Mm00442104_m1

4.2.6 Keratinocyte cell culture

The experiments described were performed with primary keratinocytes isolated from either newborn or adult aPKC$\lambda^{fl/fl}$ (ctr) or aPKC$\lambda^{epi-/-}$ mice. All experiments were done under sterile conditions.

4.2.6.1 Isolation of primary keratinocytes from newborn mice

Newborn mice were sacrificed by decapitation, the bodies were incubated for 30 min on ice. Subsequent sterilizing washes (iodine solution, sterile PBS, 70 % EtOH, each for 1 min), the skin was carefully removed from the torso and the tails was prepared for genotyping. The skin was floated dermal side down in a 0,6 cm cell culture dish filled with 1 ml of cold 0.25 % trypsin solution (Gibco) and incubated at 4 °C for 15 to 24 hrs. Each skin was transferred to a dry, sterile culture plate and spread out with the dermis facing down. The epidermis was separated from the dermis by using forceps and the epidermis was cut in little pieces with 2 scalpel blades, transferred to 2 ml eppendorf tube containing 1,5 ml growth medium. Well suspensions were shaked for 30 min at 32 °C and plated on collagen-coated 6-well plates.

4.2.6.2 Isolation of primary keratinocytes from adult tails of mice/back skin

After shaving, subcutaneous and fat tissue of 4-8 weeks old mice was removed manually and the skin was sterilized by washing in iodine solution, PBS, 70% EtOH, each for 5 min. Back and tail skin was digested with 0.25 % trypsin (without EDTA, Gibco) for 1.5 hrs at 37

°C, 5 % CO_2. Subsequently, epidermis was separated from the dermis, minced and gently agitatet for 30 min at 37 °C in keratinocytes growth medium. After straining through a 70 µm filter, cell suspensions were centrifuged (850 g, 5 min, 22 °C) and cultured as keratinocytes isolated from newborn mice (s.4.2.6.3).

4.2.6.3 Cultivation of primary keratinocytes

Primary keratinocytes were cultured on collagen type-1 (0.04 mg/ml) (Biochrom) coated dishes in FAD medium containing 50µM Ca^{2+} in the presence of mitomycin C-treated (4 µg/ml) 3T3 fibroblasts as feeders at 32 °C, 5% CO_2. Fibroblasts were cultivated on 10 cm plates and maintained in an incubator with a humified atmosphere at 37 °C and 5 % CO_2.

Reagents and media for keratinocyte cell culture

1) DMEM (FAD)-medium (Growth medium for keratinocytes)

10 % FCS, treated with Chelex

- 0.4 µg/ml hydrocortisone
- 5 µg/ml insulin
- 10 ng/ml EGF
- 10^{-10} M cholera toxin
- 100 U/ml penicillin and 100 µg/ml streptomycin
- 2 mM L-Glutamin

2) Dulbecco`s phosphate buffered saline without calcium and magnesium

3) Trypsin: 1 x Trypsin/EDTA 0.05 %

4.2.6.4 Passaging of primary keratinocytes

In order to passage the cells, growth medium was removed and the cells were trypsinized for 210 min at 37°C. After centrifugation (850 rpm, 5 min) of the obtained cell suspension in 3 fold amount of DMEM medium, wells were resuspended in growth medium and plated on freshly collagen-coated dishes.

4.2.6.5 Transfection of primary keratinocytes

Lipofectamine 2000

Keratinocytes were transfected via Lipofectamine 2000 (Invitrogen) by diluting 250 (750) ng DNA in 50 (150) µl medium w/o FCS and P/S per well for 24 (6) well plates. The same amount of medium/ well was supplemented with 4 (12) µl transfection agent and added to the DNA containing medium followed by 20 min incubation at RT. Cells were washed two times with PBS. The transfection mix was distributed dropwise on the cells and supplemented with 350 (750) µl medium w/o FCS and P/S. After 5 hrs incubation at 32 °C

and 5 % CO_2 500 µl medium containing 20 % FCS was added to the cells. After 24 – 48 hrs cells were fixed or lysed for protein extraction.

FUGENE 6

For lipofection via FUGENE 6 (Roche), cells were transferred in antibiotics-free medium 1hr before transfection. For 24 (6) well plates. 500 (1000) ng DNA was diluted in 150 µl OptiMEM medium (Invitrogen) per well. The transfection mix was incubated 15 min at room temperature and added dropwise to the growth medium. Medium was changed 18 hrs after transfection, cells were fixed or lysed for protein extraction 24 hrs after medium exchange.

4.2.6.6 Top/Fop-FLASH assays

To assay β-catenin transcriptional activity, cells were transiently transfected with 1 µg of TOP-Flash or FOP-Flash plasmid and 100 ng of pRLTK vectors. The reporter plasmids TOP-Flash or FOP-Flash contain three copies of TCF/Lef-binding site (TOP-Flash) or mutant copies of TCF/Lef binding site (Fop-Flash) upstream of a minimal thymidine kinase promoter directing transcription of luciferase gene (Promega). The pRLTK vector contains cDNA encoding for Renilla Luciferase as an internal transfection control (Promega). Cell were cotransfected with 1 µg active β-catenin (pcDNA3-S33-β-catenin) (Hans Clevers, Utrecht, the Netherlands), pEGF-C1 aPKCλ or pEGF-C1-aPKCλ-kinase dead (Peter Parker, London, England) vectors. For all co-transfections, the total mass of DNA was kept constant with appropriate amounts of the respective control vectors (pEGFP-C1 or pcDNA3.1). All experiments were performed thrice in duplicate. Firefly and Renilla activities in lysates were measured with the Promega Dual Luciferase Assay system.

4.2.6.7 Colony forming assays of primary keratinocytes

$4x10^4$ primary keratinocytes (passage 0-3) were plated in triplicates in a 6-well plate and cultured for approximately 3 weeks in the presence of fibroblasts. Fibroblasts were changed twice a week. Only keratinocytes isolated from littermates were compared. Cells were fixed with 1 % PFA for 15 min and stained for minimum 1 hr with 0.05 % crystal violet in PBS. Digital images were obtained for analysis of colony size and number using ImageJ. For each knock-out line experiments were repeated at least three times with independently isolated keratinocytes.

4.2.6.8 Proliferation assays

To measure DNA synthesis, the Cell Proliferation ELISA, BrdU (colorimetric) Kit (Roche) was used according to the manufactures instructions. The assay is based on the detection of BrdU, which is incorporated into the genomic DNA of proliferating cells. Cells grown in 96-well tissue-culture microplates were labeled by 6 hrs incubation with BrdU. During this

labeling period, BrdU were incorporated in place of thymidine into the DNA of cycling cells. The labeling medium was removed, then cells were fixed and the DNA was denatured in one step by adding FixDenat. After removing FixDenat, the BrdU-specific anti-BrdU-POD antibody was added. The immune complexes were detected by the subsequent substrate reaction. The reaction product was quantified by measuring the absorbance using a scanning multi-well spectrophotometer (ELISA reader) at an absorption wavelength of 450 nm.

4.2.7 FACS analysis /sorting of keratinocytes from adult mice

Primary keratinocytes were isolated as described in 4.2.6.2. For Lrig1 and MTS24 FACS staining, epidermis of back skin was harvested and digested using thermolysine (Sigma Aldrich) (Jensen et al., 2009). After filtering through a 70 µm and 40 µm cell strainer, single cell suspensions were incubated in 5 % FCS/PBS with antibodies for 45 minutes at 4 °C. Cell viability was assessed by 7AAD (BD Bioscience) labeling. Subsequent analysis was carried out using a FACSCanto^{TM}II Cytometer (BD Bioscience) equipped with BD FACSDiva Software. Cell sorting for RNA isolation was carried out using a FACSVantage SE System (BD Biosciene).

4.3 Protein biochemical methods

4.3.1 Isolation of the epidermis of newborn mice

Epidermis was separated from the dermis by floating skin biopsies, epidermis side up, in a 0.5 M ammoinium thiocyanate (NH_4SCN) in phosphate buffer, pH 6,8 (0,1 M Na_2HPO_4, 0,1 M KH_2PO_4) for 20 min on ice. Epidermis was either snap frozen in liquid nitrogen or immediately processed for RNA isolation or processed in protein lysates.

4.3.2 Protein extraction from epidermal splits and keratinocytes

Epidermis was grinded in a mixer mill 300 (Qiagen) for 3 min at 30 Hz in lysis buffer without detergent. Next, episermal splits were lysed in lysis buffer containing 1% NP-40, 0.5% deoxycholate, 0.2% SDS, 2 mM EDTA, 150 mM NaCl, 50 mM Tris, pH 7.4, and a cocktail of protease inhibitors (Sigma Aldrich).

Cultured keratinocytes or skin tissue were lysed in 1% Ripa lysis buffer (150 mM NaCl, 50 mM Tris pH 7.4, 4 mM EDTA , 1 % NP40, 0.5 % DOC, ddH_2O) supplemented with mammalian protease inhibitor cocktail (Sigma-Aldrich) and 2 mM PMSF (Fluka) as well as phosphatase inhibitors to prevent protein degradation by endogenous proteases or phosphatases during lysis. Afterwards lysates were rotated for 1 hr at 4 °C and were centrifuged for 10 min at 13000rpm and 4 °C and supernatants were transferred into a new reaction tube.

4.3.4 SDS-polyacrylamid-gelelectrophoresis (SDS-PAGE)

After perfoming a BCA test to determine protein concentrations (Pierce Biotechnology), the same amount of denaturized proteins were separated according to their molecular mass via SDS-polyacrylamid-gelelectrophoresis. Samples were dissolved in SDS-sample buffer and incubated for 5 min at 95 °C. 50 µg protein concentrations were loaded on the gels, which were separated at 40 mA per gel for an appropriate time in 1 x SDS running buffer. Depending on the molecular mass of the proteins of interest, gels containing 6-12 % acrylamid were used. In some cases, commercially available gradient gels (4-12 % gradient Bis-Tris Gels, Invitrogen) were applied.

4.3.5 Western Blot Analysis

Equal amounts of total protein were separated by SDS-PAGE, transferred to nitrocellulose (G&E) and probed with the appropriate antibodies. If the protein size of interest was more than 10 kD different from actin, α-actin was probed on the same filter as loading control. Otherwise, a gel was run simultaneously using the same protein amounts and probed for actin, to assure that similar amounts were indeed present.

4.3.6 Con-A precipitation

Keratinocytes on 6 cm dishes or epidermal preparations from newborn mice were lysed in 400 µl 1 % NP40 lysis buffer and subjected to a Bradford assay. Equal amounts of lysates were mixed with 60 µl of 0.5 mg/ml Concavalin-A sepharose beads. After a rotation for 2 hrs at 4 °C, the samples were centrifuged at 8000 rpm for 2 min. The supernatant, containing the cytosolic fraction, was transferred to a fresh eppendorf tube and stored at –20 °C. The beads were washed with lysis buffer and three times with ice-cold 1x PBS. 20 µl of the cytosolic fraction as well as the beads were mixed with 2x SDS-sample buffer and subjected to SDS-PAGE for further analysis.

4.3.7 Rac/Cdc42 activity assay

Epidermal skin biopsies were taken from mice and suspended in lysis buffer containing 50 mM Tris-HCl pH 7.4, 100 mM NaCl, 10 mM $MgCl_2$, protease inhibitor cocktail (Sigma Aldrich) and 4 µg biotin-CRIB-PAK peptide (Price et al., 2003). After homogenising the tissue in a mixer mill (Qiagen) 2' at 30 Hz, 1 % NP-40 was added to the lysate and rotated for 2 hrs at 4 °C. After centrifugation for 15 min at 4 °C, an aliquot of total lysate was taken after which supernatants were again rotated for 1 h at 4 °C. Lysates were incubated with streptavidin agarose-beads for 1 hr at 4 °C. Beads were washed three times with lysis buffer and cooked in loading buffer for 5 min at 95 °C. The bead lysate as well as equal amounts of total lysate were separated by SDS-PAGE, transferred to nitrocellulose and probed with either an α -Rac antibody or α-actin antibody.

4.4 Chemicals and Antibodies

4.4.1 Chemicals

Chemicals and reagents were purchased from Sigma Aldrich, BD Pharmingen, Eppendorf, Quiagen, Merck or Roth unless stated otherwise.

4.4.2 Antibodies

4.4.2.1 Primary antibodies and antisera

Table 6: Primary antibodies used for detection in western blot and immunohistochemistry

Their source, working dilution, the specific clone and producing company are shown. WB: western blot, IF: immunofluorescence. PE=Phycoerythrin.

Antigene	Source	Working dilution	Catalog number	company
actin	mouse	WB 1:10000	A3853 Lot: 6472J	Sigma Aldrich
aPKCλ	rabbit	IF: 1:200	Sc-216	Santa Cruz
aPKCζ/λ thr 410/403	rabbit	WB: 1:500	9378 Lot: F7	Cell signalling
BrdU	mouse	IF: 1: 20	347580	BD Pharmigen
β-catenin	mouse	IF: 1:250 WB: 1: 2000	610154	BD transduction labs
Cdc42	rabbit	IF 1:25	Sc 87	Santa Cruz
CD34	rat	IF 1:50	553731	BD Pharmigen
CD34-Alexa 488	rat	FACS: 1:25	553733	BD Pharmigen
CD43-Alexa-700	rat	FACS: 1:25	560518	BD Pharmigen
Cyclin B1	mouse	WB 1:250	Ab72 Lot: 931381	Abcam
GFP	chicken	1:4000	Ab13970	Abcam
Itga6/CD47f-PE	rat	FACS: 1:30	555736	BD Pharmigen
K15	mouse	IF: 1:1000	MS-1068-P0	Thermo Scientific
K75	guinea pig	IF: 1:2000 WB: 1:4000	GPK 6hf Lot: 912040	Progen
K82	guinea pig	IF: 1:2000 Wb: 1:2000	GPhHa2 Lot: 906240	Progen
K85	guinea pig	IF: 1:1000	GP-hHb5	Progen

			Lot: 802671	
K28	guinea pig	IF: 1:1000	GP- K28 Lot: 802270	Progen
K14	rabbit	IF:1:2000	PRB-155P	Covance
K10	rabbit	IF 1:1000	PRB 159P Lot: 9HC01547	Covance
Ki67	mouse	IF: 1:1000	TEC-3	TEC-3, DAKO
Lef1	rabbit	IF 1:100	2230	Cell signaling
Lgl	rabbit	IF: 1:50 WB: 1:500	/	V. Vasioukhin, Seattle, USA
Pins/LGN	rabbit	IF 1:200	/	Xiong Lang, Singapore
Loricirin	rabbit	1:1000	PRB-145P	Covance
Lrig1	goat	IF: 1:150	AF3688	R&D systems
MTS24	rat	IF: 1:50	/	A.Sonnenberg, Amsterdem,The Netherlands
MTS24	rat	IF: 1:100	/	R. Boyd, Melbourne, Australia
NfatC1	mouse	IF 1:50	SC-7294 Lot: D0708	Santa Cruz
Numb	rabbit	IF: 1:50 WB: 1:500	ab14140 Lot: 85306	Abcam
Numb	goat	IF: 1:50 WB: 1:500	ab4147-100 Lot 690683	Abcam
NuMA	rabbit	IF 1:500 WB 1:1000	NB500-174	Novus/ Acris
Par1	mouse	IF: 1:100	05-680	Upstate
Par3	rabbit	IF: 1:500 WB: 1:5000	07-330	Upstate
Rac1	mouse	WB: 1:1000	R265	Sigma-Aldrich
S100a6	rabbit	IF: 1:1000	RB-1805-A0 Lot: 1805A801F	Neomarkers
Sox9	Rabbit	IF:1:150	SC-20095 Lot: H2808	Santa Cruz

p-Smad 1/5/8	rabbit	IF 1:100	ab3848	Millipore
Survivin	rabbit	IF: 1:400	2808 Lot: 71G4B7	Cell signaling
γ-tubulin	rabbit	IF: 1:100	11321	Abcam

4.4.2.2 Secondary antibodies

Table 7: Secondary antibodies used for detection in western blot and immunohistochemistry

Their source, working dilution, the specific clone and producing company are shown. WB: western blot, IF: immunofluorescence. PE=Phycoerythrin.

Antigene	Source	Working dilution	Catalog number	company
Alexafluor 488 anti-mouse	goat	IF 1:500	A11074	Molecular Probes
Alexafluor 488 anti-rabbit	goat	IF 1:500	A21206	Molecular Probes
Alexafluor 594 anti-mouse IgG2A	goat	IF 1:500	A21135	Molecular Probes
Alexafluor 546 Anti-rat	goat	FACS: 1:200	A-11081	Molecular Probes/ Invitrogen
Alexa 647 Anti goat	donkey	FACS: 1:200	A21447	Molecular Probes/ Invitrogen
Alexa 488 anti-mouse IgG1	goat	IF: 1:500	A21121	Molecular Probes/ Invitrogen
Alexa 488 anti-guinea pig	goat	IF: 1:500	A11073	Molecular Probes/ Invitrogen
IgG-mouse anti rabbit	rabbit	IF:1:10	0931	Dako
IgG-HRP anti-rabbit	goat	WB 1:5000	170-6515	BioRad
IgG-HRP anti-mouse	goat	WB 1:5000	170-6516	BioRad
IgG-HRP anti-guinea pig	donkey	WB 1:5000	sc-2020	Santa Cruz

5 Bibliography

Akimoto, K., Takahashi, R., Moriya, S., Nishioka, N., Takayanagi, J., Kimura, K., Fukui, Y., Osada, S. i, Mizuno, K., Hirai, S. i, et al. (1996). EGF or PDGF receptors activate atypical PKClambda through phosphatidylinositol 3-kinase. *EMBO J* **15**, 788-798.

Anrather, J., Csizmadia, V., Soares, M. P. and Winkler, H. (1999). Regulation of NF-kappaB RelA phosphorylation and transcriptional activity by p21(ras) and protein kinase Czeta in primary endothelial cells. *J. Biol. Chem* **274**, 13594-13603.

Arnold, I. and Watt, F. M. (2001). c-Myc activation in transgenic mouse epidermis results in mobilization of stem cells and differentiation of their progeny. *Curr. Biol* **11**, 558-568.

Atwood, S. X. and Prehoda, K. E. (2009). aPKC Phosphorylates Miranda to Polarize Fate Determinants during Neuroblast Asymmetric Cell Division. *Current Biology* **19**, 723-729.

Baker, C. M., Verstuyf, A., Jensen, K. B. and Watt, F. M. (2010). Differential sensitivity of epidermal cell subpopulations to beta-catenin-induced ectopic hair follicle formation. *Dev. Biol* **343,** 40-50.

Barrandon, Y. and Green, H. (1985). Cell size as a determinant of the clone-forming ability of human keratinocytes. *Proc. Natl. Acad. Sci. U.S.A* **82**, 5390-5394.

Baye, L. M. and Link, B. A. (2007). Interkinetic nuclear migration and the selection of neurogenic cell divisions during vertebrate retinogenesis. *J. Neurosci.* **27**, 10143-10152.

Behrendt, K., Klatte, J., Pofahl, R., Bloch, W., Smyth, N., Tscharntke, M., Krieg, T., Paus, R., Niessen, C., Niemann, C., et al. (2012). A function for Rac1 in the terminal differentiation and pigmentation of hair. *Journal of Cell Science*.

Benitah, S. A., Frye, M., Glogauer, M. and Watt, F. M. (2005). Stem cell depletion through epidermal deletion of Rac1. *Science* **309**, 933-935.

Benton, R. and St Johnston, D. (2003). Drosophila PAR-1 and 14-3-3 inhibit Bazooka/PAR-3 to establish complementary cortical domains in polarized cells. *Cell* **115**, 691-704.

Berra, E., Diaz-Meco, M. T., Dominguez, I., Municio, M. M., Sanz, L., Lozano, J., Chapkin, R. S. and Moscat, J. (1993). Protein kinase C zeta isoform is critical for mitogenic signal transduction. *Cell* **74**, 555-563.

Betschinger, J., Mechtler, K. and Knoblich, J. A. (2003). The Par complex directs asymmetric cell division by phosphorylating the cytoskeletal protein Lgl. *Nature* **422**, 326-330.

Bickenbach, J. R., McCutecheon, J. and Mackenzie, I. C. (1986). Rate of loss of tritiated thymidine label in basal cells in mouse epithelial tissues. *Cell Tissue Kinet* **19**, 325-333.

Binczek, E., Jenke, B., Holz, B., Günter, R. H., Thevis, M. and Stoffel, W. (2007). Obesity resistance of the stearoyl-CoA desaturase-deficient (scd1-/-) mouse results from disruption of the epidermal lipid barrier and adaptive thermoregulation. *Biol. Chem.* **388**, 405-418.

Blanpain, C. and Fuchs, E. (2009). Epidermal homeostasis: a balancing act of stem cells in the skin. *Nat. Rev. Mol. Cell Biol* **10**, 207-217.

Blanpain, C., Lowry, W. E., Geoghegan, A., Polak, L. and Fuchs, E. (2004). Self-renewal, multipotency, and the existence of two cell populations within an epithelial stem cell niche. *Cell* **118**, 635-648.

Blanpain, C., Lowry, W. E., Pasolli, H. A. and Fuchs, E. (2006). Canonical notch signaling functions as a commitment switch in the epidermal lineage. *Genes Dev.* **20**, 3022-3035.

Blount, M., Goff, S. and Slusarewicz, P. (2008). In vitro degradation of the inner root sheath in human hair follicles lacking sebaceous glands. *Br. J. Dermatol* **158**, 22-30.

Botchkarev, V. A. and Sharov, A. A. (2004). BMP signaling in the control of skin development and hair follicle growth. *Differentiation* **72**, 512-526.

Braun, K. M., Niemann, C., Jensen, U. B., Sundberg, J. P., Silva-Vargas, V. and Watt, F. M. (2003). Manipulation of stem cell proliferation and lineage commitment: visualisation of label-retaining cells in wholemounts of mouse epidermis. *Development* **130**, 5241-5255.

Castilho, R. M., Squarize, C. H., Patel, V., Millar, S. E., Zheng, Y., Molinolo, A. and Gutkind, J. S. (2007). Requirement of Rac1 distinguishes follicular from interfollicular epithelial stem cells. *Oncogene* **26**, 5078-5085.

Castilho, R. M., Squarize, C. H., Chodosh, L. A., Williams, B. O. and Gutkind, J. S. (2009). mTOR mediates Wnt-induced epidermal stem cell exhaustion and aging. *Cell Stem Cell* **5**, 279-289.

Chauhan, V. P., Chauhan, A., Deshmukh, D. S. and Brockerhoff, H. (1990). Lipid activators of protein kinase C. *Life Sci* **47**, 981-986.

Chen, J., Jaeger, K., Den, Z., Koch, P. J., Sundberg, J. P. and Roop, D. R. (2008). Mice expressing a mutant Krt75 (K6hf) allele develop hair and nail defects resembling pachyonychia congenita. *J. Invest. Dermatol.* **128,** 270-279.

Clayton, E., Doupé, D. P., Klein, A. M., Winton, D. J., Simons, B. D. and Jones, P. H. (2007). A single type of progenitor cell maintains normal epidermis. *Nature* **446**, 185-189.

Corbit, K. C., Trakul, N., Eves, E. M., Diaz, B., Marshall, M. and Rosner, M. R. (2003). Activation of Raf-1 signaling by protein kinase C through a mechanism involving Raf kinase inhibitory protein. *J. Biol. Chem.* **278**, 13061-13068.

Cotsarelis, G. (0000). Epithelial Stem Cells: A Folliculocentric View. *J Invest Dermatol* **126**, 1459-1468.

Cotsarelis, G., Sun, T. T. and Lavker, R. M. (1990). Label-retaining cells reside in the bulge area of pilosebaceous unit: implications for follicular stem cells, hair cycle, and skin carcinogenesis. *Cell* **61**, 1329-1337.

Cox, D. N., Seyfried, S. A., Jan, L. Y. and Jan, Y. N. (2001). Bazooka and atypical protein kinase C are required to regulate oocyte differentiation in the Drosophila ovary. *Proc. Natl. Acad. Sci. U.S.A* **98**, 14475-14480.

Dard, N., Le, T., Maro, B. and Louvet-Vallée, S. (2009a). Inactivation of aPKCλ Reveals a

Context Dependent Allocation of Cell Lineages in Preimplantation Mouse Embryos. *PLoS ONE* **4**, e7117.

Dard, N., Louvet-Vallée, S. and Maro, B. (2009b). Orientation of Mitotic Spindles during the 8- to 16-Cell Stage Transition in Mouse Embryos. *PLoS ONE* **4**, e8171.

DasGupta, R. and Fuchs, E. (1999). Multiple roles for activated LEF/TCF transcription complexes during hair follicle development and differentiation. *Development* **126,** 4557-4568.

Demehri, S. and Kopan, R. (2009). Notch signaling in bulge stem cells is not required for selection of hair follicle fate. *Development* **136**, 891-896.

Depreter, M. G. L., Blair, N. F., Gaskell, T. L., Nowell, C. S., Davern, K., Pagliocca, A., Stenhouse, F. H., Farley, A. M., Fraser, A., Vrana, J., et al. (2008). Identification of Plet-1 as a specific marker of early thymic epithelial progenitor cells. *Proc. Natl. Acad. Sci. U.S.A.* **105,** 961-966.

Diaz-Meco, M. T. and Moscat, J. (2001). MEK5, a New Target of the Atypical Protein Kinase C Isoforms in Mitogenic Signaling. *Mol Cell Biol* **21**, 1218-1227.

Djiane, A., Yogev, S. and Mlodzik, M. (2005). The apical determinants aPKC and dPatj regulate Frizzled-dependent planar cell polarity in the Drosophila eye. *Cell* **121**, 621-631.

Dominguez, I., Diaz-Meco, M. T., Municio, M. M., Berra, E., García de Herreros, A., Cornet, M. E., Sanz, L. and Moscat, J. (1992). Evidence for a role of protein kinase C zeta subspecies in maturation of Xenopus laevis oocytes. *Mol. Cell. Biol* **12**, 3776-3783.

Doupé, D. P., Klein, A. M., Simons, B. D. and Jones, P. H. (2010). The ordered architecture of murine ear epidermis is maintained by progenitor cells with random fate. *Dev. Cell* **18**, 317-323.

Duncan, A. W., Rattis, F. M., DiMascio, L. N., Congdon, K. L., Pazianos, G., Zhao, C., Yoon, K., Cook, J. M., Willert, K., Gaiano, N., et al. (2005). Integration of Notch and Wnt signaling in hematopoietic stem cell maintenance. *Nat. Immunol.* **6**, 314-322.

Duran, A., Diaz-Meco, M. T. and Moscat, J. (2003). Essential role of RelA Ser311 phosphorylation by zetaPKC in NF-kappaB transcriptional activation. *EMBO J* **22**, 3910-3918.

Etienne-Manneville, S. and Hall, A. (2003). Cell polarity: Par6, aPKC and cytoskeletal crosstalk. *Curr. Opin. Cell Biol* **15**, 67-72.

Farese, R. V. and Sajan, M. P. (2010). Metabolic functions of atypical protein kinase C: “good” and “bad” as defined by nutritional status. *Am. J. Physiol. Endocrinol. Metab.* **298**, E385-394.

Farese, R. V., Sajan, M. P., Yang, H., Li, P., Mastorides, S., Gower, W. R., Jr, Nimal, S., Choi, C. S., Kim, S., Shulman, G. I., et al. (2007). Muscle-specific knockout of PKC-lambda impairs glucose transport and induces metabolic and diabetic syndromes. *J. Clin. Invest* **117**, 2289-2301.

Fox, T. E., Houck, K. L., O’Neill, S. M., Nagarajan, M., Stover, T. C., Pomianowski, P. T., Unal, O., Yun, J. K., Naides, S. J. and Kester, M. (2007). Ceramide recruits and activates protein kinase C zeta (PKC zeta) within structured membrane

microdomains. *J. Biol. Chem.* 282, 12450-12457.

Fuchs, E. (2007). Scratching the surface of skin development. *Nature* **445**, 834-842.

Fuchs, E. and Horsley, V. (2011). Ferreting out stem cells from their niches. *Nat. Cell Biol.* **13**, 513-518.

Fuchs, E. and Raghavan, S. (2002). Getting under the skin of epidermal morphogenesis. *Nat. Rev. Genet.* **3**, 199-209.

Galli, M., Muñoz, J., Portegijs, V., Boxem, M., Grill, S. W., Heck, A. J. R. and van den Heuvel, S. (2011). aPKC phosphorylates NuMA-related LIN-5 to position the mitotic spindle during asymmetric division. *Nat. Cell Biol.* **13**, 1132-1138.

Galvez, A. S., Duran, A., Linares, J. F., Pathrose, P., Castilla, E. A., Abu-Baker, S., Leitges, M., Diaz-Meco, M. T. and Moscat, J. (2009). Protein kinase Czeta represses the interleukin-6 promoter and impairs tumorigenesis in vivo. *Mol. Cell. Biol.* **29**, 104-115.

Gat, U., DasGupta, R., Degenstein, L. and Fuchs, E. (1998). De Novo hair follicle morphogenesis and hair tumors in mice expressing a truncated beta-catenin in skin. *Cell* **95**, 605-614.

Ghosh, S., Marquardt, T., Thaler, J. P., Carter, N., Andrews, S. E., Pfaff, S. L. and Hunter, T. (2008). Instructive role of aPKCζ subcellular localization in the assembly of adherens junctions in neural progenitors. *Proceedings of the National Academy of Sciences* **105**, 335 -340.

Göransson, O., Deak, M., Wullschleger, S., Morrice, N. A., Prescott, A. R. and Alessi, D. R. (2006). Regulation of the polarity kinases PAR-1/MARK by 14-3-3 interaction and phosphorylation. *J. Cell. Sci.* **119**, 4059-4070.

Greco, V., Chen, T., Rendl, M., Schober, M., Pasolli, H. A., Stokes, N., Dela Cruz-Racelis, J. and Fuchs, E. (2009). A two-step mechanism for stem cell activation during hair regeneration. *Cell Stem Cell* **4**, 155-169.

Guilgur, L. G., Prudêncio, P., Ferreira, T., Pimenta-Marques, A. R. and Martinho, R. G. (2012). Drosophila aPKC is required for mitotic spindle orientation during symmetric division of epithelial cells. *Development* **139**, 503-513.

Haegebarth, A. and Clevers, H. (2009). Wnt Signaling, Lgr5, and Stem Cells in the Intestine and Skin. *Am J Pathol* **174**, 715-721.

Hafner, M., Wenk, J., Nenci, A., Pasparakis, M., Scharffetter-Kochanek, K., Smyth, N., Peters, T., Kess, D., Holtkötter, O., Shephard, P., et al. (2004). Keratin 14 Cre transgenic mice authenticate keratin 14 as an oocyte-expressed protein. *Genesis* **38**, 176-181.

Halprin, K. M. (1972). Epidermal “turnover time”--a re-examination. *Br. J. Dermatol* **86**, 14-19.

Hanakawa, Y., Li, H., Lin, C., Stanley, J. R. and Cotsarelis, G. (2004). Desmogleins 1 and 3 in the companion layer anchor mouse anagen hair to the follicle. *J. Invest. Dermatol* **123**, 817-822.

Hao, Y., Du, Q., Chen, X., Zheng, Z., Balsbaugh, J. L., Maitra, S., Shabanowitz, J., Hunt, D. F. and Macara, I. G. (2010). Par3 Controls Epithelial Spindle Orientation by aPKC-Mediated Phosphorylation of Apical Pins. *Current Biology* **20**, 1809-1818.

Hashimoto, N., Kido, Y., Uchida, T., Matsuda, T., Suzuki, K., Inoue, H., Matsumoto, M., Ogawa, W., Maeda, S., Fujihara, H., et al. (2005). PKClambda regulates glucose-induced insulin secretion through modulation of gene expression in pancreatic beta cells. *J. Clin. Invest* **115**, 138-145.

Hayashi, S. and McMahon, A. P. (2002). Efficient recombination in diverse tissues by a tamoxifen-inducible form of Cre: a tool for temporally regulated gene activation/inactivation in the mouse. *Dev. Biol.* **244**, 305-318.

Helfrich, I., Schmitz, A., Zigrino, P., Michels, C., Haase, I., le Bivic, A., Leitges, M. and Niessen, C. M. (2007). Role of aPKC isoforms and their binding partners Par3 and Par6 in epidermal barrier formation. *J. Invest. Dermatol* **127**, 782-791.

Hillje, A., Worlitzer, M. M. A., Palm, T. and Schwamborn, J. C. (2011). Neural Stem Cells Maintain Their Stemness through Protein Kinase C ζ-Mediated Inhibition of TRIM32. *STEM CELLS* **29**, 1437-1447.

Hirano, Y., Yoshinaga, S., Ogura, K., Yokochi, M., Noda, Y., Sumimoto, H. and Inagaki, F. (2004). Solution Structure of Atypical Protein Kinase C PB1 Domain and Its Mode of Interaction with ZIP/p62 and MEK5. *Journal of Biological Chemistry* **279**, 31883 - 31890.

Horne-Badovinac, S., Lin, D., Waldron, S., Schwarz, M., Mbamalu, G., Pawson, T., Jan, Y., Stainier, D. Y. and Abdelilah-Seyfried, S. (2001). Positional cloning of heart and soul reveals multiple roles for PKC lambda in zebrafish organogenesis. *Curr. Biol* **11**, 1492-1502.

Horsley, V. (2011). Upward bound: follicular stem cell fate decisions. *EMBO J* **30**, 2986-2987.

Horsley, V., Aliprantis, A. O., Polak, L., Glimcher, L. H. and Fuchs, E. (2008). NFATc1 balances quiescence and proliferation of skin stem cells. *Cell* **132**, 299-310.

House, C. and Kemp, B. E. (1987). Protein kinase C contains a pseudosubstrate prototope in its regulatory domain. *Science* **238**, 1726-1728.

Huelsken, J., Vogel, R., Erdmann, B., Cotsarelis, G. and Birchmeier, W. (2001). beta-Catenin controls hair follicle morphogenesis and stem cell differentiation in the skin. *Cell* **105**, 533-545.

Hurov, J. B., Watkins, J. L. and Piwnica-Worms, H. (2004). Atypical PKC phosphorylates PAR-1 kinases to regulate localization and activity. *Curr. Biol* **14**, 736-741.

Iden, S. and Collard, J. G. (2008). Crosstalk between small GTPases and polarity proteins in cell polarization. *Nat Rev Mol Cell Biol* **9**, 846-859.

Imai, F., Hirai, S.-ichi, Akimoto, K., Koyama, H., Miyata, T., Ogawa, M., Noguchi, S., Sasaoka, T., Noda, T. and Ohno, S. (2006). Inactivation of aPKCλ results in the loss of adherens junctions in neuroepithelial cells without affecting neurogenesis in mouse neocortex. *Development* **133**, 1735 -1744.

Ito, M., Liu, Y., Yang, Z., Nguyen, J., Liang, F., Morris, R. J. and Cotsarelis, G. (2005). Stem cells in the hair follicle bulge contribute to wound repair but not to homeostasis of the epidermis. *Nat. Med* **11**, 1351-1354.

Jaks, V., Barker, N., Kasper, M., van Es, J. H., Snippert, H. J., Clevers, H. and Toftgård, R.

(2008). Lgr5 marks cycling, yet long-lived, hair follicle stem cells. *Nat. Genet* **40**, 1291-1299.

Jaks, V., Kasper, M. and Toftgård, R. (2010). The hair follicle-a stem cell zoo. *Exp. Cell Res* **316**, 1422-1428.

Jensen, K. B., Collins, C. A., Nascimento, E., Tan, D. W., Frye, M., Itami, S. and Watt, F. M. (2009). Lrig1 expression defines a distinct multipotent stem cell population in mammalian epidermis. *Cell Stem Cell* **4**, 427-439.

Joberty, G., Petersen, C., Gao, L. and Macara, I. G. (2000). The cell-polarity protein Par6 links Par3 and atypical protein kinase C to Cdc42. *Nat. Cell Biol* **2**, 531-539.

Jones, D. L. and Wagers, A. J. (2008). No place like home: anatomy and function of the stem cell niche. *Nat. Rev. Mol. Cell Biol* **9**, 11-21.

Jones, P. H., Simons, B. D. and Watt, F. M. (2007). Sic transit gloria: farewell to the epidermal transit amplifying cell? *Cell Stem Cell* **1**, 371-381.

Kalinin, A. E., Kajava, A. V. and Steinert, P. M. (2002). Epithelial barrier function: assembly and structural features of the cornified cell envelope. *Bioessays* **24**, 789-800.

Kaur, P. (2006). Interfollicular epidermal stem cells: identification, challenges, potential. *J. Invest. Dermatol* **126**, 1450-1458.

Kemphues, K. (2000). PARsing Embryonic Polarity. *Cell* **101**, 345-348.

Kemphues, K. J., Priess, J. R., Morton, D. G. and Cheng, N. S. (1988). Identification of genes required for cytoplasmic localization in early C. elegans embryos. *Cell* **52**, 311-320.

Kiso, M., Tanaka, S., Saba, R., Matsuda, S., Shimizu, A., Ohyama, M., Okano, H. J., Shiroishi, T., Okano, H. and Saga, Y. (2009). The disruption of Sox21-mediated hair shaft cuticle differentiation causes cyclic alopecia in mice. *Proc. Natl. Acad. Sci. U.S.A.* **106**, 9292-9297.

Knoblich, J. A. (2008). Mechanisms of asymmetric stem cell division. *Cell* **132**, 583-597.

Knoblich, J. A. (2010). Asymmetric cell division: recent developments and their implications for tumour biology. *Nat. Rev. Mol. Cell Biol.* **11**, 849-860.

Ko, M. S. and Marinkovich, M. P. (2010). Role of dermal-epidermal basement membrane zone in skin, cancer, and developmental disorders. *Dermatol Clin* **28**, 1-16.

Kobielak, K., Stokes, N., de la Cruz, J., Polak, L. and Fuchs, E. (2007). Loss of a quiescent niche but not follicle stem cells in the absence of bone morphogenetic protein signaling. *Proc. Natl. Acad. Sci. U.S.A.* **104**, 10063-10068.

Koike, C., Nishida, A., Akimoto, K., Nakaya, M.-aki, Noda, T., Ohno, S. and Furukawa, T. (2005). Function of Atypical Protein Kinase C Λ in Differentiating Photoreceptors Is Required for Proper Lamination of Mouse Retina. *The Journal of Neuroscience* **25**, 10290 -10298.

Korinek, V., Barker, N., Morin, P. J., van Wichen, D., de Weger, R., Kinzler, K. W., Vogelstein, B. and Clevers, H. (1997). Constitutive transcriptional activation by a beta-catenin-Tcf complex in APC-/- colon carcinoma. *Science* **275**, 1784-1787.

Koster, M. I. and Roop, D. R. (2007). Mechanisms regulating epithelial stratification. *Annu. Rev. Cell Dev. Biol* **23**, 93-113.

Kotani, K., Ogawa, W., Matsumoto, M., Kitamura, T., Sakaue, H., Hino, Y., Miyake, K., Sano, W., Akimoto, K., Ohno, S., et al. (1998). Requirement of atypical protein kinase clambda for insulin stimulation of glucose uptake but not for Akt activation in 3T3-L1 adipocytes. *Mol. Cell. Biol* **18**, 6971-6982.

Kovac, J., Oster, H. and Leitges, M. (2007). Expression of the atypical protein kinase C (aPKC) isoforms iota/lambda and zeta during mouse embryogenesis. *Gene Expr. Patterns* **7**, 187-196.

Lajtha, L. G. (1979). Stem cell concepts. *Differentiation* **14**, 23-34.

Langbein, L., Rogers, M. A., Praetzel, S., Winter, H. and Schweizer, J. (2003). K6irs1, K6irs2, K6irs3, and K6irs4 represent the inner-root-sheath-specific type II epithelial keratins of the human hair follicle. *J. Invest. Dermatol* **120**, 512-522.

Langbein, L., Rogers, M. A., Praetzel-Wunder, S., Helmke, B., Schirmacher, P. and Schweizer, J. (2006). K25 (K25irs1), K26 (K25irs2), K27 (K25irs3), and K28 (K25irs4) represent the type I inner root sheath keratins of the human hair follicle. *J. Invest. Dermatol* **126**, 2377-2386.

Lechler, T. and Fuchs, E. (2005). Asymmetric cell divisions promote stratification and differentiation of mammalian skin. *Nature* **437**, 275-280.

Lee, C.-Y., Robinson, K. J. and Doe, C. Q. (2006). Lgl, Pins and aPKC regulate neuroblast self-renewal versus differentiation. *Nature* **439**, 594-598.

Leitges, M., Sanz, L., Martin, P., Duran, A., Braun, U., García, J. F., Camacho, F., Diaz-Meco, M. T., Rennert, P. D. and Moscat, J. (2001). Targeted disruption of the zetaPKC gene results in the impairment of the NF-kappaB pathway. *Mol. Cell* **8**, 771-780.

Levy, V., Lindon, C., Harfe, B. D. and Morgan, B. A. (2005). Distinct stem cell populations regenerate the follicle and interfollicular epidermis. *Dev. Cell* **9**, 855-861.

Li, L. and Clevers, H. (2010). Coexistence of quiescent and active adult stem cells in mammals. *Science* **327**, 542-545.

Lin, D., Edwards, A. S., Fawcett, J. P., Mbamalu, G., Scott, J. D. and Pawson, T. (2000). A mammalian PAR-3-PAR-6 complex implicated in Cdc42/Rac1 and aPKC signalling and cell polarity. *Nat. Cell Biol* **2**, 540-547.

Lin, H.-Y., Kao, C.-H., Lin, K. M.-C., Kaartinen, V. and Yang, L.-T. (2011). Notch signaling regulates late-stage epidermal differentiation and maintains postnatal hair cycle homeostasis. *PLoS ONE* **6**, e15842.

Littlewood, T. D., Hancock, D. C., Danielian, P. S., Parker, M. G. and Evan, G. I. (1995). A modified oestrogen receptor ligand-binding domain as an improved switch for the regulation of heterologous proteins. *Nucleic Acids Res.* **23**, 1686-1690.

Lo Celso, C., Prowse, D. M. and Watt, F. M. (2004). Transient activation of beta-catenin signalling in adult mouse epidermis is sufficient to induce new hair follicles but continuous activation is required to maintain hair follicle tumours. *Development* **131**, 1787-1799.

Lowry, W. E., Blanpain, C., Nowak, J. A., Guasch, G., Lewis, L. and Fuchs, E. (2005). Defining the impact of beta-catenin/Tcf transactivation on epithelial stem cells. *Genes Dev* **19**, 1596-1611.

Luxenburg, C., Amalia Pasolli, H., Williams, S. E. and Fuchs, E. (2011). Developmental roles for Srf, cortical cytoskeleton and cell shape in epidermal spindle orientation. *Nat Cell Biol* **13**, 203-214.

Macara, I. G. (2004). Parsing the polarity code. *Nat. Rev. Mol. Cell Biol* **5**, 220-231.

Mackenzie, I. C. and Bickenbach, J. R. (1985). Label-retaining keratinocytes and Langerhans cells in mouse epithelia. *Cell Tissue Res.* **242**, 551-556.

Marshall, B. S., Price, G. and Powell, C. T. (2000). Rat protein kinase c zeta gene contains alternative promoters for generation of dual transcripts with 5'-end heterogeneity. *DNA Cell Biol* **19**, 707-719.

Martin, P., Duran, A., Minguet, S., Gaspar, M.-L., Diaz-Meco, M.-T., Rennert, P., Leitges, M. and Moscat, J. (2002). Role of ζPKC in B-cell signaling and function. *EMBO J* **21**, 4049-4057.

Matsumoto, M., Ogawa, W., Akimoto, K., Inoue, H., Miyake, K., Furukawa, K., Hayashi, Y., Iguchi, H., Matsuki, Y., Hiramatsu, R., et al. (2003). PKClambda in liver mediates insulin-induced SREBP-1c expression and determines both hepatic lipid content and overall insulin sensitivity. *J. Clin. Invest* **112**, 935-944.

Merrill, B. J., Gat, U., DasGupta, R. and Fuchs, E. (2001). Tcf3 and Lef1 regulate lineage differentiation of multipotent stem cells in skin. *Genes Dev.* **15**, 1688-1705.

Mertens, A. E. E., Rygiel, T. P., Olivo, C., van der Kammen, R. and Collard, J. G. (2005). The Rac activator Tiam1 controls tight junction biogenesis in keratinocytes through binding to and activation of the Par polarity complex. *J. Cell Biol.* **170**, 1029-1037.

Milner, Y., Sudnik, J., Filippi, M., Kizoulis, M., Kashgarian, M. and Stenn, K. (2002). Exogen, shedding phase of the hair growth cycle: characterization of a mouse model. *J. Invest. Dermatol* **119**, 639-644.

Miyazaki, M., Man, W. C. and Ntambi, J. M. (2001). Targeted disruption of stearoyl-CoA desaturase1 gene in mice causes atrophy of sebaceous and meibomian glands and depletion of wax esters in the eyelid. *J. Nutr* **131**, 2260-2268.

Moll, R., Franke, W. W., Schiller, D. L., Geiger, B. and Krepler, R. (1982). The catalog of human cytokeratins: patterns of expression in normal epithelia, tumors and cultured cells. *Cell* **31**, 11-24.

Morris, R. J. and Potten, C. S. (1994). Slowly cycling (label-retaining) epidermal cells behave like clonogenic stem cells in vitro. *Cell Prolif* **27**, 279-289.

Morris, R. J. and Potten, C. S. (1999). Highly persistent label-retaining cells in the hair follicles of mice and their fate following induction of anagen. *J. Invest. Dermatol* **112**, 470-475.

Morris, R. J., Fischer, S. M. and Slaga, T. J. (1985). Evidence that the centrally and peripherally located cells in the murine epidermal proliferative unit are two distinct cell populations. *J. Invest. Dermatol* **84**, 277-281.

Morris, R. J., Liu, Y., Marles, L., Yang, Z., Trempus, C., Li, S., Lin, J. S., Sawicki, J. A. and Cotsarelis, G. (2004). Capturing and profiling adult hair follicle stem cells. *Nat. Biotechnol* **22**, 411-417.

Moscat, J. and Diaz-Meco, M. T. (2000). The atypical protein kinase Cs. Functional specificity mediated by specific protein adapters. *EMBO Rep* **1**, 399-403.

Müller-Röver, S., Handjiski, B., van der Veen, C., Eichmüller, S., Foitzik, K., McKay, I. A., Stenn, K. S. and Paus, R. (2001). A comprehensive guide for the accurate classification of murine hair follicles in distinct hair cycle stages. *J. Invest. Dermatol.* **117**, 3-15.

Murray, N. R., Weems, J., Braun, U., Leitges, M. and Fields, A. P. (2009). Protein kinase C betaII and PKCiota/lambda: collaborating partners in colon cancer promotion and progression. *Cancer Res.* **69**, 656-662.

Nakanishi, H., Brewer, K. A. and Exton, J. H. (1993). Activation of the zeta isozyme of protein kinase C by phosphatidylinositol 3,4,5-trisphosphate. *J. Biol. Chem* **268**, 13-16.

Niemann, C. (2009). Differentiation of the sebaceous gland. *Dermatoendocrinol* **1**, 64-67.

Niemann, C., Unden, A. B., Lyle, S., Zouboulis, C. C., Toftgård, R. and Watt, F. M. (2003). Indian hedgehog and beta-catenin signaling: role in the sebaceous lineage of normal and neoplastic mammalian epidermis. *Proc. Natl. Acad. Sci. U.S.A.* 100 Suppl **1,** 11873-11880.

Niessen, C. M. and Gottardi, C. J. (2008). Molecular components of the adherens junction. *Biochim. Biophys. Acta* **1778**, 562-571.

Niessen, M. T. and Niessen, C. M. (2010). Regulation of cell and tissue polarity: implications for skin homeostasis and disease. *Expert Review of Dermatology* **5**, 671-687.

Nijhof, J. G. W., Braun, K. M., Giangreco, A., van Pelt, C., Kawamoto, H., Boyd, R. L., Willemze, R., Mullenders, L. H. F., Watt, F. M., de Gruijl, F. R., et al. (2006). The cell-surface marker MTS24 identifies a novel population of follicular keratinocytes with characteristics of progenitor cells. *Development* **133**, 3027-3037.

Nishimura, T. and Kaibuchi, K. (2007). Numb controls integrin endocytosis for directional cell migration with aPKC and PAR-3. *Dev. Cell* **13**, 15-28.

Nishizuka, Y. (1995). Protein kinase C and lipid signaling for sustained cellular responses. *FASEB J* **9**, 484-496.

Nowak, J. A., Polak, L., Pasolli, H. A. and Fuchs, E. (2008). Hair follicle stem cells are specified and function in early skin morphogenesis. *Cell Stem Cell* **3**, 33-43.

Ono, Y., Fujii, T., Ogita, K., Kikkawa, U., Igarashi, K. and Nishizuka, Y. (1989). Protein kinase C zeta subspecies from rat brain: its structure, expression, and properties. *Proc. Natl. Acad. Sci. U.S.A* **86**, 3099-3103.

Oster, H., Eichele, G. and Leitges, M. (2004). Differential expression of atypical PKCs in the adult mouse brain. *Brain Res. Mol. Brain Res* **127**, 79-88.

Panteleyev, A. A., Jahoda, C. A. and Christiano, A. M. (2001). Hair follicle predetermination. *J. Cell. Sci* **114**, 3419-3431.

Parsons, L. M., Grzeschik, N. A., Allott, M. L. and Richardson, H. E. (2010). Lgl/aPKC and Crb regulate the Salvador/Warts/Hippo pathway. *Fly (Austin)* **4**, 288-293.

Petersson, M., Brylka, H., Kraus, A., John, S., Rappl, G., Schettina, P. and Niemann, C. (2011). TCF/Lef1 activity controls establishment of diverse stem and progenitor cell compartments in mouse epidermis. *EMBO J* **30**, 3004-3018.

Peyre, E., Jaouen, F., Saadaoui, M., Haren, L., Merdes, A., Durbec, P. and Morin, X. (2011). A lateral belt of cortical LGN and NuMA guides mitotic spindle movements and planar division in neuroepithelial cells. *J. Cell Biol.* **193**, 141-154.

Plusa, B., Frankenberg, S., Chalmers, A., Hadjantonakis, A.-K., Moore, C. A., Papalopulu, N., Papaioannou, V. E., Glover, D. M. and Zernicka-Goetz, M. (2005). Downregulation of Par3 and aPKC function directs cells towards the ICM in the preimplantation mouse embryo. *J. Cell. Sci* **118**, 505-515.

Poliquin, L. and Shore, G. C. (1980). A method for efficient and selective recovery of membrane glycoproteins from concanavalin A-Sepharose using media containing sodium dodecyl sulfate and urea. *Anal. Biochem.* **109**, 460-465.

Potten, C. S. (1974). The epidermal proliferative unit: the possible role of the central basal cell. *Cell Tissue Kinet* **7**, 77-88.

Poulson, N. D. and Lechler, T. (2010). Robust control of mitotic spindle orientation in the developing epidermis. *J. Cell Biol.* **191**, 915-922.

Price, L. S., Langeslag, M., ten Klooster, J. P., Hordijk, P. L., Jalink, K. and Collard, J. G. (2003). Calcium signaling regulates translocation and activation of Rac. *J. Biol. Chem.* **278**, 39413-39421.

Qin, Y., Meisen, W. H., Hao, Y. and Macara, I. G. (2010). Tuba, a Cdc42 GEF, is required for polarized spindle orientation during epithelial cyst formation. *The Journal of Cell Biology* **189**, 661 -669.

Rasin, M.-R., Gazula, V.-R., Breunig, J. J., Kwan, K. Y., Johnson, M. B., Liu-Chen, S., Li, H.-S., Jan, L. Y., Jan, Y.-N., Rakic, P., et al. (2007). Numb and Numbl are required for maintenance of cadherin-based adhesion and polarity of neural progenitors. *Nat. Neurosci.* **10**, 819-827.

Raymond, K., Richter, A., Kreft, M., Frijns, E., Janssen, H., Slijper, M., Praetzel-Wunder, S., Langbein, L. and Sonnenberg, A. (2010). Expression of the orphan protein Plet-1 during trichilemmal differentiation of anagen hair follicles. *J. Invest. Dermatol* **130**, 1500-1513.

Regala, R. P., Davis, R. K., Kunz, A., Khoor, A., Leitges, M. and Fields, A. P. (2009). Atypical protein kinase C{iota} is required for bronchioalveolar stem cell expansion and lung tumorigenesis. *Cancer Res.* **69**, 7603-7611.

Rendl, M., Lewis, L. and Fuchs, E. (2005). Molecular dissection of mesenchymal-epithelial interactions in the hair follicle. *PLoS Biol* **3**, e331.

Rolls, M. M., Albertson, R., Shih, H.-P., Lee, C.-Y. and Doe, C. Q. (2003). Drosophila aPKC regulates cell polarity and cell proliferation in neuroblasts and epithelia. *The Journal of Cell Biology* **163**, 1089 -1098.

Romano, R.-A., Smalley, K., Liu, S. and Sinha, S. (2010). Abnormal hair follicle development

and altered cell fate of follicular keratinocytes in transgenic mice expressing DeltaNp63alpha. *Development* **137**, 1431-1439.

Rosse, C., Linch, M., Kermorgant, S., Cameron, A. J. M., Boeckeler, K. and Parker, P. J. (2010). PKC and the control of localized signal dynamics. *Nat Rev Mol Cell Biol* **11**, 103-112.

Sabherwal, N., Tsutsui, A., Hodge, S., Wei, J., Chalmers, A. D. and Papalopulu, N. (2009). The apicobasal polarity kinase aPKC functions as a nuclear determinant and regulates cell proliferation and fate during Xenopus primary neurogenesis. *Development* **136**, 2767-2777.

Schlegelmilch, K., Mohseni, M., Kirak, O., Pruszak, J., Rodriguez, J. R., Zhou, D., Kreger, B. T., Vasioukhin, V., Avruch, J., Brummelkamp, T. R., et al. (2011). Yap1 acts downstream of α-catenin to control epidermal proliferation. *Cell* **144**, 782-795.

Schneider, M. R., Schmidt-Ullrich, R. and Paus, R. (2009). The hair follicle as a dynamic miniorgan. *Curr. Biol.* **19**, R132-142.

Seifert, K., Ibrahim, H., Stodtmeister, T., Winklbauer, R. and Niessen, C. M. (2009). An adhesion-independent, aPKC-dependent function for cadherins in morphogenetic movements. *J. Cell. Sci.* **122**, 2514-2523.

Selbie, L. A., Schmitz-Peiffer, C., Sheng, Y. and Biden, T. J. (1993). Molecular cloning and characterization of PKC iota, an atypical isoform of protein kinase C derived from insulin-secreting cells. *J. Biol. Chem* **268**, 24296-24302.

Sengupta, A., Duran, A., Ishikawa, E., Florian, M. C., Dunn, S. K., Ficker, A. M., Leitges, M., Geiger, H., Diaz-Meco, M., Moscat, J., et al. (2011). Atypical protein kinase C (aPKC{zeta} and aPKC{lambda}) is dispensable for mammalian hematopoietic stem cell activity and blood formation. *Proc. Natl. Acad. Sci. U.S.A* **108**, 9957-9962.

Senoo, M., Pinto, F., Crum, C. P. and McKeon, F. (2007). p63 Is essential for the proliferative potential of stem cells in stratified epithelia. *Cell* **129**, 523-536.

Shi, S.-H., Jan, L. Y. and Jan, Y.-N. (2003). Hippocampal neuronal polarity specified by spatially localized mPar3/mPar6 and PI 3-kinase activity. *Cell* **112**, 63-75.

Shtutman, M., Zhurinsky, J., Simcha, I., Albanese, C., D'Amico, M., Pestell, R. and Ben-Ze'ev, A. (1999). The cyclin D1 gene is a target of the beta-catenin/LEF-1 pathway. *Proc. Natl. Acad. Sci. U.S.A.* **96**, 5522-5527.

Smart, I. H. (1970). Variation in the plane of cell cleavage during the process of stratification in the mouse epidermis. *Br. J. Dermatol* 82, 276-282.

Smith, C. A., Lau, K. M., Rahmani, Z., Dho, S. E., Brothers, G., She, Y. M., Berry, D. M., Bonneil, E., Thibault, P., Schweisguth, F., et al. (2007). aPKC-mediated phosphorylation regulates asymmetric membrane localization of the cell fate determinant Numb. *EMBO J.* **26**, 468-480.

Snippert, H. J., Haegebarth, A., Kasper, M., Jaks, V., van Es, J. H., Barker, N., van de Wetering, M., van den Born, M., Begthel, H., Vries, R. G., et al. (2010). Lgr6 marks stem cells in the hair follicle that generate all cell lineages of the skin. *Science* **327**, 1385-1389.

Soloff, R. S., Katayama, C., Lin, M. Y., Feramisco, J. R. and Hedrick, S. M. (2004). Targeted

deletion of protein kinase C lambda reveals a distribution of functions between the two atypical protein kinase C isoforms. *J. Immunol* **173**, 3250-3260.

Sotiropoulou, P. A., Candi, A. and Blanpain, C. (2008). The majority of multipotent epidermal stem cells do not protect their genome by asymmetrical chromosome segregation. *Stem Cells* **26**, 2964-2973.

Srinivas, S., Watanabe, T., Lin, C. S., William, C. M., Tanabe, Y., Jessell, T. M. and Costantini, F. (2001). Cre reporter strains produced by targeted insertion of EYFP and ECFP into the ROSA26 locus. *BMC Dev. Biol.* **1**, 4.

St Johnston, D. and Sanson, B. (2011). Epithelial polarity and morphogenesis. *Curr. Opin. Cell Biol.* **23**, 540-546.

Stachelscheid, H., Ibrahim, H., Koch, L., Schmitz, A., Tscharntke, M., Wunderlich, F. T., Scott, J., Michels, C., Wickenhauser, C., Haase, I., et al. (2008). Epidermal insulin/IGF-1 signalling control interfollicular morphogenesis and proliferative potential through Rac activation. *EMBO J.* **27**, 2091-2101.

Standaert, M. L., Bandyopadhyay, G., Kanoh, Y., Sajan, M. P. and Farese, R. V. (2001). Insulin and PIP3 activate PKC-zeta by mechanisms that are both dependent and independent of phosphorylation of activation loop (T410) and autophosphorylation (T560) sites. *Biochemistry* **40**, 249-255.

Stratis, A., Pasparakis, M., Markur, D., Knaup, R., Pofahl, R., Metzger, D., Chambon, P., Krieg, T. and Haase, I. (2006). Localized Inflammatory Skin Disease Following Inducible Ablation of I Kappa B Kinase 2 in Murine Epidermis. *J Invest Dermatol* **126**, 614-620.

Sugiyama, Y., Akimoto, K., Robinson, M. L., Ohno, S. and Quinlan, R. A. (2009). A cell polarity protein aPKClambda is required for eye lens formation and growth. *Dev. Biol* **336**, 246-256.

Suzuki, A. and Ohno, S. (2006). The PAR-aPKC system: lessons in polarity. *Journal of Cell Science* **119**, 979 -987.

Suzuki, A., Akimoto, K. and Ohno, S. (2003). Protein Kinase C λ/ι (PKCλ/ι): A PKC Isotype Essential for the Development of Multicellular Organisms. *Journal of Biochemistry* **133**, 9 -16.

Tabler, J. M., Yamanaka, H. and Green, J. B. A. (2010). PAR-1 promotes primary neurogenesis and asymmetric cell divisions via control of spindle orientation. *Development* **137**, 2501-2505.

Tabuse, Y., Izumi, Y., Piano, F., Kemphues, K. J., Miwa, J. and Ohno, S. (1998). Atypical protein kinase C cooperates with PAR-3 to establish embryonic polarity in Caenorhabditis elegans. *Development* **125**, 3607-3614.

Trempus, C. S., Morris, R. J., Ehinger, M., Elmore, A., Bortner, C. D., Ito, M., Cotsarelis, G., Nijhof, J. G. W., Peckham, J., Flagler, N., et al. (2007). CD34 expression by hair follicle stem cells is required for skin tumor development in mice. *Cancer Res* **67**, 4173-4181.

Tumbar, T., Guasch, G., Greco, V., Blanpain, C., Lowry, W. E., Rendl, M. and Fuchs, E. (2004). Defining the Epithelial Stem Cell Niche in Skin. *Science* **303**, 359 -363.

Tunggal, J. A., Helfrich, I., Schmitz, A., Schwarz, H., Günzel, D., Fromm, M., Kemler, R., Krieg, T. and Niessen, C. M. (2005). E-cadherin is essential for in vivo epidermal barrier function by regulating tight junctions. *EMBO J.* **24**, 1146-1156.

Van Mater, D., Kolligs, F. T., Dlugosz, A. A. and Fearon, E. R. (2003). Transient activation of beta -catenin signaling in cutaneous keratinocytes is sufficient to trigger the active growth phase of the hair cycle in mice. *Genes Dev.* **17**, 1219-1224.

Vidal, V. P. I., Chaboissier, M.-C., Lützkendorf, S., Cotsarelis, G., Mill, P., Hui, C.-C., Ortonne, N., Ortonne, J.-P. and Schedl, A. (2005). Sox9 is essential for outer root sheath differentiation and the formation of the hair stem cell compartment. *Curr. Biol.* **15**, 1340-1351.

Wang, L. C., Liu, Z. Y., Gambardella, L., Delacour, A., Shapiro, R., Yang, J., Sizing, I., Rayhorn, P., Garber, E. A., Benjamin, C. D., et al. (2000). Regular articles: conditional disruption of hedgehog signaling pathway defines its critical role in hair development and regeneration. *J. Invest. Dermatol.* **114**, 901-908.

Wang, G., Krishnamurthy, K. and Bieberich, E. (2009). Regulation of primary cilia formation by ceramide. *J. Lipid Res.* **50**, 2103-2110.

Watt, F. M. (2001). Stem cell fate and patterning in mammalian epidermis. *Curr. Opin. Genet. Dev* **11**, 410-417.

Watt, F. M. and Jensen, K. B. (2009). Epidermal stem cell diversity and quiescence. *EMBO Mol Med* **1**, 260-267.

Watt, F. M., Estrach, S. and Ambler, C. A. (2008). Epidermal Notch signalling: differentiation, cancer and adhesion. *Curr. Opin. Cell Biol.* **20**, 171-179.

Wend, P., Holland, J. D., Ziebold, U. and Birchmeier, W. (2010). Wnt signaling in stem and cancer stem cells. *Semin. Cell Dev. Biol.* **21**, 855-863.

Williams, S. E., Beronja, S., Pasolli, H. A. and Fuchs, E. (2011a). Asymmetric cell divisions promote Notch-dependent epidermal differentiation. *Nature* **470**, 353-358.

Win, H. Y. and Acevedo-Duncan, M. (2008). Atypical protein kinase C phosphorylates IKKalphabeta in transformed non-malignant and malignant prostate cell survival. *Cancer Lett* **270**, 302-311.

Wirtz-Peitz, F., Nishimura, T. and Knoblich, J. A. (2008). Linking cell cycle to asymmetric division: Aurora-A phosphorylates the Par complex to regulate Numb localization. *Cell* **135**, 161-173.

Wu, X., Quondamatteo, F., Lefever, T., Czuchra, A., Meyer, H., Chrostek, A., Paus, R., Langbein, L. and Brakebusch, C. (2006). Cdc42 controls progenitor cell differentiation and beta-catenin turnover in skin. *Genes Dev.* **20**, 571-585.

Yang, L. and Peng, R. (2010). Unveiling hair follicle stem cells. *Stem Cell Rev* **6**, 658-664.

Yang, J.-Q., Leitges, M., Duran, A., Diaz-Meco, M. T. and Moscat, J. (2009a). Loss of PKCλ/ι impairs Th2 establishment and allergic airway inflammation in vivo. *Proceedings of the National Academy of Sciences* **106**, 1099 -1104.

Yang, L., Wang, L. and Yang, X. (2009b). Disruption of Smad4 in mouse epidermis leads to depletion of follicle stem cells. *Mol. Biol. Cell* **20**, 882-890.

Zhang, J., He, X. C., Tong, W.-G., Johnson, T., Wiedemann, L. M., Mishina, Y., Feng, J. Q. and Li, L. (2006). Bone morphogenetic protein signaling inhibits hair follicle anagen induction by restricting epithelial stem/progenitor cell activation and expansion. *Stem Cells* **24**, 2826-2839.

Zhang, Y. V., Cheong, J., Ciapurin, N., McDermitt, D. J. and Tumbar, T. (2009). Distinct self-renewal and differentiation phases in the niche of infrequently dividing hair follicle stem cells. *Cell Stem Cell* **5**, 267-278.

Zhang, Y. V., White, B. S., Shalloway, D. I. and Tumbar, T. (2010). Stem cell dynamics in mouse hair follicles: a story from cell division counting and single cell lineage tracing. *Cell Cycle* **9**, 1504-1510.

Zheng, Z., Zhu, H., Wan, Q., Liu, J., Xiao, Z., Siderovski, D. P. and Du, Q. (2010). LGN regulates mitotic spindle orientation during epithelial morphogenesis. *J. Cell Biol* **189**, 275-288.

Zouboulis, C. C., Baron, J. M., Böhm, M., Kippenberger, S., Kurzen, H., Reichrath, J. and Thielitz, A. (2008). Frontiers in sebaceous gland biology and pathology. *Exp. Dermatol* **17**, 542-551.

8 Acknowledgements

Many thanks to....

Prof. Dr Carien Niessen for providing me with this fascinating project and giving me the opportunity to work in her lab. Thank you for teaching me incredibly much, for showing me my strengths and weaknesses, for continuiously positive support and an open door at all times.

Prof. Thomas Langer for reviewing my thesis and being part of my thesis committee.

Prof. Matthias Hammerschidt and **Isabel Witt** for joining my defense committee.

All present and former members of the **Niessen lab**. Thanks to stimulating discussions, help with experiments and general advice. Such a friendly, funny and warm working atmosphere is anything but granted. I am proud to be part of this extraordinary team!!!

Dr. Jeanie Scott and **Dr. Karla Seifert** for teaching me so much about skin, lab work and science life.

Dr. Rehan Villani, **Christian Günschmann** and **Susanne Vorhagen** for proofreading the manuscript.

Nadine Niehoff for help in cell culture and her wonderful clear way of seeing the things.

Alexandra Schwickert for genotyping and great commitment.

Annika Schmitz for listening to me in my desperate moments, for always laughing with and about me and for being the proof that being colleagues and real friends at the same time is possible.

The **Haase, Iden and Niemann lab** for a great athmosphere, helpful discussions and a lot of advice.

Sabine Haffke for this wonderful friendship.

All **my friends**, especially the girls: Bine, Ellen, Isa, Sarah, Tina, Anne, Jule, Andrea, Moni, Yvonne, Dana and Petra for perfectly counterbalancing my lab life and brightening up each day! Thank you for always supporting me and still loving me even if I was always tired and a bit too late the last 4 years.

My wonderful family, for always believing in me and supporting me in such a warm, kind and endless way. You made me feel safe every single day.

Dennis Fink for being my perfect counterpart, for cheering me up and calming me down when I needed it, for understanding my weird habits, for always believing in me, for being my best friend and the love of my life.

9 Erklärung

Ich versichere, dass ich die von mir vorgelegte Dissertation selbständig angefertigt, die benutzten Quellen und Hilfsmittel vollständig angegeben und die Stellen der Arbeit – einschließlich Tabellen, Karten und Abbildungen -, die anderen Werken im Wortlaut oder dem Sinn nach entnommen sind, in jedem Einzelfall als Entlehnung kenntlich gemacht habe; dass diese Dissertation noch keiner anderen Fakultät oder Universität zur Prüfung vorgelegen worden ist sowie, dass ich eine solche Veröffentlichung vor Abschluss des Promotionsverfahren nicht vornehmen werde. Die Bestimmungen dieser Promotionsordnung sind mir bekannt. Die von mir vorgelegte Dissertation ist von Prof. Dr. Thomas Langer betreut worden.

Köln, den Michaela Niessen